The activities of the gelsolin homology domains of Flightless-I in actin dynamics

Réka Pintér

Supervisor: Dr. Beáta Bugyi

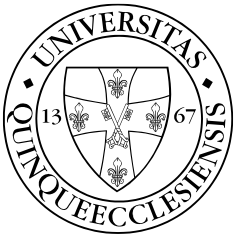

University of Pécs

Medical School

Department of Biophysics

2023

Interdisciplinary Medical Sciences D93 Doctoral School

Leader of the Doctoral School: Prof. Dr. Balázs Sümegi†, ifj. Prof. Dr. Ferenc Gallyas

Program: Investigating functional protein dynamics using biophysical methods (B-130/199)

Leader of the program: Prof. Dr. Miklós Nyitrai

Supervisor: Dr. Beáta Bugyi

Table of contents

1. INTRODUCTION

1.1. Actin cytoskeleton

Cell migration, shape changes or movement of subcellular components are essential for many unicellular or multicellular organisms. Forces that power these diverse motility processes originate, on the one hand, from the actin cytoskeleton[1].

The cytoskeleton is a complex, dynamic network present in the cytoplasm of all cells, including bacteria and archaea. In eukaryotes, it is composed of microfilaments, intermediate filaments and microtubules and determines the structural and dynamic properties of the cell. It is involved in cell stability, cell growth, proliferation, import and export of nutrients and signaling intermediates, migration of pathogens and immune cells. One of the main components of the cytoskeleton is the microfilament system, which are linear polymers composed of the protein; actin (Figure 1)[1-3].

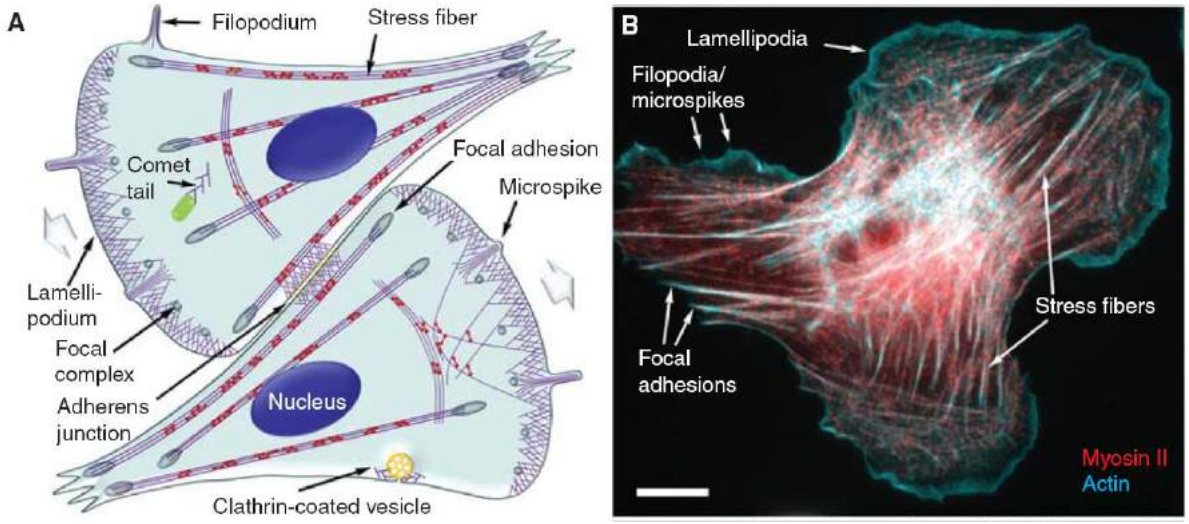

Figure 1. *(A) Components of the actin cytoskeleton in fibroblast-like cells. (B) Fluorescence micrograph of a rat embryo fibroblast showing actin filaments (cyan) and myosin II (red)[1].*

The actin cytoskeleton undergoes continuous remodeling through interactions with a large repertoire of actin-binding proteins (ABPs). These actin remodeling proteins have multiple functions and regulate actin filament assembly and disassembly by e.g., severing pre-existing filaments, capping filament ends or promoting filament

formation; nucleation[1,4-6]. The dynamic remodeling of the actin cytoskeleton requires a spatial and temporal arrangement of ABPs. The ABPs, besides controlling actin dynamics, are also involved in the assembly of actin filaments into higher-order structures, like networks and bundles. Other ABPs allow filaments to interact with cellular membranes. Many of the ABPs bind to the same site of the actin molecule; therefore, they are expected to compete. On the other hand, the ABPs can interact with each other and form ternary complexes such as capping protein and mDia1[1,5,7].

1.1.1. Actin

Actin is a major functional and structural protein present in the cytoplasm of most eukaryotic cells. Yeast and amoebas have a single actin gene, whereas in vertebrates six actin isoforms can be differentiated and divided into two classes, muscle and non-muscle isoactins[8,9]. Actin isoforms are highly conserved and play important roles in nearly all aspects of eukaryotic cell biology[2]. Actin can be found in the highest concentration in muscle fibers (~ 20% of the total cellular protein); however, it also presents in significant amounts in non-muscle cells. In vertebrates, the four actin isoforms (α-skeletal, α-cardiac, α- and γ-smooth muscle) are present in muscle cells and participate in muscle contraction as a component of myofibril. β- and γ-cytoplasmic actins are ubiquitous and expressed in non-muscle cells, where they are involved in cell motility, cell shape determination, intracellular transport, and mitosis. Isoactins cannot replace each other, indicating that although actins have a very slight variation in sequence and have similar physicochemical properties, they are functionally different[8,10]. Due to their specific biological functions, mutations in actin-coding genes may cause changes, incomplete operation or loss-of-related functions, which can lead to severe human diseases, including deafness, cancer and developmental disorders[10-12].

Actin can exist in two forms: as monomer (globular or G-actin) and polymer (filamentous or F-actin). The monomeric actin is composed of 375 amino acids and its molecular mass is roughly 42.3 kDa[2]. The molecule consists of two main domains, which are known as the outer and inner domains. The structure can be further divided into four subdomains (S1-4). The cleft between S2 and S4 (pointed end or '- end') represents the ATP and associated divalent cation binding site (Mg^{2+} or Ca^{2+}), which is a center of enzymatic catalysis[13]. ATP binds with higher affinity to G-actin than ADP and Mg^{2+} is the dominant cation in cells, which determines how tightly or weakly the

ATP binds. The cleft between subdomains 1 and 3 (barbed end or '+ end') composes the major binding site for many ABPs (Figure 2)[2,14].

Actin filaments are formed by the polymerization of monomers. The F-actin structure is considered to be a double-stranded, left-handed helix with a rotation of 166° around the helical axis and has an axial translation of 27.5 $Å^2$. The position of actin monomers is arranged, giving the distinct structural polarity of F-actin. G-actin has poor ATPase activity; the catalytic rate is very low (7×10^{-6} s^{-1}). During polymerization the ATPase activity increases, triggering ATP hydrolysis and phosphate release[2,13].

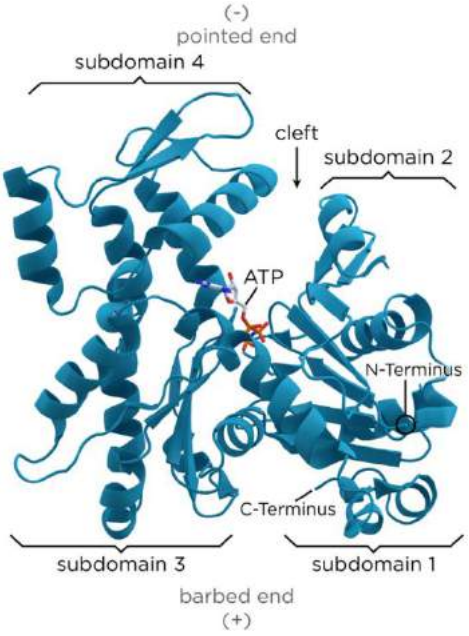

Figure 2. *Structure of the actin monomer[14].*

1.1.1.1. Assembly of actin filaments - nucleation and elongation

The process of actin assembly into filaments is polymerization. Polymerization occurs at suitable solvent conditions, including high ionic strength (e.g., [KCl] = 50 mM, [$MgCl_2$] = 1 mM), neutral or slightly acidic pH and elevated temperature[15,16]. The main features of polymerization are nucleation, elongation and steady-state (Figure 3). During *nucleation* monomers (G) associate to form dimers (G2) and then trimers (G3) that act as nuclei for polymerization. Dimers are less stable than trimers. Filaments lengthen during the *elongation* phase, where actin monomers are added to the polymer[2,6,17,18]. Elongation involves the assembly and disassembly of monomers which

are continuous at both ends of the actin filament. We differentiate a fast-growing barbed end ('+ end') and a slow-growing pointed end ('- end')[19]. The association mainly occurs at the barbed end and dissociation at the pointed end. The subunits of the barbed end primarily bind ATP, while the subunits of the pointed end ADP-bound. In the steady-state, the length of the filament remains constant while continuous association and dissociation of subunits occur. This steady-state assembly and disassembly is known as treadmilling. Small but limited concentration of actin monomers coexists with the filament population, which results in a constant monomer:filament ratio[2]. A dissociation equilibrium constant can be determined for both ends, which is known as critical concentration ($c_{critical}$). It can be calculated as the ratio of the association (k_+) and dissociation (k-) rate constants. The critical concentration marks the level of G-actin concentration above which polymerization takes place spontaneously. The value of critical concentration is ~ 0.1 µM at the barbed end and ~ 0.6 µM at the pointed end[6,20].

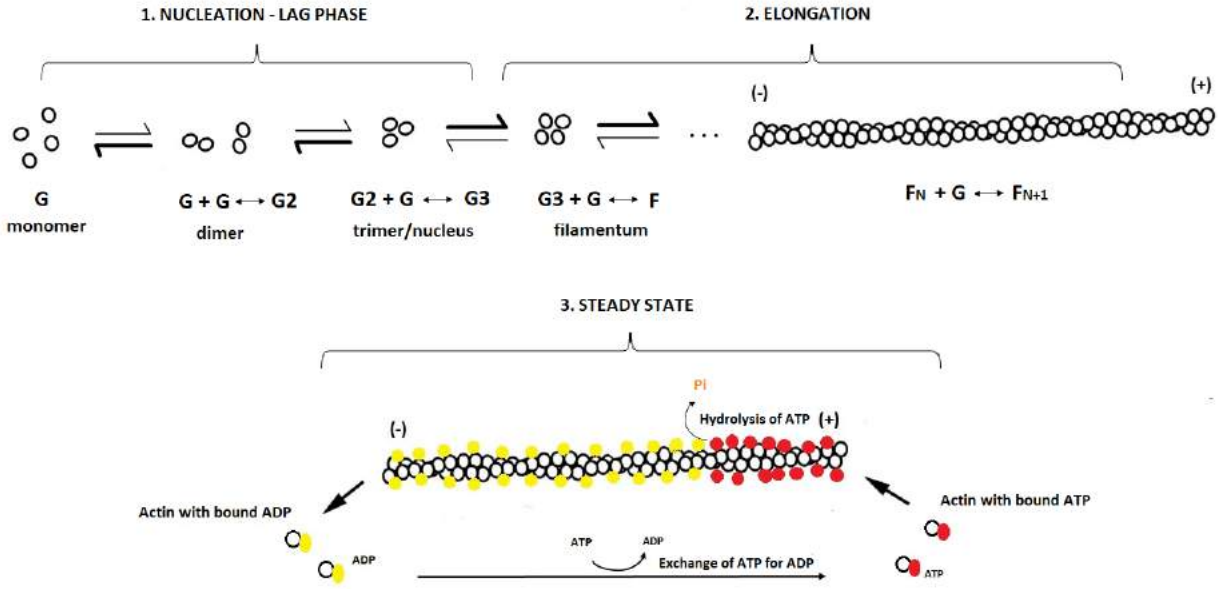

Figure 3. *The phases of actin filament assembly.*

1.1.1.2. Assembly of actin filaments - annealing

The length and number of polymers can be influenced by fragmentation and annealing at steady-state. In the course of fragmentation actin filaments can be broken into smaller pieces by mechanical forces or thermal fluctuations[21]. Annealing occurs

when these short filaments bind end-to-end resulting in an increase in filament length. While the length of filaments increases, their number decreases. Annealing does not necessarily require ATP hydrolysis and is probably part of a repairing mechanism that occurs spontaneously after shearing or sonication[21,22].

1.1.2. Regulation of actin cytoskeleton by actin-binding proteins

Numerous types of ABPs can influence the disassembly and assembly of actin; actin dynamics. These proteins can bind to monomers and/or filaments modifying their structure, thus changing actin's biological function. A large number of ABPs are known, which are generally classified according to their binding mode/effect on actin. The ABPs can be classified into the following groups[2].

1) ***G-actin-binding proteins*** can sequester monomers by forming complexes with them preventing their polymerization (e.g., profilin, thymosin-β) (Figure 4). In non-muscle cells, the concentration of actin monomers is about 100 μM which is approximately 50% of the total actin concentration. For the cells to maintain this large amount of unpolymerized actin stores, monomer-binding proteins are required[23,24].

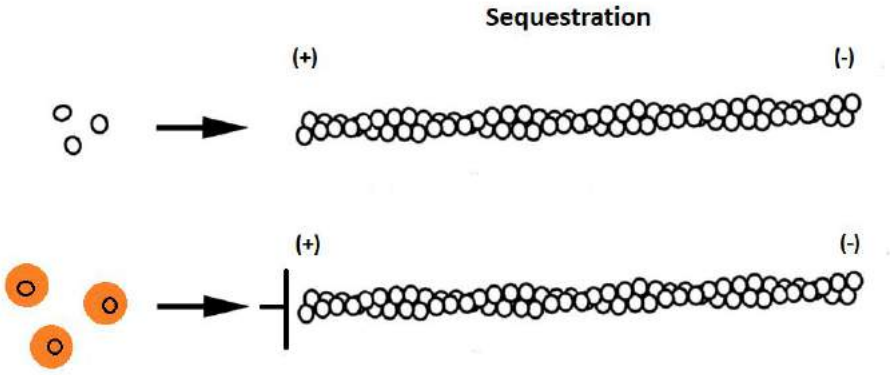

Figure 4. *Sequestration of actin monomers.*

2) ***Filament end-binding proteins*** can cap the ends of the filament, inhibiting the monomer exchange at the barbed end (e.g., CapZ) or at the pointed end (e.g., tropomodulin) (Figure 5).

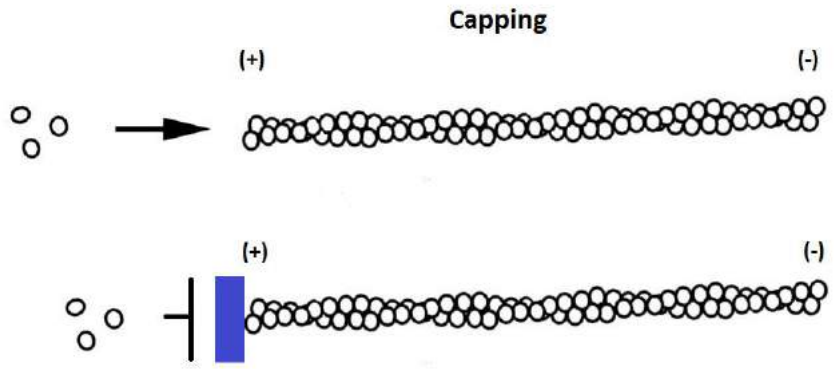

Figure 5. *Capping proteins cap the filament ends.*

3) ***Depolymerizers*** promote the conversion of F-actin to G-actin (e.g., ADF/cofilins). ADF/cofilin proteins bind to F-actin, inducing conformational change, which leads to the loss of filament integrity and disassembly (Figure 6).

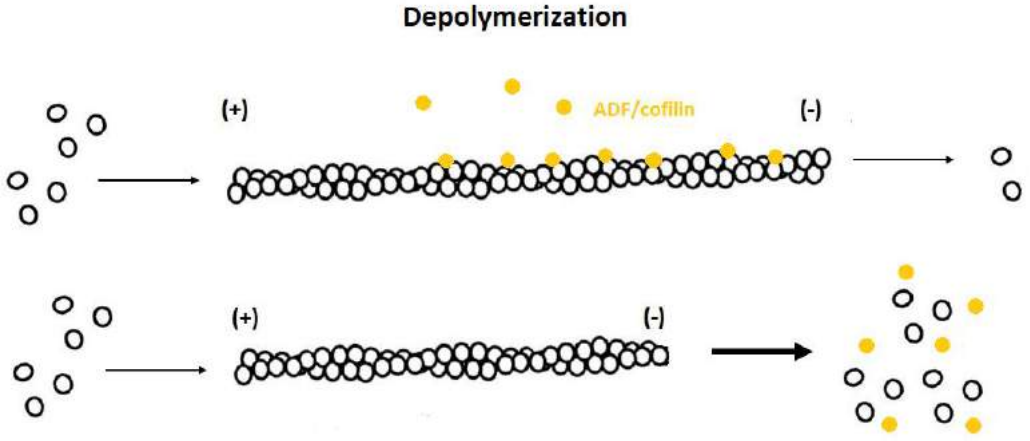

Figure 6. *Depolymerizing proteins.*

4) ***Severing proteins*** can fragment actin filaments into smaller pieces by binding to their side (e.g., gelsolin) (Figure 7). During fragmentation, several shorter filaments are produced (increased filament end formation), to which actin monomers can bind, thus enhancing polymerization[2,25].

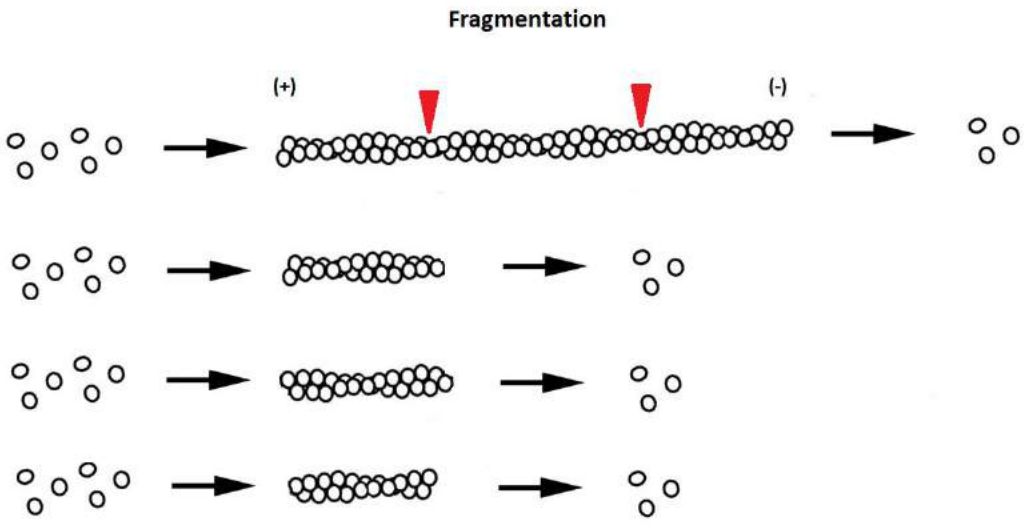

Figure 7. *Severing proteins fragment actin filaments.*

5) ***Cross-linking*** proteins organize filaments into larger-scale structures, branched filaments or make three-dimensional networks (e.g., Arp2/3 complex, actinins) (Figure 8). For example, the Arp2/3 complex nucleates a new filament from the side of an existing filament[26,2,3,6,24].

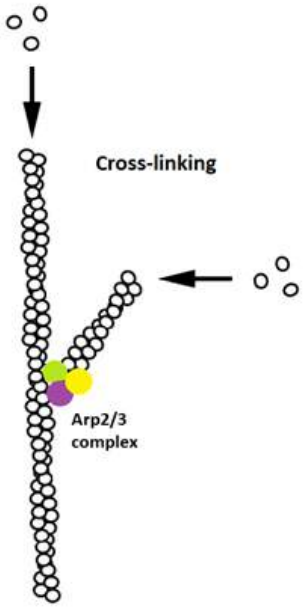

Figure 8. *Actin cross-linking proteins organize filaments into higher-order structures.*

6) ***Stabilizing proteins*** stabilize actin filaments by preventing depolymerization (e.g., tropomyosin) (Figure 9).

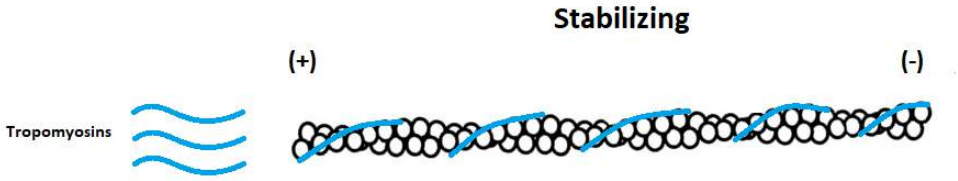

Figure 9. *F-actin stabilizing proteins.*

7) ***Actin-nucleating proteins*** facilitate nucleation and filament formation (e.g., formins, Arp2/3 complex, gelsolin) (Figure 10). Spontaneous actin polymerization is relatively slow in cells; these nucleation factors bind to G-actin and allow rapid polymerization[2,3,27]. Formins both nucleate actin and act as elongation factors that associate with the plus end of the filament and can modify the elongation rate[6,28].

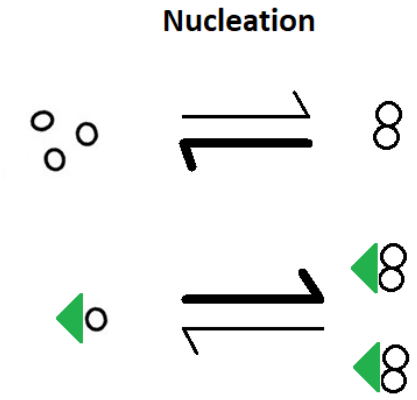

Figure 10. *Nucleating proteins facilitate nucleation and actin filament formation.*

8) **Motor proteins** are class of mechanochemical enzymes (e.g., myosins). Myosins are actin-based motor proteins that move along the actin filament toward the plus end. They convert chemical energy into mechanical work by the hydrolysis of ATP. They are essential in processes such as cell movement, cell division, vesicular transport or muscle contraction[29,30].

ABPs can have multiple functions and generally cannot be classified into one functional group. For example, gelsolin shows actin filament severing and capping activities or the Arp2/3 complex can nucleate filaments and form branch points in actin networks[2,31].

1.1.2.1. Profilin

Profilin is a cytoskeleton-regulating protein that can be found in all eukaryotic cells and it is among the most highly expressed proteins in the cytoplasm[2]. The protein can participate in several cellular functions and have multiple roles (e.g., signal transmission, catalyzing nucleotide exchange on G-actin). Profilin is a small protein (~ 13 kDa) that prefers Mg^{2+}-ATP-G-actin against ADP-G-actin[3]. It binds to G-actin with a high affinity, inhibiting nucleation and pointed end elongation. Profilin can also bind to the '+ end' of F-actin but with relatively weak affinity (K_F ~ 20 μM) as compared to G-actin (K_F ~ 0.1 μM)[2,32]. It was found that profilin increases fluctuation in the length of actin filaments and can interact with other barbed end regulators on F-actin. For example, the protein can bind to Arp2 in the Arp2/3 complex or inhibit FH1FH2 domain association to barbed ends[33].

1.1.2.2. Formins

Formins are multi-domain proteins that can catalyze the nucleation and formation of linear actin filaments. They contain several conserved domains including the formin homology domains 1 and 2 (FH1 and FH2)[3,6]. The FH1 domain is responsible for the binding of profilin and the FH2 domain is essential for actin monomer/filament interactions. Formins are classified into seven families: Dia, FMN, FHOD, delfilin, INF, FRL and DAAM. In general, the cells can express multiple formins that differ in their filament nucleation/elongation activities[3,34].

Based on the sequence homology and function, DAAM proteins belong to the DRF subfamily (diaphanous-related formin). These formins are regulated by autoinhibition through their diaphanous inhibitory domain (DID) and diaphanous autoregulatory (DAD) domains. The two domains interact with each other, inhibiting the actin binding of the FH2 domain. This intramolecular autoinhibitory interaction can be released with the binding of Rho GTPases; thereby DRFs become activated[35-37].

1.1.2.3. Gelsolin superfamily

The gelsolin superfamily is a highly conserved protein family whose members are present in mammalian as well as in non-mammalian organisms. They play an important role in cytoskeletal rearrangement, and control actin organization by severing actin filaments, capping filament ends and nucleating actin assembly[38]. These proteins are also involved in cellular processes, including cell motility, control of apoptosis, regulation of phagocytosis or platelet formation and activation[2,38]. The family includes gelsolin, villin, adseverin, capG, advillin, supervillin and Flightless-I. All these proteins contain three or six gelsolin homology domains[39].

Gelsolin (GSN) is an 80 kDa protein with six gelsolin homology (GH) domains, referred to as GH1-GH6. It can be divided into two tandem homologous halves, the N-terminal (GH13) and C-terminal (GH46) GH domains (Figure 11). Gelsolin exists as a cytosolic and a plasma isoform as well. It is expressed in a wide range of cell types and a key regulator of actin filament assembly and disassembly[38,40,41]. Gelsolin is capable of binding, severing and capping F-actin and controlling actin polymerization at barbed ends. The activity of gelsolin is controlled by calcium ions (Ca^{2+}), intracellular pH and phosphoinositides[39]. In the absence of Ca^{2+}, gelsolin exists in a closed/inactive form that does not interact with actin[31,38,42]. Gelsolin activity is stimulated by calcium ions, which induces a conformational rearrangement that exposes the actin-binding regions (GH1, GH2 and GH4). The two halves of gelsolin are separated from each other and this open form will interact with actin (Figure 11)[31]. Gelsolin activation requires micromolar free Ca^{2+} concentration in cells. The C-terminus plays important role in the sensing of Ca^{2+} effects and regulation of actin-binding. The N-terminus can bind to two actin monomers and is directly involved in the severing of F-actin. In contrast to the C-terminal half, the function of the N-terminal half is Ca^{2+}-independent. After severing, gelsolin remains attached to the filament and caps the plus end[2,31,38]. Intracellular pH can also affect the

activities of gelsolin. At lowered pH, the calcium ion requirement for both severing and nucleating activities decreases; low pH can also activate gelsolin in the absence of Ca^{2+} [38].

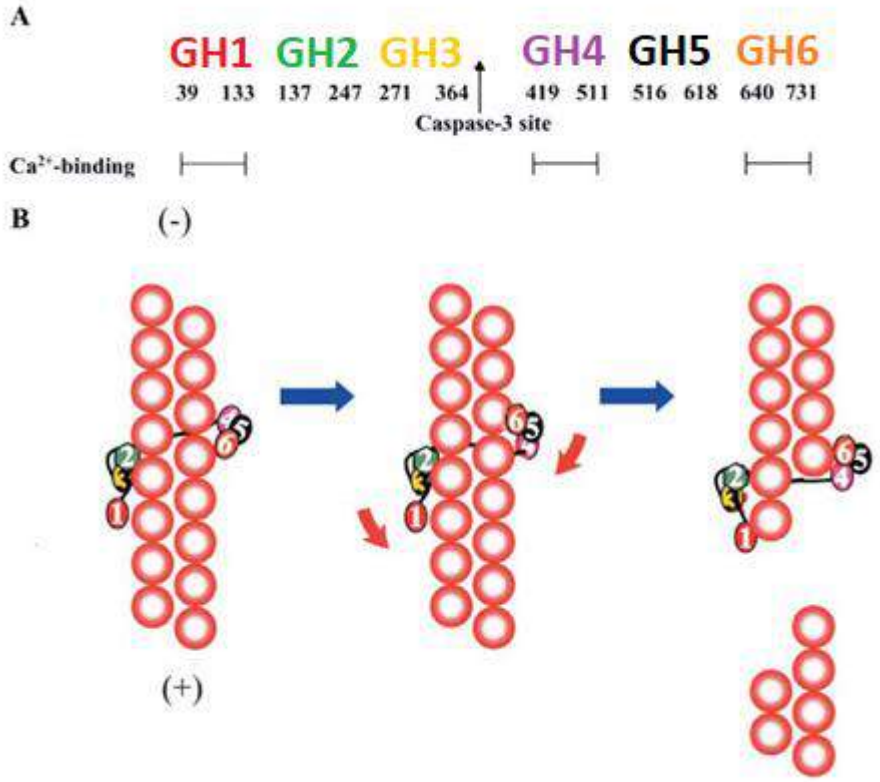

Figure 11. *(A) Domain organization of gelsolin. Figure A is a modified version of the original figure published in reference[38]. (B) Severing of actin filament by gelsolin[38].*

1.1.2.3.1. Flightless-I

Flightless-I (Fli-I) is a relatively newly identified actin-associated protein, which was originally discovered in *Drosophila melanogaster*. The mutations in the *Fli-I* gene lead to abnormal myofibrillar arrangements in the flight muscles causing the loss of flight ability. The severe form of the mutations can cause incomplete cellularization during early embyogenesis[43-45]. Flightless-I is a member of the GH domain family. These actin-binding proteins have multiple functions and play an important role in the remodeling of the actin cytoskeleton. The founding member of this family, the 6 GH domain gelsolin is characterized in the most detail. It is a multifunctional protein

possessing actin filament severing, filament end capping and *de novo* nucleation activities[31].

Like the other members of the gelsolin family, Flightless-I is evolutionary highly conserved implying that it has vital functions. It was proved that Fli-I protein is required for actin distribution during cellularization in *Drosophila* and mouse[46,47]. In support of this, homozygous Fli-I knockout mutation in mice leads to early embryogenic lethality, which indicates the essential role of the protein in embryonic development[48]. It is noteworthy that homozygous null gelsolin[49], CapG[50] or villin[51] mutant mice are viable and fertile. Flightless-I is expressed widely in human tissues; it is abundant in skeletal, myocardial and nerve cells[31,44,45]. In cells, Flightless-I presents in the nucleus where it may act as a hormone-regulated nuclear receptor coactivator (Figure 12)[52]. Fli-I may facilitate the interaction of coactivator complexes containing actin or actin-like proteins[47].

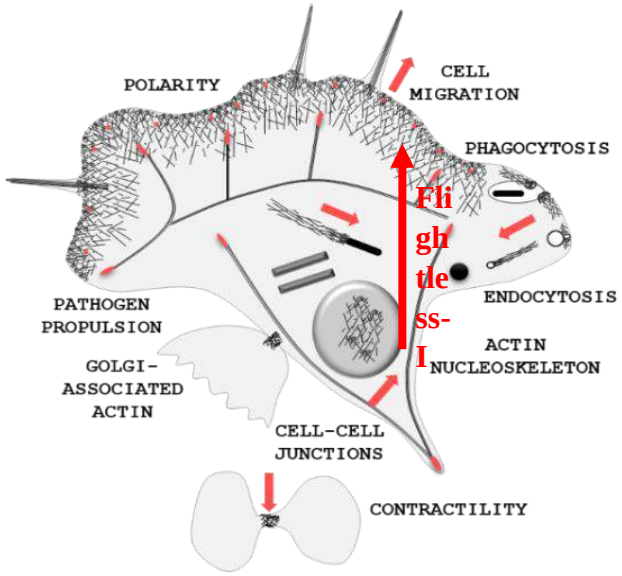

Figure 12. *Fli-I can translocate from the nucleus to the cytoplasm.*

In the presence of serum, Fli-I can translocate from the nucleus to the cytoplasm where it plays a key role in cell migration, which is thought to be linked to its negative influences on wound healing and tissue regeneration[45,53-55]. Previously it has been shown that reducing the level of Flightless-I in wounds either genetically or by using a Fli-I neutralizing antibody decreases the severity of dermal fibrosis and hypertrophic

scarring[56-58]. The human Flightless-I is involved in epidermolysis bullosa and Smith-Magenis syndrome causing developmental and behavioral abnormalities[54,59].

Fli-I can also take part in the regulation of ovulation and embryogenesis. It was explored, that the *Caenorhabditis elegans* Fli-I homolog has a key role in determining the asymmetric cell division and establishing the anterior-posterior polarity of the zygote. The *Fli-I* gene regulates somatic cell cytokinesis and germline development and interacts with the phosphoinositol signaling pathway in the regulation of ovulation[60].

Flightless-I alloys leucine-reach repeats (LRR) and gelsolin homology domains, which confers unique structural characteristics to the protein (Figure 13)[45].

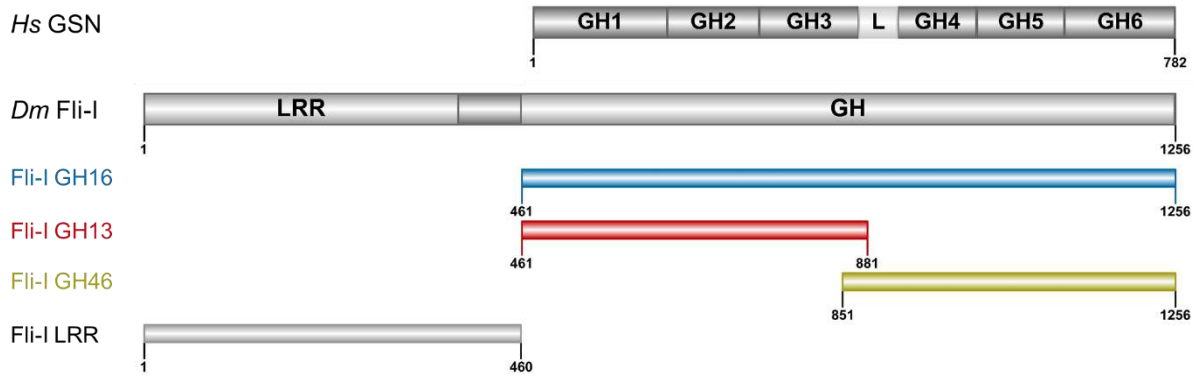

Figure 13. *Domain organization of gelsolin (GSN) and Flightless-I (Fli-I). The protein fragments investigated in our study are also shown. The figure was made by IBS 1.0.2.[61]. Hs: Homo sapiens, Dm: Drosophila melanogaster, GSN: gelsolin, Fli-I: Flightless-I, LRR: leucine-rich repeat, GH: gelsolin homology, L: linker region.*

Flightless-I has been shown to interact functionally with various proteins; it participates in cell signaling, regulates cytoskeleton re-organization or influences actin dynamics and cell migration[5]. The LRR region consists of 16 tandem leucine-rich repeat motifs found in several proteins with diverse cellular localization and functions[62,63]. The LRR is potentially involved in protein-protein interactions. C-terminally to the LRR, Flightless-I contains six gelsolin homology domains which are potential actin-binding regions. Although the actin-binding ability of Flightless-I was proposed, the functional outcome is still elusive[64,65]. Incubation of crude yeast extract containing *Caenorhabditis elegans* Flightless-I with actin agarose suggested that Fli-I associates with G-actin even in the presence of 10 mM EGTA indicating Ca^{2+}-independent interaction[64]. In co-

sedimentation experiments Fli-I appeared in the pellet with actin filaments; also it increased the amount of unpolymerized actin in the supernatant, interpreted as F-actin severing activity[64]. Pyrenyl polymerization experiments suggested that actin assembly is retarded by mouse Fli-I in a concentration-dependent manner, while disassembly is not markedly influenced[65]. This led to the conclusion that Fli-I possesses actin filament capping but not severing activity. The authors also corroborated that the effects of Fli-I were independent of Ca^{2+} in the range of 0 - 1 mM[65]. Arora et al. (2015) have shown that the Fli-I GH16 domain inhibited actin polymerization, while the truncated Fli-I GH2-6 had no effect[66]. These results suggest that the actin-related function of Flightless-I is associated with its GH1 domain. Recent data have suggested that Fli-I may enhance the actin nucleation activity of formin proteins, including Daam1 and mDia1 by binding to Daam1/mDia1 through its GH46 region[67].

Although several studies have been performed regarding the effects of Fli-I on actin dynamics, the underlying molecular mechanism is still controversial and incomplete. To get more insight into the biological functioning of Fli-I we aimed to analyze the actin activities of its different regions, including the gelsolin homology domains, as well as the leucine-rich repeat segment by protein biochemical and biophysical approaches.

2. OBJECTIVE AND AIMS

Although several studies have been performed regarding the effects of Fli-I on actin dynamics, we still face a lack of understanding of the molecular mechanisms underlying its biological functioning. Flightless-I possesses a leucine-reach repeat (LRR) and gelsolin-homology domains (GH), which provide a unique structure for Flightless-I allowing it to act as an actin remodeling protein. Fli-I is a highly conserved member of the gelsolin family; it differs in function and structure from the other members of the family.

We aimed to investigate the activities of Flightless-I underlying its cytoplasmic functions. We studied the interactions of different, recombinantly produced Fli-I constructs with actin by using protein biochemical and biophysical approaches *in vitro*. Gelsolin homology domains are potentially responsible for the actin-binding activities; therefore, we primarily investigated the effects of GH domains of Fli-I on actin dynamics. We examined the interactions of the LRR domain with actin as well. The small actin-binding protein, profilin plays an important role in the building of the cellular actin structures; thus, we also studied whether profilin influences the actin activities of Flightless-I.

My work addressed the following questions:

- What are the activities of Flightless-I LRR and GH domains in actin dynamics?
- How each region (LRR/GH domains) of the protein contributes to these activities?
- What are the similarities and differences between the regulation and actin interaction of gelsolin and Flightless-I?
- Does profilin influence the actin activities of Flightless-I? If it does so, what are the effects of profilin on the actin activities of Flightless-I?

3. MATERIALS AND METHODS

3.1. Protein expression and purification

3.1.1. Flightless-I

For bacterial protein expression, cDNAs of *Drosophila melanogaster* Flightless-I (GenBank accession no. Q24020) were inserted into pGEX-6P1 vector encoding the GH16 domains and into pGEX-2T vector encoding the LRR, GH13 or GH46 domains by our collaborator (József Mihály, Biological Research Centre, Szeged). Constructs were expressed as glutathione S-transferase (GST) fusion proteins in the *Escherichia coli* BL21(DE3)pLysS strain (Novagen). Transformed bacteria were grown at 37°C in Luria Broth (Lennox) EZMix^{TM} powder microbial growth medium (Sigma-Aldrich). Protein expression was induced by the addition of 0.5 mM isopropyl β-D-1-thiogalactopyranoside (IPTG) at $OD_{600\ nm}$ ~ 0.6-0.8. After overnight expression at 20°C the bacterial pellet was collected by centrifugation (Hermle Z326K; 10,000 g, 10 minutes, 4°C) and stored at - 80°C until use.

For protein purification the bacterial pellet was lysed by sonication in Lysis buffer (20 mM Tris-HCl pH8.0, 1 M NaCl, 5 mM $CaCl_2$, 1 mM ATP, 0.5% Triton X-100, 1% sucrose, 2 mM DTT, 5% glycerol supplemented with 0.1 mM PMSF, and Protease Inhibitor Cocktail (Sigma-Aldrich P8465)). The cell lysate was centrifuged (Hitachi CP 80NX; 10,000 g, 25 minutes, 4°C) and the supernatant was poured into a baker and gently stirred with 0.8% (w/v) polyethylenimine (PEI, Sigma-Aldrich) (pH7.9, stock concentration 5%) on ice. After the precipitation of nucleic acids, the solution was centrifuged (Hitachi CP 80NX; 17,300 g, 10 minutes, 4°C) and finely powdered ammonium sulfate (AS, Sigma-Aldrich) was added to the supernatant to 60% saturation by gently stirring for 30–45 minutes to precipitate the protein. The solution was cleared by centrifugation (Hitachi CP 80NX; 21,700 g, 25 minutes, 4°C). The pellet was resuspended in Lysis buffer and precipitated repeatedly by adding 60% saturated AS solution to remove PEI. The solution was centrifuged (Hitachi CP 80NX; 21,700 g, 25 minutes, 4°C) and the pellet was resuspended in Low salt buffer (20 mM Tris-HCl pH7.9, 50 mM NaCl, 1% sucrose, 5% glycerol and 1 mM DTT). The solution was stirred with Glutathione Sepharose 4B (Sigma-Aldrich) at 4°C overnight. The next day it was slowly loaded onto column and washed with Low salt buffer. The column was

incubated at room temperature two times for 10 minutes with Elution buffer ((Low salt buffer supplemented with 50 mM glutathione (Glutathione Reduced, Sigma-Aldrich), pH7.9) to elute GST-tagged proteins. The eluate was concentrated with Amicon-Ultra 50 kDa tube (Merck Millipore) by centrifugation (Sartorius Sigma; 3000 g, 5 minutes, 4°C) and loaded onto PD10 column (GE Healthcare) for buffer exchange to Storing buffer (20 mM Tris-HCl pH7.9, 50 mM NaCl, 1% sucrose, 5% glycerol, 1 mM DTT). The constructs were clarified by ultracentrifugation (Beckman Coulter Optima MAX-XP; 300,000 g, 30 min, 4°C) before flash freeze in liquid nitrogen and stored at – 80°C until use. Control experiments showed that a freeze/thaw cycle does not affect the actin activities/functionality of the Fli-I constructs (*data not shown*).

3.1.2. Preparation and isolation of actin and actin-binding proteins: gelsolin, profilin and Disheveled-associated activator of morphogenesis (DAAM)

Ca^{2+}-ATP-G-actin was isolated from rabbit skeletal acetone powder according to the standard protocol of Spudich and Watt[68]. Actin was gel filtered on *Sephadex G-2000* column (GE Healthcare) to separate actin oligomers, capping protein and other minor contaminants from the actin monomers. G-actin was stored in buffer G (4 mM Tris-HCl pH7.8, 0.1 mM $CaCl_2$, 0.2 mM ATP, 0.005% NaN_3, 0.5 M β-mercaptoethanol) after the isolation. The actin-bound Ca^{2+} was replaced by Mg^{2+} by adding 200 μM EGTA and 50 μM $MgCl_2$. Human gelsolin (GSN) and mouse profilin1 were purified as described previously[69,70]. The DAAM subfragments (cDAAM, DAAM FH1-FH2) were isolated according to Vig et al. (2017)[71].

3.2 Fluorescent labeling of actin

Actin was labeled at Cys^{374} by N-(1-pyrenyl) iodoacetamide (pyrene, Thermo Fisher Scientific) or at Lys^{328} by Alexa Fluor488 carboxylic acid succinimidyl ester and by Alexa Fluor568 carboxylic acid succinimidyl ester (Alexa488NHS and Alexa568NHS, Invitrogen) for fluorescence spectroscopic and microscopic experiments.

N-(1-pyrenyl) iodoacetamide (pyrene) labeling: G-actin (2 mg/ml) was polymerized with 100 mM KCl and 2 mM $MgCl_2$ for 2 hours at room temperature. F-actin was incubated at room temperature for 18 hours with a 1.1 molar excess of N-(1-

pyrenyl) iodoacetamide (Sigma-Aldrich). The protein was at a concentration of 1 mg/ml and pyrene was introduced as a 5 mg/ml solution in dimethyl sulfoxide (DMSO). Pyrene-actin solution was centrifuged to pellet F-actin (Beckman Coulter Optima MAX-XP; 300,000 g, 30 minutes, 20°C). The pellet was resuspended in A buffer, homogenized in a potter, and dialyzed overnight. The solution was cleared by centrifugation (Beckman Coulter Optima MAX-XP; 300,000 g, 30 minutes, 4°C). The labeling efficiency was determined spectrophotometrically and was typically found to be ~ 80% (chapter 3.2.1.).

Tetramethylrhodamine N-succinimidyl ester (NHSR) labeling: G-actin (2 mg/ml) was dialyzed against F buffer (20 mM PIPES, 0.2 mM $CaCl_2$, 0.2 mM ATP and 0.1 M KCl, pH6.9). To the F-actin solution 0.3 mM NHSR (Alexa488NHS and Alexa568NHS) was added from a 100 mM stock solution in DMF, and incubated at room temperature for 1 hour. The reaction was stopped by the addition of 10 mM Tris-HCl, pH7.8. The solution was centrifuged (Beckman Coulter Optima MAX-XP; 40,000 g, 40 minutes, 20°C) to pellet Rh-F-actin. The pellet was resuspended in 2 ml A buffer (5 mM Tris-HCl pH7.8, 1 mM DTT, 0.1 mM $CaCl_2$, 0.2 mM ATP, 0.01% NaN_3) homogenized in a potter. The actin was gel filtered on a PD-10 column to remove unbound rhodamine, then polymerized by the addition of 1 mM $MgCl_2$ and 0.1 M KCl for 30 minutes at room temperature. The solution was centrifuged (Beckman Coulter Optima MAX-XP; 40,000 g, 40 minutes, 20°C), the pellet was resuspended in A buffer and dialyzed overnight. The solution was cleared by centrifugation (Beckman Coulter Optima MAX-XP; 40,000 g, 30 minutes, 4°C). The labeling efficiency was determined spectrophotometrically and was typically found to be ~ 40% (chapter 3.2.1.).

3.2.1. Calculation of protein concentration and protein:dye molar ratio

The degree of labeling was calculated by determining the protein and fluorophore molar concentrations based on UV-VIS absorbance measurements (Jaco V550 UV/VIS Spectrophotometer). Correction factor was used to determine the exact amount of fluorescent dyes (Table 1). Fluorescent dyes also absorb at 280 nm; therefore, the following calculation was used to adjust for the A_{280} contributed by the dye: $A_{280nm,\ correction} = A_{280nm} - (CF_{280nm} \times A_{max})$.

Table 1. Properties of fluorescent dyes used in our study.

Fluorophore	MW (Da)	Wavelength corresponding to maximum absorption (λ_{max}) (nm)	Extinction coefficient (ε) (M^{-1} cm^{-1})	Correction factor (CF_{280nm})
Pyrene	297	344	22000	0.127
Alexa488NHS	643	495	71000	0.11
Alexa568NHS	88.92	577	91300	0.46

The degree of labeling was calculated as the quotient of the molar concentration of protein and the fluorescent dye. The protein concentrations were measured spectrophotometrically using the extinctions coefficient at 280 nm. The extinction coefficients and the molecular weights of the proteins were derived from their amino acid sequence (ExPAsy ProtParam tool http://web.expasy.org/protparam/) (Table 2). The purity of the proteins was checked by absorption photometry by calculating the A_{280}/A_{260} ratio[72].

Table 2. Characteristics of the examined proteins and protein fragments.

Protein	MW (Da)	ε 280nm
Flightless-I GH 16	120128.4	185070 M^{-1} cm^{-1}
Flightless-I GH 13	75441.5	113845 M^{-1} cm^{-1}
Flightless-I GH 46	74456.2	114710 M^{-1} cm^{-1}
Flightless-I LRR	78382.7	56840 M^{-1} cm^{-1}
Actin	42300	0.63 mg x ml^{-1} x cm^{-1}
Gelsolin	85697.52	115280 M^{-1} cm^{-1}
Profilin	14800	1.13 mg x ml^{-1} x cm^{-1}
DAAM FH1-FH2	8139	65780 M^{-1} cm^{-1}
cDAAM (DAAM FH1-FH2-DAD-CT)	9239	65780 M^{-1} cm^{-1}

3.3. Fluorescence spectroscopy

3.3.1. Bulk actin assembly/disassembly measurements

The effects of Flightless-I constructs on actin dynamics were studied with pyrenyl polymerization assays. The fluorescence emission of pyrene is relatively low in the case of G-actin and proportionally increases with the amount of actin filaments formed during polymerization. Actin assembly and disassembly were measured by monitoring the change in pyrenyl fluorescence emission using a Safas Xenius FLX spectrofluorimeter (λ_{ex} = 365 nm, and λ_{em} = 407 nm).

3.3.1.1. Actin assembly

Polymerization of Mg^{2+}-G-actin (2.5 µM, containing 2% or 5% pyrenyl-actin in the presence and absence of profilin, respectively) was initiated by the addition of 1 mM $MgCl_2$ and 50 mM KCl in the absence and presence of different concentrations of Fli-I proteins. The measurements were performed either in the presence of 1 mM EGTA (Ca^{2+}-free environment) or 1 mM $CaCl_2$ to address the Ca^{2+} effects on the actin activities of Fli-I. The profilin:G-actin samples contained 6 µM profilin, considering the dissociation equilibrium constant of profilin:G-actin to be K_D ~ 0.2 µM, ~ 95% of the monomeric actin was bound to profilin under these conditions. To quantitatively analyze the effects of Fli-I on actin dynamics, the polymerization rates were determined from the slope of the linear part of the pyrenyl traces at each condition. The relative polymerization rates were derived as the ratio of the polymerization rate measured in the presence and absence of different amounts of Fli-I proteins. The relative polymerization rate ($v_{relative}$) of profilin:actin as a function of $[Fli - I]$ was fit by the following equation:

$$v_{relative} = 1 - \frac{1-\frac{v_{min}}{v_0}}{1+\frac{IC50}{[Fli-I]}} \qquad (Eq.\ 1)$$

where v_0 and v_{min} are the relative polymerization rates in the absence and the presence of saturating amount [Fli-I], respectively, and IC_{50} is the Fli-I concentration corresponding to 50% inhibition.

The [Fli-I] dependence of the rate of cDAAM catalyzed actin assembly (v) was fit by the following equation:

$$\frac{v-v_{max}}{v_{min}-v_{max}} = \frac{A_0+F_0+K_D-\sqrt{(A_0+F_0+K_D)^2-4A_0F_0}}{2F_0} \quad (Eq.\ 2)$$

where v_{min} and v_{max} are the polymerization rates in the absence and the presence of saturating amount of [Fli-I]; A_0 and F_0 are the total cDAAM and Fli-I concentration, respectively, K_D is the dissociation equilibrium constant of the cDAAM:Fli-I complex.

3.3.1.2. Actin disassembly

Mg^{2+}-ATP-G-actin (50 nM, 50% pyrenyl labeled) was polymerized overnight with the addition of 1 mM $MgCl_2$ and 50 mM KCl. The actin polymer disassembly kinetics were followed by the decrease in pyrenyl fluorescence emission in the absence or presence of Fli-I (105 nM) or GSN (5 nM), in calcium-containing environment ([$CaCl_2$] = 1 mM).

3.3.2. Steady-state anisotropy measurements

Steady-state anisotropy of AlexaFluor488 succinimidyl ester labeled Mg^{2+}-ATP-G-actin (Alexa488NHS-G-actin) was measured to study the Fli-I:G-actin interaction. The anisotropy measurements were performed in a Fluorolog-3 spectrofluorometer (Horiba Jobin Yvon, $\lambda_{excitation}$ = 488 nm, $\lambda_{emission}$ = 516 nm, $slit_{excitation}/slit_{emission}$ = 5/5 nm). Alexa488NHS-G-actin (0.2 µM) was incubated with LatrunculinA (LatA, 4 µM) for 15 minutes at room temperature. The Fli-I constructs were added at different concentrations to the samples and the solutions were further incubated for 1 h at 22ºC either in the presence of 1 mM EGTA (Ca^{2+}-free condition) or 1 mM $CaCl_2$. In profilin-containing samples, profilin (4 µM) was added to actin after the incubation with LatA. The samples were incubated for 1 hour at 22ºC before adding Fli-I constructs to them. LatA binds to actin monomers and prevents them from polymerizing; thus, the increase in the steady-state anisotropy of LatA-bound actin is expected to result from the binding of Fli-I to actin monomers. For quantitative analysis, the Fli-I concentration dependence

of the steady-state anisotropy (r) measured either in the absence or presence of profilin and was calculated as:

$$\frac{r-r_A}{r_{AF}-r_A} = \frac{A_0+F_0+K_D-\sqrt{(A_0+F_0+K_D)^2-4A_0F_0}}{2F_0} \qquad (Eq.\ 3)$$

where A_0 and F_0 are the total G-actin and Fli-I concentration, respectively, r_A is the steady-state anisotropy of Alexa488NHS-G-actin, r_{AF} is the steady-state anisotropy of Alexa488NHS-G-actin at saturating amount of Fli-I, K_D is the dissociation equilibrium constant of the G-actin:Fli-I complex.

3.4 Total internal reflection fluorescence microscopy

3.4.1. Actin assembly/disassembly measurements

The effects of Fli-I and profilin on the assembly/disassembly of actin were studied by total internal reflection fluorescence microscopy (TIRFM), which allowed us to observe the activities of actin-binding proteins at the level of individual filaments.

Glass flow cells were incubated with 1 volume of N-ethymaleimide (NEM) myosin for 1 min, washed extensively with 2 volumes of myosin buffer (F buffer supplemented with 0.5 M KCl; F buffer = G buffer supplemented with 1 mM $MgCl_2$ and 50 mM KCl) and 1 volume of 1% (w/v) bovine serum albumin (BSA, dissolved in F buffer). Finally, flow cells were equilibrated with 2 volumes of TIRF buffer (0.5% (w/v) methylcellulose, 0.5% (w/v) BSA, 10 mM 1,4-diazabicyclo[2,2,2]octane (DABCO), 100 mM DTT dissolved in F buffer). A mixture of G-actin (0.5 µM, 10% Alexa488NHS labeled) and different concentrations of Fli-I constructs were injected into the flow cell to follow the assembly of G-actin in the absence or presence of Fli-I.

Two-color TIRF experiments were performed to follow the filament growth in the absence and presence of Fli-I and profilin. In profilin-containing samples, the profilin concentration was 2 µM. G-actin (0.5 µM, 10% Alexa488NHS labeled) was polymerized in the flow cell by the addition of 1 mM $MgCl_2$ and 50 mM KCl for 10 minutes to form 'green' actin filaments, and then unpolymerized actin was washed out by 1 volume of TIRF buffer. A mixture of G-actin (0.5 µM, 10% Alexa568NHS labeled), profilin (2 µM) and Fli-I in TIRF buffer was transferred into the flow cell.

In assembly assays, filament number was derived 15 – 17 min after the initiation of actin assembly. Time-lapse images were analyzed by either the MultipleKymograph plugin of Fiji or by manually tracking filament growth to obtain the length (µm) and the elongation rate of actin filaments (subunit×s^{-1}). Filament length was converted to subunits using 370 subunits/µm filament[73,74]. The elongation rate (v) was related to the critical concentration of actin assembly (c_c ~ 0.1 µM[18,73]), the association rate constant of actin monomers to filament barbed ends (k_+) and the total actin concentration ($[G_0]$) by the following equation:

$$v = k_+([G_0] - cc) \quad (Eq.\ 4)$$

In disassembly assays, G-actin (0.5 µM, 10% Alexa488NHS labeled) was polymerized for 35 min in the flow cell. The flow cells were equilibrated with TIRF buffer supplemented with different amounts of Fli-I or gelsolin. Images were captured 5 – 7 min after the initiation of actin disassembly.

3.4.2. Measurement of end-to-end annealing of actin filaments

End-to-end annealing assays were performed to examine the protein-protein interactions specifically at the filament ends. G-actin (1 µM, containing either 10% Alexa488NHS or 10% Alexa568NHS labeled actin) was polymerized for 1 h at room temperature, F-actin was stabilized by unlabeled phalloidin (1:1 molar ratio) overnight. Actin filaments labeled with different fluorophores were mixed in the absence or presence of Fli-I and then fragmented by a 26G syringe (10×). Samples were diluted to 2 nM F-actin into TIRF buffer, adsorbed onto poly-L-lysine-functionalized coverslip (Sigma-Aldrich, P4707) and processed for microscopy analysis. Images were captured immediately after fragmentation (t = 0 min) and after 60 min (t = 60 min).

3.4.3. Steady-state measurement of actin filament number

G-actin (2 µM, unlabeled) was polymerized overnight either in the absence or presence of Fli-I GH16 (800 nM). Filaments were stabilized by Alexa Fluor™ 488 phalloidin (1:1 molar ratio, Thermo Fisher Scientific), diluted to 5 nM into TIRF buffer and adsorbed onto poly-L-lysine-functionalized coverslip (Sigma-Aldrich, P4707) for imaging.

3.4.4. Imaging and image analysis

Images were captured with an Olympus IX81 microscope equipped with a laser-based TIRF module (laser lines: 491 nm, 561 nm, APON TIRF 60x NA1.45 oil immersion objective, Hamamatsu Orca-ER high-resolution digital B/W CCD camera). Time-lapse images of actin assembly/disassembly were captured every 10.5 s. The number and length of actin filaments were derived from a 66×66 µm^2 region of the images by using Fiji.

3.5. Statistical analysis

The data represented in the dissertation were derived from at least two independent experiments. Values are displayed as mean ± standard deviation. Statistical analysis (Student's t-test) was performed by Microsoft Excel (ns $p > 0.05$, * $p \leq 0.05$, ** $p \leq 0.01$, *** $p \leq 0.001$, **** $p \leq 0.0001$). The significance levels and the number of independent samples are given in the text or the corresponding figure.

4. RESULTS AND DISCUSSION

4.1. The GH domains of Flightless-I interact with actin and affect actin dynamics in a Ca^{2+}-independent manner

It is well established that the Ca^{2+} binding of gelsolin is a prerequisite for the activation of its actin interactions and activities[44]. Proteolytic cleavage of the protein at the caspase 3 site results in a Ca^{2+}-independent N-terminal (GH13) and a Ca^{2+}-dependent C-terminal (GH46) halves[25,38,75]. Comparative sequence analysis of gelsolin and Fli-I reveals that the tail latch and many of the type-2 Ca^{2+} binding sites are not conserved in Fli-I (Figure 14). This indicates that, as opposed to gelsolin, the actin activities of Fli-I do not rely on Ca^{2+} binding. In support of this, previous work did not find any effect of Ca^{2+} on the actin-binding of Flightless-I proteins from mouse and *Caenorhabditis elegans*[64,65]. To corroborate this, the actin interactions and activities of Fli-I were investigated in the absence and presence of Ca^{2+} ions (Figure 15).

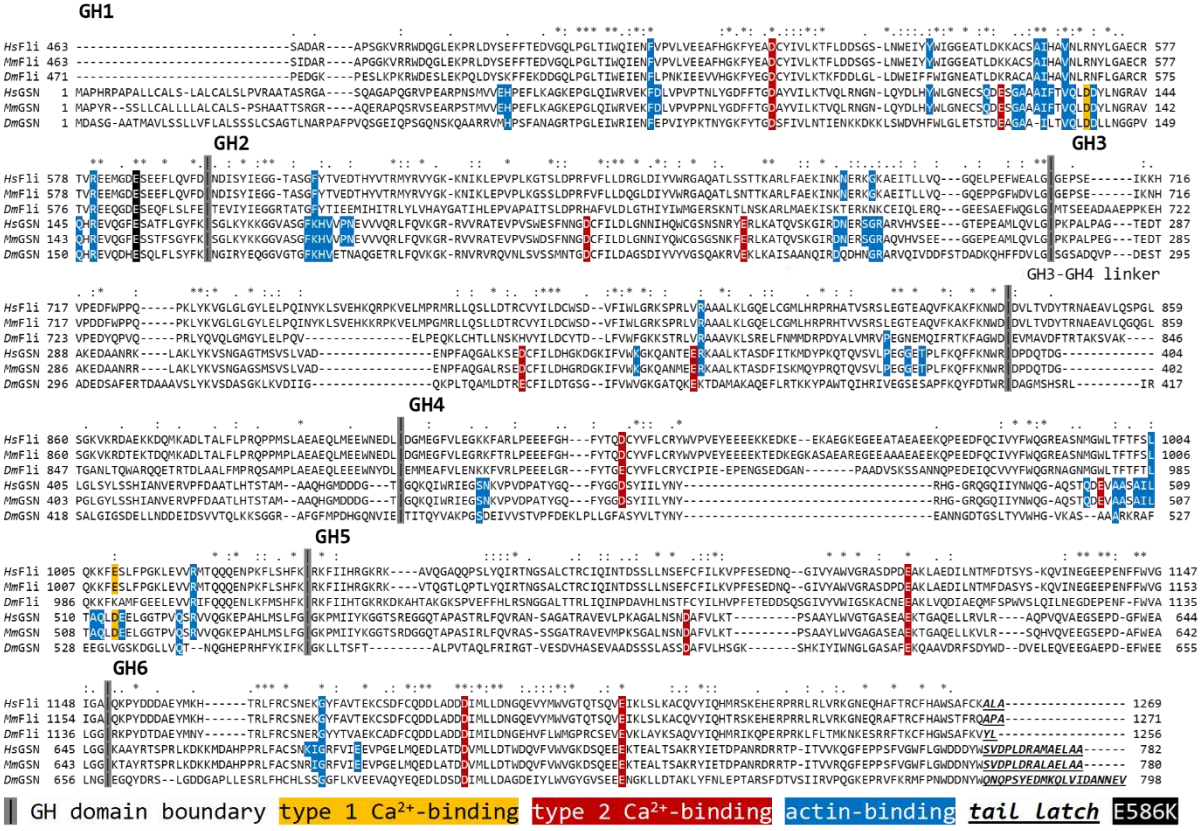

Figure 14. *Domain organization and sequence characteristics of full-length human gelsolin (GSN) and Drosophila melanogaster Flightless-I (Fli-I) and the constructs investigated in this study.*

Comparative bioinformatics analysis of the gelsolin homology domains of Fli-I and gelsolin from different species. Hs: Homo sapiens, Mm: Mus musculus, Dm: Drosophila melanogaster, Fli-I: Flightless-I, GSN: gelsolin, UniProt IDs: Q13045 (Hs Fli-I), Q9JJ28 (Mm Fli-I), Q24020 (Dm Fli-I), P06396 (Hs GSN), P13020 (Mm GSN), Q07171 (Dm GSN). The analysis was performed by ClustalX.

For this purpose, constructs containing all the six gelsolin homology domains (Fli-I GH16), as well as an N-, and a C-terminal fragment of Flightless-I comprising the first and second half of the GH domains, Fli-I GH13 and GH46, respectively were studied (Figure 13 and 15).

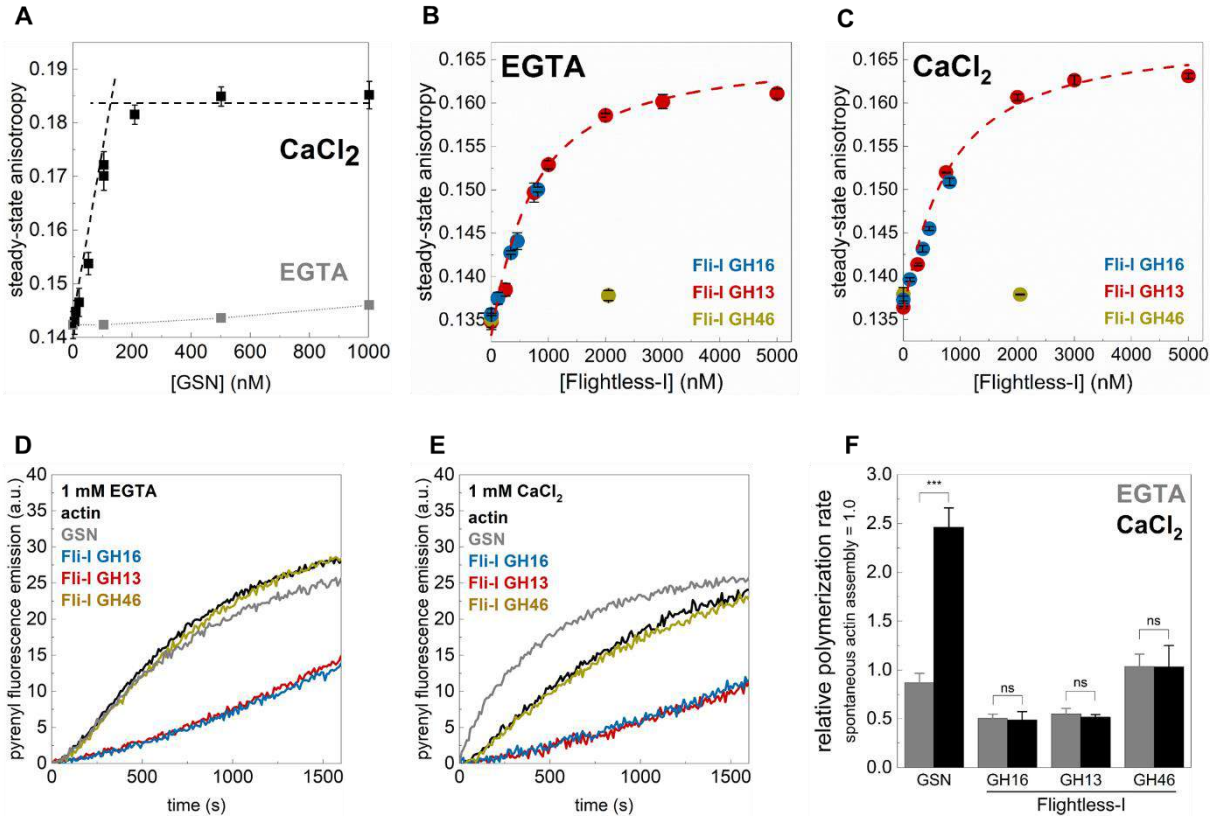

Figure 15. The gelsolin homology domains of Flightless-I interact with actin and affect actin dynamics in a Ca^{2+}-independent manner

(A) *Steady-state anisotropy of Alexa488NHS-G-actin (0.2 µM) as a function of [GSN] in the presence of 1 mM EGTA (Ca^{2+}-free condition) or 1 mM $CaCl_2$, as indicated. Black dashed lines show the linear fits of the data segments measured at low and high [GSN]. The breakpoint was found at [GSN] ~ 150 nM indicating a ~ 1 GSN:2 G-actin stoichiometry. Data are shown as mean ± SD, n = 3.* ***(B, C)*** *Steady-state anisotropy of Alexa488NHS-G-actin (0.2 µM) as a function of [Fli-I] in the presence of 1 mM EGTA (Ca^{2+}-free condition)* ***(B)*** *or 1 mM $CaCl_2$* ***(C)****. Red dashed lines show the fit of the data according to Eq. 3. The fit gave the following dissociation equilibrium constants; 1 mM EGTA: $K_{D(Fli\text{-}I\ GH13)}$ = 576 ± 18.2 nM, 1 mM $CaCl_2$: $K_{D(Fli\text{-}I\ GH13)}$ = 638 ± 151.2 nM. Data are shown as mean ± SD, n = 3.* ***(D, E)*** *Representative pyrenyl emission kinetics recorded in the absence or presence of Fli-I or GSN (5 nM) and the presence of 1 mM EGTA* ***(D)*** *or 1 mM $CaCl_2$* ***(E)****, as indicated. Conditions: [actin] = 2.5 µM (5% pyrenyl labeled).* ***(F)*** *Relative polymerization rates derived from pyrenyl transients shown on panels* ***(D, E)****. Data are shown as mean ± SD, n = 2 – 4.*

The interaction of Fli-I GH16 with G-actin was tested in steady-state anisotropy (*anisotropy*) measurements by monitoring the anisotropy of fluorescently labeled G-actin (0.2 µM Alexa488NHS-G-actin) (Figure 15B, C). Gelsolin is known to bind monomeric actin and forms a GA_2 (1 GSN:2 G-actin) complex in a Ca^{2+}-dependent fashion (reference[38] and Figure 15A). Consistently, in control measurements we found that GSN binds extremely weakly to G-actin in the absence of Ca^{2+} (1 mM EGTA condition), while the addition of $CaCl_2$ (1 mM) profoundly strengthens the interaction (Figure 15A). The breakpoint titration is consistent with the 1 GSN:2 G-actin stoichiometry (breakpoint at [GSN] ~ 150 nM*)*, as well as the high affinity of the complex. The addition of Fli-I GH16 to monomeric actin, even in the absence of $CaCl_2$ (1 mM EGTA condition) resulted in an increase in anisotropy from ~ 0.136 ± 0.000 to ~ 0.150 ± 0.000 at the maximum amount of protein that we could test in these experiments (Figure 15B). This suggests direct binding of the GH domains of Fli-I and G-actin. A similar response in a broader concentration range could be detected in the case of Fli-I GH13 (Figure 15B). The analysis of the anisotropy data gave a dissociation equilibrium constant of K_D(Fli-I GH13) = 576 ± 182 nM of the Fli-I GH13:G-actin complex (Figure 15B, *Eq. 3*). The analysis of the [Fli-I] dependence of the anisotropy measured in the presence of $CaCl_2$ (1 mM) revealed similar binding trend and affinity as detected in the absence of the divalent cation (K_D(Fli-I GH13) = 638 ± 152 nM, Figure

15C), indicating that the interaction of Fli-I with G-actin is not affected by the presence of Ca^{2+}. Importantly, no significant change in anisotropy was found when Fli-I GH46 (2050 nM) was added to G-actin suggesting that this region does not interact significantly with actin (Figure 15B, C).

Subsequently, the calcium response of the effects of Fli-I on actin assembly was monitored in pyrenyl polymerization experiments (Figure 15D-F). In control measurements, we found that gelsolin does not significantly affect actin polymerization in Ca^{2+}-free environment (1 mM EGTA condition), while it accelerates actin assembly kinetics in the presence of $CaCl_2$ (1 mM) (~ 2.46 ± 0.19fold increase, $n = 3$, $p \leq 0.001$) (Figure 15D, E). This observation agrees well with previous data[72, 76-78]. Fli-I GH16 (5 nM) inhibited actin assembly both in the absence and presence of Ca^{2+} ($n = 2 – 3$, $p > 0.05$) (Figure 15D, E). The inhibitory effect of Fli-I on the rate of actin polymer formation is in agreement with previous reports[65]. Qualitatively and quantitatively the same response was detected for Fli-I GH13 (5 nM) (Figure 15D, E). In contrast, when Fli-I GH46 was added at the same concentration as the two other constructs (5 nM) it did not have any effect on actin assembly, independently from the presence of calcium (Figure 15D, E).

Altogether, these observations suggest that in contrast to gelsolin, the actin interactions and activities of Flightless-I are Ca^{2+}-independent. On the other hand, it is interesting to note that both G-actin interaction and actin assembly inhibition of the Fli-I GH16 domains are reconstituted by GH13, suggesting the lack of direct interaction between Fli-I GH46 and actin.

4.2. The GH domains of Flightless-I affect actin assembly from free G-actin in a biphasic manner which relies on the GH13 regions

To address the biochemical activities of Flightless-I (Fli-I) in actin dynamics, the effects of Fli-I on actin assembly kinetics from free G-actin were investigated in bulk pyrenyl polymerization experiments (Figure 16). The data revealed that the effects of Fli-I GH16 on polymer formation follow a biphasic concentration-response. At lower concentrations (< ~ 10 nM) it inhibits the overall rate of actin polymerization; in contrast, higher concentrations of Fli-I GH16 (> ~ 25 nM) accelerate the assembly kinetics of free G-actin above the rate of spontaneous assembly (Figure 16A, E). The

biphasic concentration dependence of the influence of the Fli-I GH domains on polymerization kinetics suggests multiple activities in actin dynamics. We found that Fli-I GH13 can influence actin dynamics in a qualitatively and quantitatively similar manner as Fli-I GH16 in the entire concentration range tested in the experiments (Figure 16B, E). In contrast, the GH46 region does not have any effect on actin polymerization in the concentration range in which the two other fragments of Fli-I were tested (Figure 16C, E). These results are consistent with our previous data and further support that the GH13 region of Fli-I is responsible for the actin activities of the GH domains of the protein.

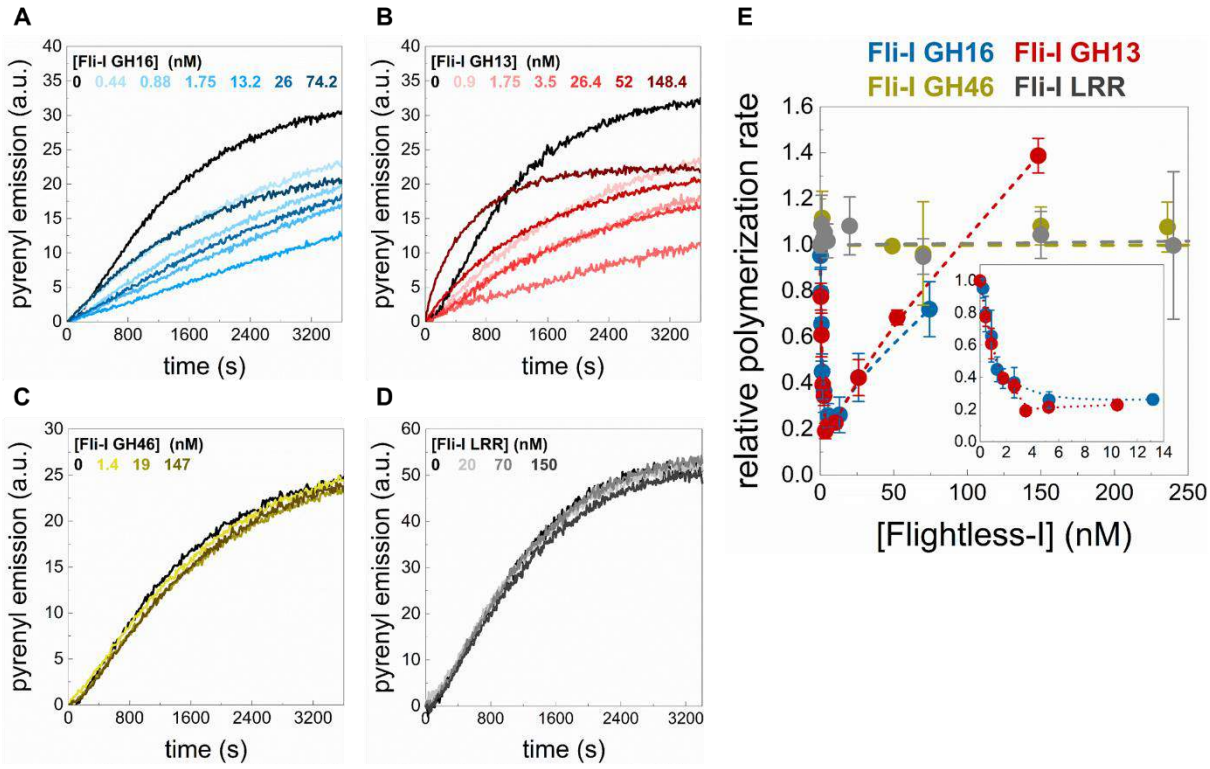

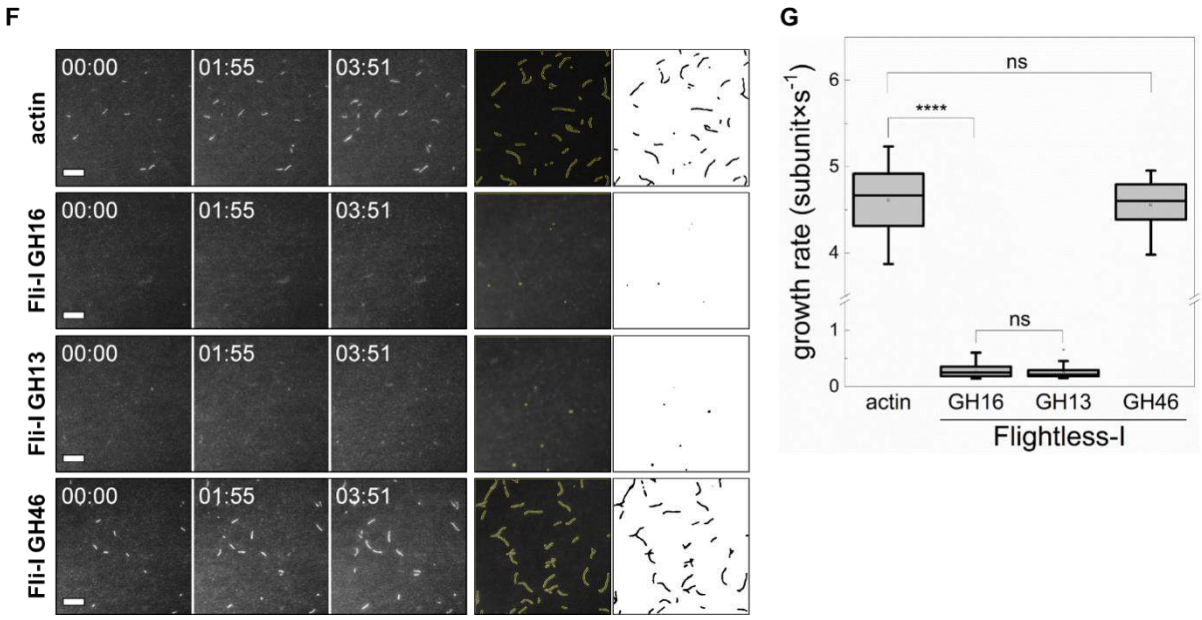

Figure 16. The gelsolin homology domains of Flightless-I affect actin assembly that relies on the GH13 domains

(A-D) *Representative pyrenyl fluorescence emission kinetics recorded in the absence or presence of different concentrations of Fli-I, as indicated. Conditions: [actin] = 2.5 µM (5% pyrenyl labeled).* ***(E)*** *Relative polymerization rate as a function of [Fli-I], as indicated. Data are shown as mean ± SD, n = 2 – 7. Inset: enlarged view of the data corresponding to low (< 14 nM) Fli-I concentrations.* ***(F)*** *Left panels: Representative montages of actin assembly followed by TIRFM in the absence or presence of Fli-I, as indicated. Right panels: Representative skeletonized TIRFM images used for filament number analysis showing the field of view of a 66×66 µm^2 region in the absence or presence of Fli-I, as indicated. Conditions: [actin] = 0.5 µM (10% Alexa488NHS labeled), [Fli-I GH16] = 10 nM, [Fli-I GH13] = 10 nM, [Fli-I GH46] = 100 nM.* ***(G)*** *Filament growth rate from G-actin in the absence or presence of different Fli-I constructs, as indicated derived from time-lapse TIRFM images shown on* ***(F)****, n = 20 – 60.*

We also investigated the effects of the LRR region of Flightless-I on actin dynamics. In steady-state anisotropy experiments, no significant change was detected upon titration of actin monomers (0.2 µM Alexa488NHS-G-actin) with Fli-I LRR (r = 0.130 ± 0.001 in the presence of 800 nM LRR). Fli-I LRR does not affect actin

assembly in pyrenyl polymerization measurements (Figure 16D, E). These findings indicate that the isolated LRR does not interact with actin[62].

Upon interaction with fluorescently labeled actin (e.g., by pyrene, IAEDANS) some proteins can modify the structural properties of actin resulting in a change in the spectral properties of the actin-bound fluorophore (e.g., Leiomodin (Lmod), Wiskott-Aldrich Syndrome Homology 2 domains of Sarcomere Length Short (SALS-WH2)[79,80]). This effect could result in an apparent change in pyrenyl kinetics, even in the absence of any functional effects on actin polymerization. To address this issue, actin assembly at the level of individual polymers was visualized by using total internal reflection fluorescence microscopy (TIRFM) in the absence and presence of different regions of Flightless-I (Figure 16F, G). In control samples, polymers spontaneously nucleated (N = 34.64 ± 8.07 polymer, n = 58) and elongated at a rate of v = 4.61 ± 0.36 subunit×s^{-1} (n = 23), which corresponds to the well-established barbed end association rate constant of free G-actin (k_+ = 11.53 ± 0.90 $\mu M^{-1}s^{-1}$ [6,81], *Eq. 4.*). Addition of Fli-I GH16 (10 nM) to actin resulted in almost complete inhibition of polymer growth (0.24 ± 0.10 subunit×s^{-1}, n = 39, $p \leq 0.0001$), as well as a marked reduction in the observable polymer number (N = 6.58 ± 4.26 polymer, n = 36, $p \leq 0.0001$). In agreement with the results of pyrenyl polymerization experiments, the effects of Fli-I GH16 on polymer assembly can be recapitulated by Fli-I GH13; as 10 nM Fli-I GH13 resulted in similar assembly inhibition as observed for 10 nM Fli-I GH16 (N = 6.43 ± 4.97 polymer, n = 32, p = 0.897; v = 0.28 ± 0.12 subunit×s^{-1}, n = 33, p = 0.158). Consistently with the observations made in the fluorescence spectroscopy experiments, we found that Fli-I GH46 does not have a significant effect on either polymer number or growth rate in TIRFM assays (N = 35.77 ± 6.70 polymer, n = 22, p = 0.565; v = 4.56 ± 0.30 subunit×s^{-1}, n = 20, p = 0.589).

Altogether, TIRFM data support the results obtained from pyrenyl fluorescence experiments; when present at low amounts Fli-I inhibits actin assembly and this activity relies on the GH13 segment of the protein.

4.3. The GH domains of Flightless-I inhibit actin filament growth by barbed end capping

Fluorescence spectroscopy data indicate that the gelsolin homology domains of Fli-I affect the assembly of free G-actin by having multiple activities in actin dynamics. The polymerization inhibition that we observe at low nM concentrations reflects high-affinity interactions and can result from the prevention of subunit addition to filament ends. This can be manifested by sequestration upon binding to monomeric actin and/or by capping upon filament end interactions. While accelerated assembly detected in the presence of higher amounts of Fli-I is attributed to lower-affinity interactions and can originate from facilitated nucleation of monomers and/or severing actin polymers, thereby creating filament ends capable of elongation.

Based on the experimental conditions in our TIRFM assays (0.5 μM free G-actin), actin polymer growth is dominated by barbed end assembly. Considering the dissociation equilibrium constant of the Fli-I:G-actin interaction derived from anisotropy measurements (Figure 15B, C), 10 nM Flightless-I – which causes polymer growth inhibition in TIRFM experiments – is expected to bind to ~ 1% of monomeric actin; i.e., ~ 5 nM. This would result in a negligible reduction (~ 1.4%) in polymer growth rate as predicted by *Eq. 4*. Thus, G-actin sequestration that relies on monomer binding by Flightless-I does not explain the marked polymerization inhibition that we observe at nanomolar protein concentrations. Consequently, our data point towards filament end-related activities.

To experimentally address barbed end capping activity, the end-to-end annealing kinetics of pre-formed, mechanically fragmented filaments were monitored both in the absence and presence of Fli-I by dual-color TIRFM (Figure 17). In the absence of Fli-I, the spontaneous lengthwise association, i.e., the annealing of actin filament fragments was supported by the increase in the filament length with time, as well as by the appearance of spectrally inhomogeneous filament segments. In the presence of either Fli-I GH16 or GH13 the filaments remained short and were characterized by homogeneous fluorescence emission indicating that annealing is inhibited. No such inhibitory effect was detected when Fli-I GH46 was added to actin, in agreement with our previous observations.

Altogether, the above data indicate that Fli-I inhibits end-to-end annealing by binding to filament barbed end. Therefore, we propose that inhibition of actin assembly by Fli-I results from the prevention of actin incorporation at barbed ends upon direct capping of filament ends.

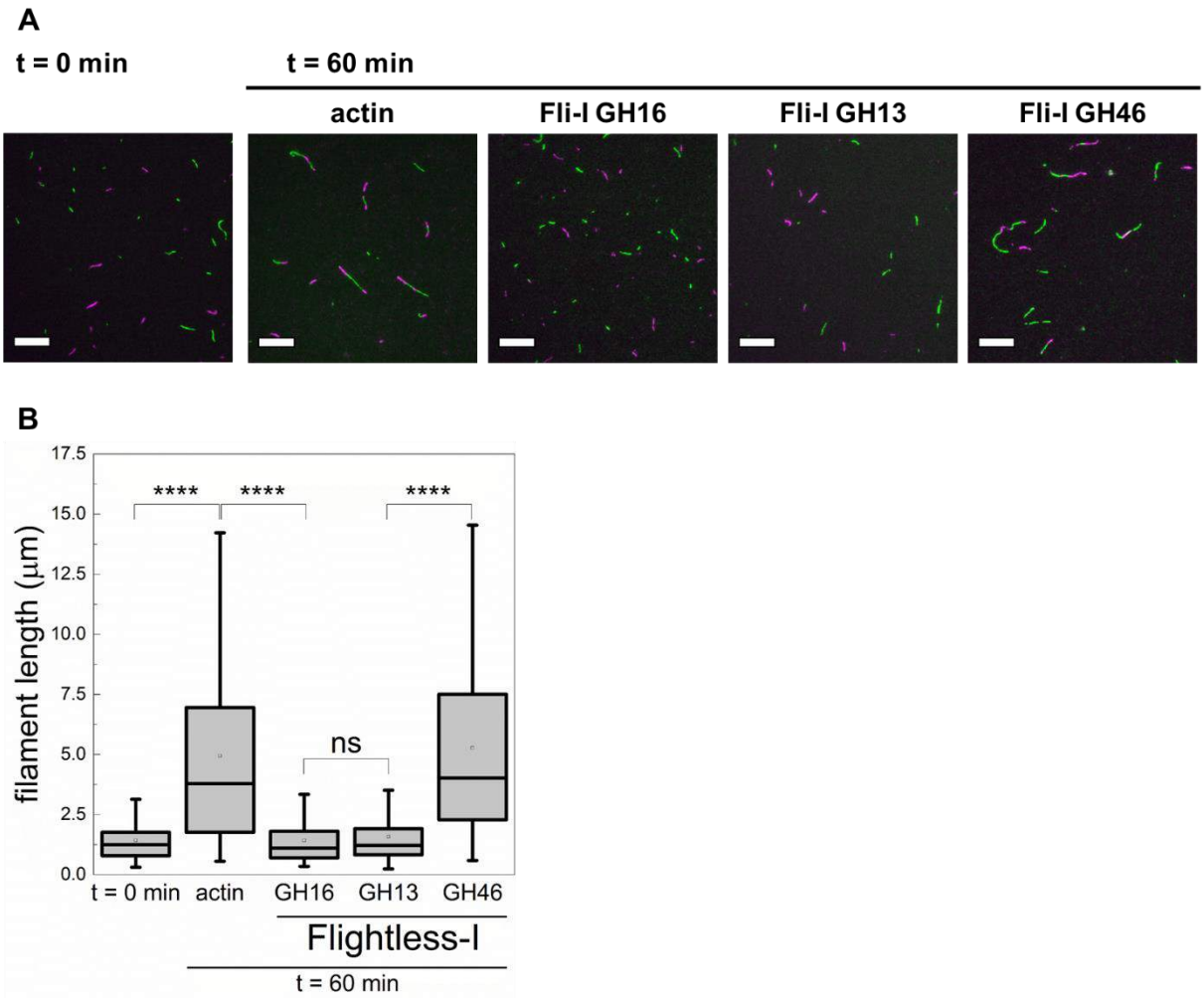

Figure 17. The GH domains of Flightless-I inhibit actin filament end-to-end annealing

(A) *Representative montages of actin filament end-to-end annealing followed by TIRFM in the absence or presence of different Fli-I constructs, as indicated. The t = 0 min corresponds to the initial fragmentation of filaments, while t = 60 min indicates the time interval after fragmentation. Conditions: [actin] = 500 nM (10% Alexa488NHS and 10% Alexa568NHS labeled), [Fli-I] = 120 nM. Scale bar = 10 µm.* ***(B)*** *Filament length at t = 0 and 60 min in the absence or presence of Fli-I, derived from TIRFM images shown on* ***(A)****,* $n_{samples}$ *= 3 – 9,* $n_{filaments}$ *= 136 – 174.*

4.4. The GH domains of Flightless-I do not depolymerize/disassemble filaments but facilitate the formation of nucleation intermediates

In pyrenyl polymerization experiments, we noted that the addition of a relatively large amount of Fli-I resulted in facilitated polymerization, which can be manifested through enhanced nucleation and/or cutting of actin filaments and generating more ends for elongation. To test the fragmentation ability of Fli-I, dilution-induced bulk disassembly/depolymerization kinetics measurements were performed (Figure 18A, B). In control experiments, we found that the spontaneous disassembly/depolymerization of actin filaments is relatively slow; in contrast, gelsolin (5 nM, in the presence of 1 mM $CaCl_2$) accelerated disassembly kinetics (Figure 18A, B), consistently with previous findings[79]. In the presence of Fli-I at a concentration that can enhance actin polymerization in pyrenyl fluorescence experiments (105 nM, Figure 16E), no significant increase in the rate of filament disassembly was observed as compared to spontaneous depolymerization, neither in the absence (*data not shown*) nor in the presence of 1 mM $CaCl_2$ (Figure 18A, B).

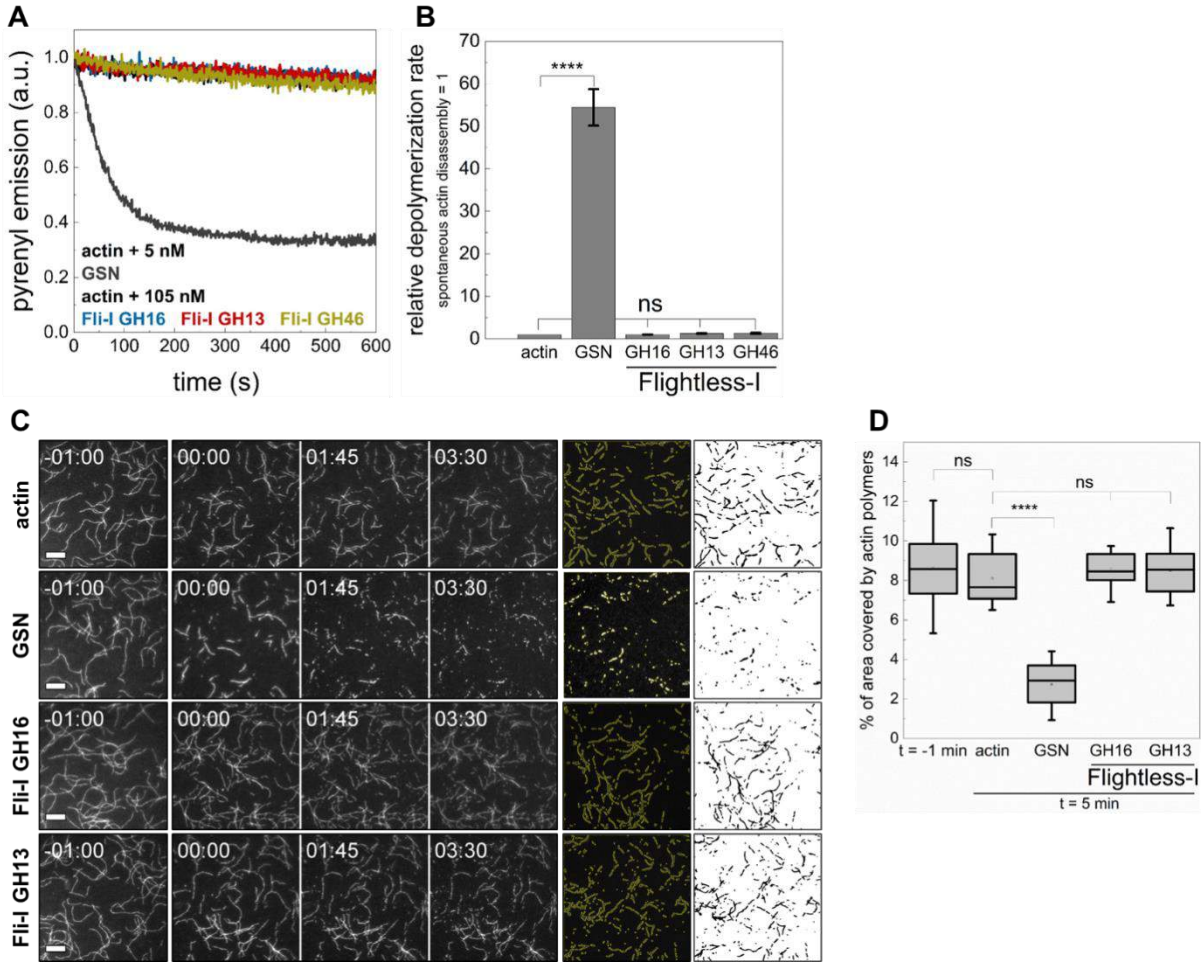

Figure 18. The GH domains of Flightless-I do not sever filaments but facilitate the formation of nucleation intermediates

(A) *Kinetics of actin polymer disassembly as followed by the decrease in pyrenyl fluorescence emission in the absence or presence of Fli-I or GSN, as indicated. Conditions: [actin] = 50 nM (50% pyrenyl labeled), [GSN] = 5 nM, [Fli-I] = 105 nM, [$CaCl_2$] = 1 mM.* ***(B)*** *Relative depolymerization rate derived from pyrene transients shown on panel* ***(A)****, n = 2 – 3.* ***(C)*** *Left panels: Representative montages of actin disassembly followed by TIRFM in the absence or presence of Fli-I or GSN, as indicated. The frame labeled by -01:00 and 00:00 shows the field of view just before and right after the addition of GH homology proteins, respectively. Right panels: Representative skeletonized TIRFM images used for filament number analysis showing the field of view of a 66×66 μm^2 region in the absence or presence of Fli-I or GSN, as indicated. Conditions: [actin] = 0.5 µM (10% Alexa488NHS labeled), [GSN] = 0.5 nM, [Fli-I] = 105 nM. Scale bar = 10 µm, time = min:s.* ***(D)*** *Percent of area covered by actin filaments 5 – 7 min after the addition of GH homology proteins derived from TIRFM images shown on* ***(C)****, n = 12 – 51.*

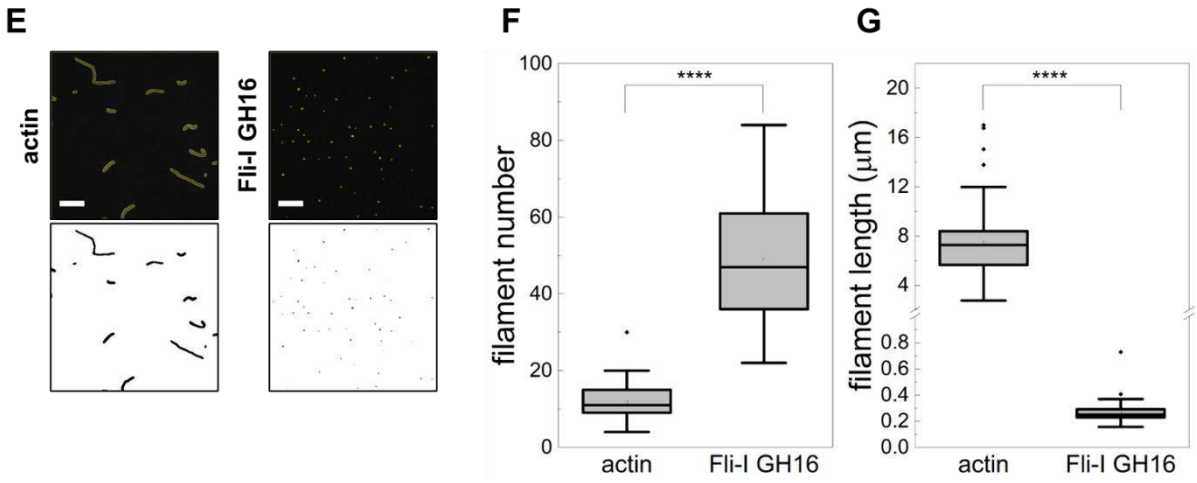

(E) *Representative skeletonized TIRFM images used for filament number and length analysis showing the field of view of a 66×66 μm^2 region in the absence or presence of Fli-I GH16, as indicated. Conditions: [actin] = 2 µM (10% Alexa488NHS labeled), [Fli-I GH16] = 800 nM. Scale bar = 10 µm.* ***(F)*** *Number of filaments assembled from G-actin either spontaneously or in the presence of Fli-I GH16, as indicated derived from TIRFM images shown on* ***(E)****, n = 69 – 73.* ***(G)*** *Length of filaments assembled from*

*G-actin either spontaneously or in the presence of Fli-I GH16, as indicated derived from TIRFM images shown on **(E)**, n = 69 – 73. Filament length assembled from G-actin either spontaneously or in the presence of Fli-I GH16 derived from TIRFM images shown on **(E)**, n = 69 – 73.****p<0.0001.*

Alternatively, the disassembly/depolymerization efficiency of gelsolin and Fli-I was visualized in TIRFM experiments by adding GH domain proteins to preassembled filaments (Figure 18C, D). The disassembly/depolymerization activity was quantified by measuring the area covered by filamentous actin after 5 - 7 min following GSN or Fli-I addition. The presence of gelsolin (0.5 nM, in the presence of 1 mM $CaCl_2$) resulted in a marked decrease in the actin filament area as compared to the control (A(actin) = 337.47 ± 84.92 μm^2, n = 10, A(GSN) = 165.95 ± 49.05 μm^2, n = 12, $p \leq 0.0001$). In contrast, the addition of either the GH16 or GH13 fragments of Fli-I (105 nM) to actin filaments did not influence significantly this parameter (A(Fli-I GH16) = 373.44 ± 38.458 μm^2, n = 14, p = 0.224, A(Fli-I GH13) = 370.31 ± 54.58 μm^2, n = 12, p = 0.373). Based on these results, we conclude that, in contrast to gelsolin, the GH domains of Fli-I possess filament disassembly/depolymerization activity.

Considering the monomer binding ability of Fli-I revealed by anisotropy measurements we hypothesize that the assembly-promoting activity of Fli-I results from its ability to *de novo* nucleate actin filaments, similarly to gelsolin[9]. To test the nucleation ability of Fli-I the number of actin filaments formed in the absence and presence of Fli-I GH16 was measured at steady-state by TIRFM (Figure 18E-G). For this purpose, actin filaments were formed spontaneously or in the presence of a high concentration of Fli-I GH16 (800 nM) overnight, followed by phalloidin stabilization and dilution. In the absence of Fli-I GH16 the number of actin filaments was found to be N = 11.78 ± 5.12, while Fli-I GH16 increased this parameter significantly by ~ 4.2fold (N = 49.06 ± 15.20, $p \leq 0.0001$) (Figure 18F). On the other hand, the steady-state length of filaments was markedly reduced in the presence of Fli-I GH16 as compared to the control samples, further supporting barbed end capping by Fli-I (Figure 18G). It is worth noting that due to the inhibited lengthening of the filaments by Fli-I, the size of some filaments may be under the resolution limit of the microscope; therefore, the filament number is expected to be underestimated in our experiments. Nonetheless, the above observation indicates that Fli-I can promote actin assembly by facilitating the *de novo* formation of nucleation intermediates.

4.5 Profilin directs the activities of Flightless-I towards barbed end capping

Cellular actin structures are built from profilin:G-actin (PA); therefore, we aimed to investigate whether the presence of profilin influences the actin assembly activities of Fli-I. In pyrenyl polymerization experiments we found that both Fli-I GH16 and GH13 inhibit the assembly of profilin:G-actin at subnanomolar concentrations (Figure 19A-D). However, in contrast to their effects on the assembly of free G-actin, they failed to increase the bulk polymerization rate of profilin:G-actin at higher concentrations. The analysis of the Fli-I concentration dependence of the bulk polymerization rate gave IC_{50} values of IC_{50}(Fli-I GH16) = 0.93 ± 0.12 nM and IC_{50}(Fli-I GH13) = 0.13 ± 0.01 nM (Figure 19D, *Eq. 1*). This indicates that Fli-I prevents the assembly of profilin:G-actin with high-affinity barbed end capping. Similarly to the lack of the effect of Fli-I GH46 on actin assembly from free G-actin, this construct failed to influence the bulk polymerization of profilin:G-actin (Figure 19C, D).

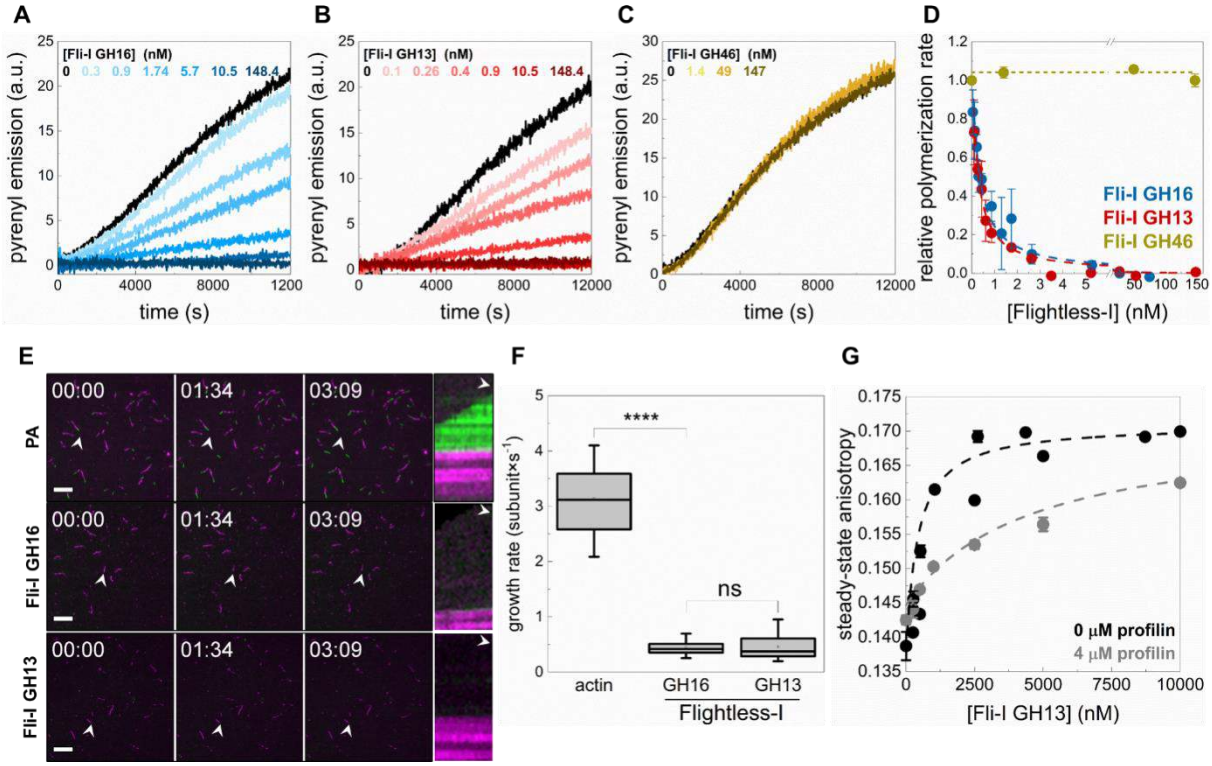

Figure 19. Profilin directs the activities of Flightless-I towards barbed end capping

(A-C) *Polymerization kinetics of profilin:G-actin (PA) followed by the change in pyrenyl emission in the absence and presence of different concentrations of Fli-I, as indicated. Conditions: [actin] = 2.5 µM (2% pyrenly labeled), [profilin] = 6 µM.* ***(D)*** *Relative polymerization rate as a function of [Fli-I], as indicated. Data are shown as mean ± SD, n = 2 – 7. Inset: enlarged view of the data corresponding to low (< 10 nM) Fli-I concentrations. Dashed lines in the corresponding colors show the fit to the data (Eq. 1). The fit gave IC_{50}(Fli-I GH16) = 0.93 ± 0.12 nM and IC_{50}(Fli-I GH13) = 0.13 ± 0.01 nM.* ***(E)*** *Representative montages of actin assembly (green) from preformed F-actin seeds (magenta) followed by TIRFM in the absence or presence of Fli-I, as indicated. Arrowheads highlight the filament which were tracked for kymographs. Conditions: [actin] = 0.5 µM (10% Alexa488NHS or Alexa568 NHS labeled), [profilin] = 2 µM, [Fli-I] = 10 nM. Scale bar = 10 µm, time = min:s.*

(F) *Filament growth rate from profilin:G-actin in the absence or presence of Fli-I, as indicated derived from time-lapse TIRFM images shown on* ***(E)****, n = 37 – 62.* ***(G)*** *Steady-state anisotropy of Alexa488NHS-G-actin (0.2 µM) in complex with profilin (4 µM) as a function of [Fli-I]. Data are shown as mean ± SD, n = 2 – 3. Dashed lines in the corresponding color show the fit of the data according to Eq. 3. The fit gave the following dissociation equilibrium constants: K_D(Fli-I GH13) = 411.43 ± 22.69 nM (in the absence of profilin), K_D(Fli-I GH13) = 4511.6 ± 631.92 nM (in the presence of profilin).*

The results of dual-color TIRFM experiments performed to study profilin:G-actin assembly corroborated our observations made in pyrenyl spectroscopic assays (Figure 19E, F). Polymer growth (green portion) was observed from preformed F-actin seeds (magenta portion) both in the absence and presence of Fli-I (Figure 19E). In control samples, in the absence of Fli-I, profilin:G-actin assembled at the barbed ends of preformed F-actin seeds with a rate of v(PA) = 3.14 ± 0.58 subunit×s^{-1} (n = 37), which is consistent with the slightly reduced association rate constant of profilin:G-actin to the barbed ends as compared to free G-actin (k_+ = 7.86 ± 1.45 subunit×s^{-1} [3,71]) (Figure 19F). In the presence of Fli-I GH16 (10 nM) or GH13 (10 nM) the number of elongating barbed ends, as well as the rate of profilin:G-actin association to preassembled F-actin seeds markedly decreased (v(Fli-I GH16) = 0.45 ± 0.14 subunit×s^{-1} (n = 62), v(Fli-I GH13) = 0.46 ± 0.23 subunit×s^{-1} (n = 57, $p \leq 0.0001$) (Figure 19E, F).

The lack of the polymerization-promoting effects that we detected in the presence of profilin indicates that the interaction of Fli-I with monomeric actin is compromised by profilin. To test this, the steady-state anisotropy of fluorescently labeled actin (0.2 μM Alexa488NHS-G-actin) in complex with profilin (4 μM) was measured upon titration with Fli-I GH13 (Figure 19G). The analysis revealed that the binding strength of Fli-I GH13 to profilin:G-actin is reduced (K_D(Fli-I GH13) > 4000 nM) as compared to free G-actin (K_D(Fli-I GH13) ~ 500 – 600 nM, Figure 15B, C). This result suggests that Fli-I and profilin competitively bind to monomeric actin.

4.6 The GH46 domains of Flightless-I interacts with the C-terminus of DAAM and inhibit its actin assembly activities

In the above experiments, we did not detect any direct actin interaction or activity of the GH46 domains of Fli-I. In previous studies, this region of the human Flightless-I protein was identified to interact with the C-terminal region of formins, including human mDia1 and Disheveled-associated activator of morphogenesis (Daam) 1[67]. The interaction seems to be specific to Fli-I since the binding was not detected for the GH46 domains of gelsolin. Based on this, we sought to investigate the effects of Fli-I GH46 on *Drosophila melanogaster* DAAM-catalyzed actin assembly. An N-terminally truncated DAAM construct comprising the formin homology (FH) domains FH1FH2 and the C-terminal Diaphanous autoinhibitory domain (DAD)-CT regions (cDAAM; DAAM FH1FH2-DAD-CT), as well as the isolated DAAM FH1FH2 domains were studied in pyrenyl polymerization experiments (Figure 20). Both DAAM FH1FH2 and FH1FH2-DAD-CT promoted actin assembly, albeit with different efficiencies, in agreement with our previous findings[82]. We found that while Fli-I GH46 did not influence FH1FH2-mediated actin polymerization, it inhibited the cDAAM-catalyzed actin assembly in a concentration-dependent fashion. At saturating amount of Fli-I GH46, the assembly rate corresponded to that of characteristic to the FH1FH2. The analysis gave dissociation equilibrium constant of the Fli-I GH46:cDAAM interaction of K_D = 254.7 ± 189.4 (*Eq. 2*). This indicates that Fli-I GH46 interacts with DAAM and its main binding site is the DAD-CT region corroborating previous findings[67]. Altogether, besides its activities directly targeting actin, this interaction can provide an indirect way for Fli-I to regulate actin dynamics through the DAAM-mediated pathway.

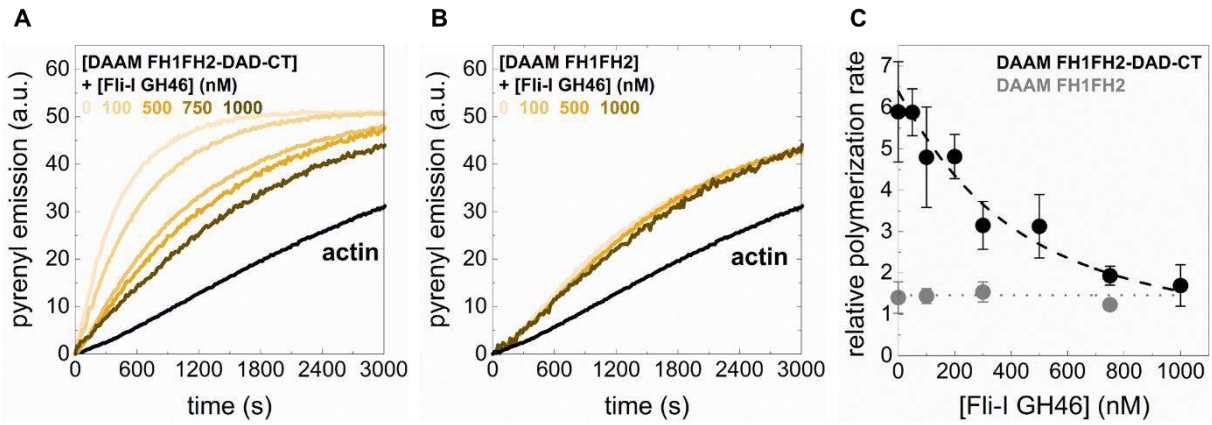

Figure 20. The GH46 domains of Flightless-I interact with the C-terminus of DAAM and inhibit its actin assembly activities

(A, B) *Representative pyrenyl emission kinetics recorded in the absence and presence of cDAAM (FH1FH2-DAD-CT) or DAAM FH1FH2 at different concentrations of Fli-I GH46, as indicated. Conditions: 2.5 µM actin (5% pyrenyl labeled) [DAAM] = 250 nM.* ***(C)*** *Relative polymerization rates as a function of [Fli-I GH46]. The dashed line in the corresponding color shows the fit of the data according to Eq. 2. The fit gave the dissociation equilibrium constant of the Fli-I GH46:cDAAM interaction of* K_D *= 254.7 ± 189.4 nM.*

4.7. Flightless-I disrupts the actin cytoskeleton *in vivo*

Our collaborator (József Mihály, Biological Research Centre, Szeged) tested the effect of Fli-I overexpression in developing *Drosophila* egg chambers, to estimate the *in vivo* significance of our *in vitro* findings. The experiments and data shown in Figure 21 were performed by József Mihály's research group. They created transgenic lines for Fli-I GH16, GH13 and GH46 under UAS control and expressed the proteins with *mat-tub4-Gal4* in the germline cells of the ovary. The results of the overexpression studies suggest that Fli-I GH16 and GH13 can influence actin organization of the nurse cells and disturb the formation of various types of actin structures, while GH46 has no such effect. The impact of GH13 is completely consistent with the *in vitro* barbed end capping activity of GH13 which provides a potential molecular mechanism for the *in vivo* effect. We conclude that our *in vitro* and *in vivo* data both support that the Fli-I GH13 domain inhibits actin polymerization, whereas GH46 has no significant effect on actin dynamics.

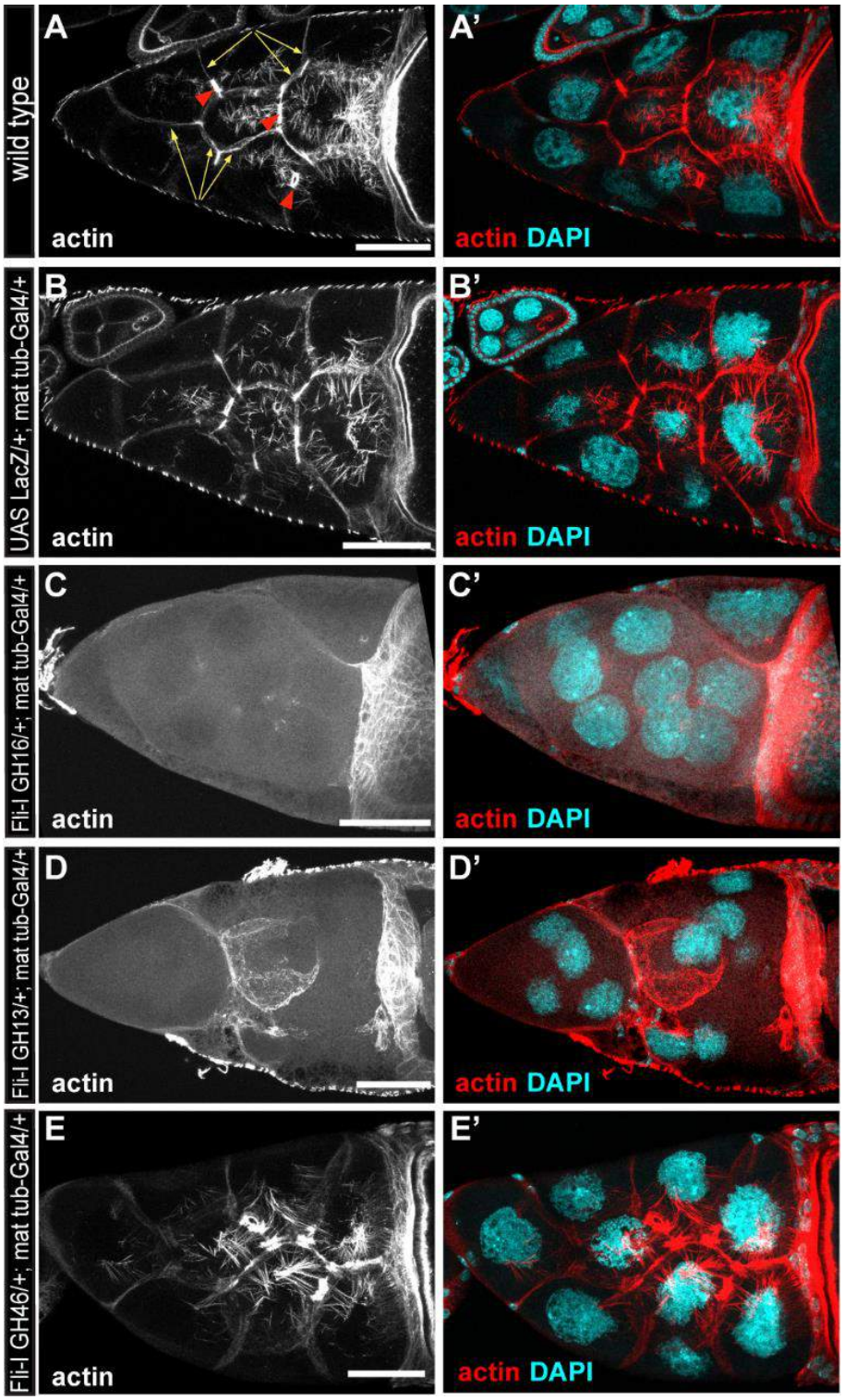

Figure 21. The effect of the gelsolin homology domains of Fli-I on actin organization in Drosophila egg chambers

(A, A') *Actin organization in nurse cells of wild-type Drosophila egg chamber in stage 10B is characterized by cortical actin (yellow arrows), ring canals (red arrowheads) and cytoplasmic actin cables growing from the plasma membrane to the nucleus. Actin*

is shown in ***(A)*** *in grayscale, an overlay of DAPI (in cyan) and actin (in red) are shown in* ***(A')***. ***(B, B')*** *Maternal expression of a UAS-lacZ control does not affect actin organization in the nurse cells.* ***(C-D')*** *Maternal expression of UAS-Fli-I-GH16* ***(C, C')*** *or UAS-Fli-IGH13* ***(D, D')*** *severely impairs cytokinesis in the nurse cells resulting in fused cells with reduced cortical actin level, ring canals are not evident and the nuclear positioning cytoplasmic actin cables are also missing.* ***(E, E')*** *By contrast, in UAS-Fli-I GH46 expressing egg chambers actin organization is not altered as compared to wild type. Anterior edge of the oocyte is visible on the right side of each panel; anterior is on the left, posterior is on the right. Scale bar = 50µm.*

5. CONCLUSION

In my Ph.D. work, I investigated the effect of Flightless-I on actin dynamics. Flightless-I protein was originally characterized in fruit fly where gene mutation in the GH domains resulted in an irregular actin organization and defective flight muscles. Like the other members of the gelsolin family, the protein has multiple functions and plays an important role in actin cytoskeleton organization. Flightless-I is widely expressed in tissues, mostly in skeletal, myocardial and nerve cells. It presents in the nucleus, where it acts as a hormone-regulated nuclear receptor coactivator. In the presence of serum, Fli-I can translocate from the nucleus to the cytoplasm, where it plays a role in cell migration, which is thought to be linked to its negative influences on wound healing and tissue regeneration. *Fli-I* maps with the Smith-Magenis microdeletion region in 17p11.2, suggesting the involvement of the protein in developmental and behavioral abnormalities.

To better understand the activities of Flightless-I and reveal the molecular mechanisms underlying these processes, I investigated the interactions of different, recombinantly produced Fli-I constructs with actin by using protein biochemical, biophysical and fluorescence microscopy (single and dual-color TIRFM) methods *in vitro*. I also studied the effect of the actin-binding protein profilin on the actin activities of Fli-I.

My main results are as follows:

- Flightless-I LRR and GH domains were successfully expressed and produced in the *Escherichia coli* system.
- Flightless-I interacts with both actin monomers (low-affinity interaction) and polymer barbed ends (high-affinity interaction).
- Flightless-I affects actin assembly in a biphasic manner. Fli-I GH16 and GH13 inhibit actin polymerization at lower concentrations (high affinity capping activity) and increase the rate of actin assembly at higher concentrations (low-affinity nucleation activity).
- Unlike gelsolin, the GH domains of Flightless-I have no severing activity.
- Fli-I GH46 and LRR have no direct effects on actin dynamics. The actin interactions and activities of Fli-I rely on the GH13 region.

- The actin-binding protein, profilin allows Fli-I to cap barbed ends and block actin polymer growth, but it inhibits its interaction with actin monomers and thereby, its nucleation activity.
- In contrast to gelsolin, the actin activities of Fli-I are not calcium-dependent, which can be explained by the lack of the conservation of type II calcium-binding sites between the two proteins.
- Fli-I GH46 binds to the DAD-CT region of DAAM and thereby tunes the actin assembly activities of DAAM.

In conclusion, our results indicate that in the cytoplasmic environment, Flightless-I interferes with actin dynamics by capping polymer ends, which may explain its negative effects on cell migration, and, thus wound healing and tissue regeneration.

6. FUTURE INTEREST

According to literature data[67], as well as to our findings presented in *Figure 20*, Fli-I interacts with the C terminal DAD-CT region of DAAM through its GH46 domain. The DAD-CT of DAAM is known to play an important role in the regulation of the actin activities of the FH1FH2 domains of DAAM; it forms an intramolecular contact with the N-terminal diaphanous inhibitory domain (DID), which renders DAAM inactive[71]. The binding of RhoGTPases to the GTPase binding domain of DAAM can relieve this inhibitory interaction, leading to DAAM activation. Altogether, these imply that Fli-I GH46 may have a role in the activation of DAAM. On the other hand, our research group has shown that the DAD-CT region is involved in the microtubule-binding ability of DAAM and potentially in the co-regulation of the actin-microtubule dynamics[71,84].

Based on the above, the focus of my future research interest is formulated by the following hypotheses.

Hypothesis 1: The interaction of Fli-I with the DAD-CT of DAAM provides an alternative/complementary activation pathway of DAAM, in which the DID domain is competed off by Fli-I GH46. Thereby, Fli-I can regulate actin dynamics indirectly through the activation of the DAAM-mediated pathway. To test this hypothesis, I aim to examine the interaction of DAAM and Fli-I GH46 in the presence of DID by using the above methodology.

Hypothesis 2: The interaction of Fli-I GH46 with DAD-CT can potentially influence the microtubule-binding, as well as the actin-microtubule crosslinking activity of DAAM. To tackle this hypothesis, I aim to investigate the DAAM-microtubule double and the DAAM-actin-microtubule triple interactions in the presence of different regions of Fli-I by using the above methodology with complementary TIRFM assays that allow the simultaneous observation of actin and microtubule polymers[84].

7. LIST OF ABBREVIATIONS

AS	ammonium sulfate
ATP	adenosine triphosphate
Alexa488NHS	Alexa Fluor488 carboxylic acid succinimidyl ester
Alexa568NHS	Alexa Fluor568 carboxylic acid succinimidyl ester
BSA	bovine serum albumin
DAAM	Disheveled-associated activator of morphogenesis
cDAAM	C-terminal Disheveled-associated activator of morphogenesis
DABCO	1,4-diazabicyclo[2.2.2]octane
DAD	diaphanous autoregulatory domain
DID	diaphanous inhibitory domain
DMSO	dimethyl sulfoxide
DRF	Diaphanous-related formins
DTT	dithiothreitol
EGTA	ethylene glycol-bis(β-aminoethyl ether)-*N*,*N*,*N*′,*N*′-tetraacetic acid)
F-actin	filamentous, polymer actin
FH1 domain	formin homology domain 1
FH2 domain	formin homology domain 2
Fli-I	Flightless-I
Fli-I GH13	Flightless-I GH 13 domains
Fli-I GH16	Flightless-I GH 16 domains
Fli-I GH46	Flightless-I GH 46 domains
GH	gelsolin homology domain
GA2	gelsolin:G-actin complex
G-actin	globular, monomeric actin
G2	actin dimer
G3	actin trimer
GSN	gelsolin
GST	glutathione *S*-transferases

IC_{50}	concentration required for half-maximal inhibition
IPTG	isopropyl β-D-1-thiogalactopyranoside
K_D	dissociation equilibrium constant
LatA	LatrunculinA
LRR	leucine-rich repeat
NHSR	tetramethylrhodamine N-succinimidyl ester
PA	profilin:G-actin complex
PEI	polyethylenimine
PMSF	phenylmethylsulfonyl fluoride
S1-4	actin subdomains 1-4
TIRFM	total internal reflection fluorescence microscopy

8. ACKNOWLEDGEMENTS

Firstly, I would like to thank my supervisor **Dr. Beáta Bugyi** for the continuous support of my Ph.D. study and related research, and for her patience, motivation, and immense knowledge. Her guidance helped me in all the time of research and writing of this thesis. I could not have imagined having a better advisor and mentor for my Ph.D. study.

My sincere thanks also go to **Prof. Dr. Miklós Nyitrai** and **Dr. András Lukács**, who provided me the opportunity to fulfill my Ph.D. studies in the Department of Biophysics.

I would like to thank **Dr. József Mihály** and his research team (Biological Research Centre, Szeged) for providing us with the plasmids of Flightless-I and performing the in vivo experiments shown in Figure 21. I would like to thank **Szilárd Szikora** for providing us with the Fiji plugin used in image analysis.

I thank **Dr. Andrea Teréz Vig**, **Dr. Tamás Huber** and **Dr. Péter Gaszler** for their help and professional advice during my research.

I also thank my co-workers in the Department for their help and advice during my work.

Last but not least, I would like to thank my family, my parents, and my husband, that they believed in me, supporting me spiritually throughout my Ph.D. research, writing this thesis and my life in general.

9. LIST OF REFERENCES

1. Svitkina T. The Actin Cytoskeleton and Actin-Based Motility. *Cold Spring Harb Perspect Biol*. 01 02 2018;10(1)doi:10.1101/cshperspect.a018267
2. dos Remedios CG, Chhabra D, Kekic M, et al. Actin binding proteins: regulation of cytoskeletal microfilaments. *Physiol Rev*. Apr 2003;83(2):433-73. doi:10.1152/physrev.00026.2002
3. Merino F, Pospich S, Raunser S. Towards a structural understanding of the remodeling of the actin cytoskeleton. *Semin Cell Dev Biol*. 06 2020;102:51-64. doi:10.1016/j.semcdb.2019.11.018
4. Cowin AJ, Adams DH, Strudwick XL, et al. Flightless I deficiency enhances wound repair by increasing cell migration and proliferation. *J Pathol*. Apr 2007;211(5):572-581. doi:10.1002/path.2143
5. Kopecki Z, Cowin AJ. Flightless I: an actin-remodelling protein and an important negative regulator of wound repair. *Int J Biochem Cell Biol*. 2008;40(8):1415-9. doi:10.1016/j.biocel.2007.04.011
6. Bugyi B, Carlier MF. Control of actin filament treadmilling in cell motility. *Annu Rev Biophys*. 2010;39:449-70. doi:10.1146/annurev-biophys-051309-103849
7. Shekhar S, Kerleau M, Kühn S, et al. Formin and capping protein together embrace the actin filament in a ménage à trois. *Nat Commun*. Nov 13 2015;6:8730. doi:10.1038/ncomms9730
8. Dugina V, Zwaenepoel I, Gabbiani G, Clément S, Chaponnier C. Beta and gamma-cytoplasmic actins display distinct distribution and functional diversity. *J Cell Sci*. Aug 15 2009;122(Pt 16):2980-8. doi:10.1242/jcs.041970
9. Lodish H, Berk A, Zipursky L, Matsudaira P, Baltimore D, Darnell J. *Molecular Cell Biology*. 4th Edition ed. W.H. Freeman; 1999:1184.
10. Müller M, Diensthuber RP, Chizhov I, et al. Distinct functional interactions between actin isoforms and nonsarcomeric myosins. *PLoS One*. 2013;8(7):e70636. doi:10.1371/journal.pone.0070636
11. Rubenstein PA, Wen KK. Insights into the effects of disease-causing mutations in human actins. *Cytoskeleton (Hoboken)*. Apr 2014;71(4):211-29. doi:10.1002/cm.21169
12. Rubenstein PA. The functional importance of multiple actin isoforms. *Bioessays*. Jul 1990;12(7):309-15. doi:10.1002/bies.950120702
13. Dominguez R, Holmes KC. Actin structure and function. *Annu Rev Biophys*. 2011;40:169-86. doi:10.1146/annurev-biophys-042910-155359
14. Graceffa P, Dominguez R. Crystal structure of monomeric actin in the ATP state. Structural basis of nucleotide-dependent actin dynamics. *J Biol Chem*. Sep 05 2003;278(36):34172-80. doi:10.1074/jbc.M303689200
15. Grazi E, Trombetta G. Effects of temperature on actin polymerized by Ca2+. Direct evidence of fragmentation. *Biochem J*. Nov 15 1985;232(1):297-300. doi:10.1042/bj2320297
16. Wang F, Sampogna RV, Ware BR. pH dependence of actin self-assembly. *Biophys J*. Feb 1989;55(2):293-8. doi:10.1016/S0006-3495(89)82804-8
17. Pollard TD. Rate constants for the reactions of ATP- and ADP-actin with the ends of actin filaments. *J Cell Biol*. Dec 1986;103(6 Pt 2):2747-54. doi:10.1083/jcb.103.6.2747
18. Sept D, McCammon JA. Thermodynamics and kinetics of actin filament nucleation. *Biophys J*. Aug 2001;81(2):667-74. doi:10.1016/S0006-3495(01)75731-1
19. HANSON J, LOWY J. THE STRUCTURE OF ACTIN FILAMENTS AND THE ORIGIN OF THE AXIAL PERIODICITY IN THE I-SUBSTANCE OF VERTEBRATE STRIATED MUSCLE. *Proc R Soc Lond B Biol Sci*. Oct 27 1964;160:449-60. doi:10.1098/rspb.1964.0055
20. Blanchoin L, Pollard TD. Hydrolysis of ATP by polymerized actin depends on the bound divalent cation but not profilin. *Biochemistry*. Jan 15 2002;41(2):597-602. doi:10.1021/bi011214b

21. Murphy DB, Gray RO, Grasser WA, Pollard TD. Direct demonstration of actin filament annealing in vitro. *J Cell Biol*. Jun 1988;106(6):1947-54. doi:10.1083/jcb.106.6.1947
22. Sept D, Xu J, Pollard TD, McCammon JA. Annealing accounts for the length of actin filaments formed by spontaneous polymerization. *Biophys J*. Dec 1999;77(6):2911-9. doi:10.1016/s0006-3495(99)77124-9
23. Huff T, Müller CS, Otto AM, Netzker R, Hannappel E. beta-Thymosins, small acidic peptides with multiple functions. *Int J Biochem Cell Biol*. Mar 2001;33(3):205-20. doi:10.1016/s1357-2725(00)00087-x
24. Witke W. The role of profilin complexes in cell motility and other cellular processes. *Trends Cell Biol*. Aug 2004;14(8):461-9. doi:10.1016/j.tcb.2004.07.003
25. Pope B, Way M, Weeds AG. Two of the three actin-binding domains of gelsolin bind to the same subdomain of actin. Implications of capping and severing mechanisms. *FEBS Lett*. Mar 11 1991;280(1):70-4. doi:10.1016/0014-5793(91)80206-i
26. Mullins RD, Kelleher JF, Xu J, Pollard TD. Arp2/3 complex from Acanthamoeba binds profilin and cross-links actin filaments. *Mol Biol Cell*. Apr 1998;9(4):841-52. doi:10.1091/mbc.9.4.841
27. Weston L, Coutts AS, La Thangue NB. Actin nucleators in the nucleus: an emerging theme. *J Cell Sci*. Aug 01 2012;125(Pt 15):3519-27. doi:10.1242/jcs.099523
28. Firat-Karalar EN, Welch MD. New mechanisms and functions of actin nucleation. *Curr Opin Cell Biol*. Feb 2011;23(1):4-13. doi:10.1016/j.ceb.2010.10.007
29. Geeves MA, Fedorov R, Manstein DJ. Molecular mechanism of actomyosin-based motility. *Cell Mol Life Sci*. Jul 2005;62(13):1462-77. doi:10.1007/s00018-005-5015-5
30. *Molecular interactions of actin: actin-myosin interaction and actin based regulation ; [... Fourth Pentennial Actin Conference held at the new Sheraton Maui in Hawaii in 1997]*. Results and problems in cell differentiation. Springer; 2002.
31. Nag S, Larsson M, Robinson RC, Burtnick LD. Gelsolin: the tail of a molecular gymnast. *Cytoskeleton*. Jul 2013;70(7):360-84. doi:10.1002/cm.21117
32. Pollard TD, Borisy GG. Cellular motility driven by assembly and disassembly of actin filaments. *Cell*. Feb 21 2003;112(4):453-65. doi:10.1016/s0092-8674(03)00120-x
33. Pernier J, Shekhar S, Jegou A, Guichard B, Carlier MF. Profilin Interaction with Actin Filament Barbed End Controls Dynamic Instability, Capping, Branching, and Motility. *Dev Cell*. Jan 25 2016;36(2):201-14. doi:10.1016/j.devcel.2015.12.024
34. Goode BL, Eck MJ. Mechanism and function of formins in the control of actin assembly. *Annu Rev Biochem*. 2007;76:593-627. doi:10.1146/annurev.biochem.75.103004.142647
35. Yamashita M, Higashi T, Suetsugu S, et al. Crystal structure of human DAAM1 formin homology 2 domain. *Genes Cells*. Nov 2007;12(11):1255-65. doi:10.1111/j.1365-2443.2007.01132.x
36. Barkó S, Bugyi B, Carlier MF, et al. Characterization of the biochemical properties and biological function of the formin homology domains of Drosophila DAAM. *J Biol Chem*. Apr 23 2010;285(17):13154-69. doi:10.1074/jbc.M109.093914
37. Lu J, Meng W, Poy F, Maiti S, Goode BL, Eck MJ. Structure of the FH2 domain of Daam1: implications for formin regulation of actin assembly. *J Mol Biol*. Jun 22 2007;369(5):1258-69. doi:10.1016/j.jmb.2007.04.002
38. Silacci P, Mazzolai L, Gauci C, Stergiopulos N, Yin HL, Hayoz D. Gelsolin superfamily proteins: key regulators of cellular functions. *Cell Mol Life Sci*. Oct 2004;61(19-20):2614-23. doi:10.1007/s00018-004-4225-6
39. Feldt J, Schicht M, Garreis F, Welss J, Schneider UW, Paulsen F. Structure, regulation and related diseases of the actin-binding protein gelsolin. *Expert Rev Mol Med*. 01 30 2019;20:e7. doi:10.1017/erm.2018.7
40. Ghoshdastider U, Popp D, Burtnick LD, Robinson RC. The expanding superfamily of gelsolin homology domain proteins. *Cytoskeleton (Hoboken)*. Nov 2013;70(11):775-95. doi:10.1002/cm.21149

41. Urosev D, Ma Q, Tan AL, Robinson RC, Burtnick LD. The structure of gelsolin bound to ATP. *J Mol Biol*. Mar 31 2006;357(3):765-72. doi:10.1016/j.jmb.2006.01.027
42. Salazar R, Bell SE, Davis GE. Coordinate induction of the actin cytoskeletal regulatory proteins gelsolin, vasodilator-stimulated phosphoprotein, and profilin during capillary morphogenesis in vitro. *Exp Cell Res*. May 25 1999;249(1):22-32. doi:10.1006/excr.1999.4460
43. Campbell HD, Fountain S, Young IG, et al. Genomic structure, evolution, and expression of human FLII, a gelsolin and leucine-rich-repeat family member: overlap with LLGL. *Genomics*. May 15 1997;42(1):46-54. doi:10.1006/geno.1997.4709
44. Campbell HD, Schimansky T, Claudianos C, et al. The Drosophila melanogaster flightless-I gene involved in gastrulation and muscle degeneration encodes gelsolin-like and leucine-rich repeat domains and is conserved in Caenorhabditis elegans and humans. *Proc Natl Acad Sci U S A*. Dec 01 1993;90(23):11386-90. doi:10.1073/pnas.90.23.11386
45. Davy DA, Ball EE, Matthaei KI, Campbell HD, Crouch MF. The flightless I protein localizes to actin-based structures during embryonic development. *Immunology and cell biology*. Aug 2000;78(4):423-9. doi:10.1046/j.1440-1711.2000.00926.x
46. Straub KL, Stella MC, Leptin M. The gelsolin-related flightless I protein is required for actin distribution during cellularisation in Drosophila. *J Cell Sci*. Jan 1996;109 (Pt 1):263-70. doi:10.1242/jcs.109.1.263
47. Lee YH, Campbell HD, Stallcup MR. Developmentally essential protein flightless I is a nuclear receptor coactivator with actin binding activity. *Mol Cell Biol*. Mar 2004;24(5):2103-17. doi:10.1128/MCB.24.5.2103-2117.2004
48. Campbell HD, Fountain S, McLennan IS, et al. Fliih, a gelsolin-related cytoskeletal regulator essential for early mammalian embryonic development. *Mol Cell Biol*. May 2002;22(10):3518-26. doi:10.1128/MCB.22.10.3518-3526.2002
49. Witke W, Sharpe AH, Hartwig JH, Azuma T, Stossel TP, Kwiatkowski DJ. Hemostatic, inflammatory, and fibroblast responses are blunted in mice lacking gelsolin. *Cell*. Apr 07 1995;81(1):41-51. doi:10.1016/0092-8674(95)90369-0
50. Witke W, Li W, Kwiatkowski DJ, Southwick FS. Comparisons of CapG and gelsolin-null macrophages: demonstration of a unique role for CapG in receptor-mediated ruffling, phagocytosis, and vesicle rocketing. *J Cell Biol*. Aug 20 2001;154(4):775-84. doi:10.1083/jcb.200101113
51. Pinson KI, Dunbar L, Samuelson L, Gumucio DL. Targeted disruption of the mouse villin gene does not impair the morphogenesis of microvilli. *Dev Dyn*. Jan 1998;211(1):109-21. doi:10.1002/(SICI)1097-0177(199801)211:1<109::AID-AJA10>3.0.CO;2-7
52. Archer SK, Behm CA, Claudianos C, Campbell HD. The flightless I protein and the gelsolin family in nuclear hormone receptor-mediated signalling. *Biochem Soc Trans*. Dec 2004;32(Pt 6):940-2. doi:10.1042/BST0320940
53. Ruzehaji N, Mills SJ, Melville E, Arkell R, Fitridge R, Cowin AJ. The influence of Flightless I on Toll-like-receptor-mediated inflammation in a murine model of diabetic wound healing. *Biomed Res Int*. 2013;2013:389792. doi:10.1155/2013/389792
54. Kopecki Z, Arkell RM, Strudwick XL, et al. Overexpression of the Flii gene increases dermal-epidermal blistering in an autoimmune ColVII mouse model of epidermolysis bullosa acquisita. *J Pathol*. Nov 2011;225(3):401-13. doi:10.1002/path.2973
55. Davy DA, Campbell HD, Fountain S, de Jong D, Crouch MF. The flightless I protein colocalizes with actin- and microtubule-based structures in motile Swiss 3T3 fibroblasts: evidence for the involvement of PI 3-kinase and Ras-related small GTPases. *J Cell Sci*. Feb 2001;114(Pt 3):549-62. doi:10.1242/jcs.114.3.549
56. Jackson JE, Kopecki Z, Adams DH, Cowin AJ. Flii neutralizing antibodies improve wound healing in porcine preclinical studies. *Wound Repair Regen*. 2012 Jul-Aug 2012;20(4):523-36. doi:10.1111/j.1524-475X.2012.00802.x
57. Adams DH, Ruzehaji N, Strudwick XL, et al. Attenuation of Flightless I, an actin-remodelling protein, improves burn injury repair via modulation of transforming growth factor

(TGF)-beta1 and TGF-beta3. *Br J Dermatol*. Aug 2009;161(2):326-36. doi:10.1111/j.1365-2133.2009.09296.x
58. Cameron AM, Turner CT, Adams DH, et al. Flightless I is a key regulator of the fibroproliferative process in hypertrophic scarring and a target for a novel antiscarring therapy. *Br J Dermatol*. Apr 2016;174(4):786-94. doi:10.1111/bjd.14263
59. Chen KS, Gunaratne PH, Hoheisel JD, et al. The human homologue of the Drosophila melanogaster flightless-I gene (flil) maps within the Smith-Magenis microdeletion critical region in 17p11.2. *Am J Hum Genet*. Jan 1995;56(1):175-82.
60. Deng H, Xia D, Fang B, Zhang H. The Flightless I homolog, fli-1, regulates anterior/posterior polarity, asymmetric cell division and ovulation during Caenorhabditis elegans development. *Genetics*. Oct 2007;177(2):847-60. doi:10.1534/genetics.107.078964
61. Liu W, Xie Y, Ma J, et al. IBS: an illustrator for the presentation and visualization of biological sequences. *Bioinformatics*. Oct 15 2015;31(20):3359-61. doi:10.1093/bioinformatics/btv362
62. Liu YT, Yin HL. Identification of the binding partners for flightless I, A novel protein bridging the leucine-rich repeat and the gelsolin superfamilies. *J Biol Chem*. Apr 03 1998;273(14):7920-7. doi:10.1074/jbc.273.14.7920
63. Matsushima N, Miyashita H, Mikami T, Kuroki Y. A nested leucine rich repeat (LRR) domain: the precursor of LRRs is a ten or eleven residue motif. *BMC Microbiol*. Sep 09 2010;10:235. doi:10.1186/1471-2180-10-235
64. Goshima M, Kariya K-i, Yamawaki-Kataoka Y, et al. Characterization of a Novel Ras-Binding Protein Ce-FLI-1 Comprising Leucine-Rich Repeats and Gelsolin-like Domains. *Biochemical and Biophysical Research Communications*. 1999/04/02/ 1999;257(1):111-116. doi:https://doi.org/10.1006/bbrc.1999.0420
65. Mohammad I, Arora PD, Naghibzadeh Y, et al. Flightless I is a focal adhesion-associated actin-capping protein that regulates cell migration. *FASEB J*. Aug 2012;26(8):3260-72. doi:10.1096/fj.11-202051
66. Arora PD, Wang Y, Bresnick A, Janmey PA, McCulloch CA. Flightless I interacts with NMMIIA to promote cell extension formation, which enables collagen remodeling. *Mol Biol Cell*. Jun 15 2015;26(12):2279-97. doi:10.1091/mbc.E14-11-1536
67. Higashi T, Ikeda T, Murakami T, et al. Flightless-I (Fli-I) regulates the actin assembly activity of diaphanous-related formins (DRFs) Daam1 and mDia1 in cooperation with active Rho GTPase. *J Biol Chem*. May 21 2010;285(21):16231-8. doi:10.1074/jbc.M109.079236
68. Spudich JA, Watt S. The regulation of rabbit skeletal muscle contraction. I. Biochemical studies of the interaction of the tropomyosin-troponin complex with actin and the proteolytic fragments of myosin. *J Biol Chem*. Aug 10 1971;246(15):4866-71.
69. Perelroizen I, Marchand JB, Blanchoin L, Didry D, Carlier MF. Interaction of profilin with G-actin and poly(L-proline). *Biochemistry*. Jul 19 1994;33(28):8472-8. doi:10.1021/bi00194a011
70. Nag S, Ma Q, Wang H, et al. Ca2+ binding by domain 2 plays a critical role in the activation and stabilization of gelsolin. *Proc Natl Acad Sci U S A*. Aug 18 2009;106(33):13713-8. doi:10.1073/pnas.0812374106
71. Vig AT, Földi I, Szikora S, et al. The activities of the C-terminal regions of the formin protein disheveled-associated activator of morphogenesis (DAAM) in actin dynamics. *J Biol Chem*. 08 18 2017;292(33):13566-13583. doi:10.1074/jbc.M117.799247
72. Manchester KL. Value of A260/A280 ratios for measurement of purity of nucleic acids. *Biotechniques*. Aug 1995;19(2):208-10.
73. Hanson J, Lowy. J. The structure of F-actin and of actin filaments isolated from muscle. *Journal of Molecular Biology*. 1963;6:46-60.
74. von der Ecken J, Müller M, Lehman W, Manstein DJ, Penczek PA, Raunser S. Structure of the F-actin–tropomyosin complex. *Nature*. 2015/03/01 2015;519(7541):114-117. doi:10.1038/nature14033

75. Kothakota S, Azuma T, Reinhard C, et al. Caspase-3-generated fragment of gelsolin: effector of morphological change in apoptosis. *Science*. Oct 10 1997;278(5336):294-8. doi:10.1126/science.278.5336.294
76. Kis-Bicskei N, Becsi B, Erdodi F, et al. Tropomyosins Regulate the Severing Activity of Gelsolin in Isoform-Dependent and Independent Manners. *Biophysical journal*. Feb 27 2018;114(4):777-787. doi:10.1016/j.bpj.2017.11.3812
77. Yin HL, Stossel TP. Control of cytoplasmic actin gel-sol transformation by gelsolin, a calcium-dependent regulatory protein. *Nature*. Oct 18 1979;281(5732):583-6. doi:10.1038/281583a0
78. Coué M, Korn ED. Interaction of plasma gelsolin with G-actin and F-actin in the presence and absence of calcium ions. *J Biol Chem*. Dec 05 1985;260(28):15033-41.
79. Tóth M, Majoros AK, Vig AT, et al. Biochemical Activities of the Wiskott-Aldrich Syndrome Homology Region 2 Domains of Sarcomere Length Short (SALS) Protein. *J Biol Chem*. Jan 08 2016;291(2):667-80. doi:10.1074/jbc.M115.683904
80. Szatmári D, Bugyi B, Ujfalusi Z, Grama L, Dudás R, Nyitrai M. Cardiac leiomodin2 binds to the sides of actin filaments and regulates the ATPase activity of myosin. *PLoS One*. 2017;12(10):e0186288. doi:10.1371/journal.pone.0186288
81. Pollard TD. Regulation of actin filament assembly by Arp2/3 complex and formins. *Annu Rev Biophys Biomol Struct*. 2007;36:451-77. doi:10.1146/annurev.biophys.35.040405.101936
82. Vig AT, Foldi I, Szikora S, et al. The activities of the C-terminal regions of the formin protein disheveled-associated activator of morphogenesis (DAAM) in actin dynamics. *J Biol Chem*. Aug 18 2017;292(33):13566-13583. doi:10.1074/jbc.M117.799247
83. Perrimon N, Smouse D, Miklos GL. Developmental genetics of loci at the base of the X chromosome of Drosophila melanogaster. *Genetics*. Feb 1989;121(2):313-31. doi:10.1093/genetics/121.2.313
84. Szikora S, Földi I, Tóth K, et al. The formin DAAM is required for coordination of the actin and microtubule cytoskeleton in axonal growth cones. *J Cell Sci*. Aug 01 2017;130(15):2506-2519. doi:10.1242/jcs.203455

10. LIST OF PUBLICATIONS

Publications related to the dissertation

Réka Pintér, Tamás Huber, Péter Bukovics, Péter Gaszler, Andrea Vig, Mónika Ágnes Tóth, Gabriella Gazsó-Gerhát, Dávid Farkas, Ede Migh, József Mihály, and Beáta Bugyi. The activities of the gelsolin homology domains of Flightless-I in actin dynamics. Front Mol Biosci. 2020; 7:575077
Impact factor: 5.246, Q1
Total citations/Independent citations: 2/1

Andrea Teréz Vig, István Földi, Szilárd Szikora, Ede Migh, Rita Gombos, Mónika Ágnes Tóth, Tamás Huber, **Réka Pintér**, Gábor Csaba Talián, József Mihály, and Beáta Bugyi. The activities of the c-terminal regions of the formin protein disheveled-associated activator of morphogenesis (daam) in actin dynamics. J. Biol. Chem. 2017; 292(33):13566–13583.
Impact factor: 4.011, Q1/D1
Total citations/Independent citations: 11/3

Conference presentations related to the dissertation

Péter Gaszler, **Réka Pintér**, Péter Bukovics, Rauan Sakenov, Tamás Huber, Andrea Teréz Vig, Mónika Ágnes Tóth, Veronika Takács-Kollár, Beata Bugyi. Comparative Analyses of the Gelsolin Homology Domains of Gelsolin and Flightless-I. The 2nd International Electronic Conference on Biomolecules: Biomacromolecules and the Modern World Challenges/online, November 1-15th 2022

Péter Gaszler, Rahmah Hanifatul, **Réka Pintér**, Péter Bukovics, Rauan Sakenov, Tamás Huber, Andrea Teréz Vig, Mónika Ágnes Tóth, Beáta Bugyi. Structural and functional analyses of the gelsolin homology domains of Flightless-I in actin dynamics. FASEB Journal 2021; 35:00391 (Abstract)
Impact factor: 5.835, Q1

Réka Pintér, Budiman Hanifatul Rahmah, Rauan Sakenov, Tamás Huber, Péter Bukovics, Péter Gaszler, Beáta Bugyi. The activities of the gelsolin homology domains of Flightless-I in actin dynamics. Proceedings of the EFOP-3.6.2-16-2017-00006 (LIVE LONGER) project, University of Szeged, Szeged. 2020; p. 95-95, ISBN: 9789633067642. (Abstract)

Réka Pintér, Péter Gaszler, Tamás Huber, Andrea Teréz Vig, Mónika Ágnes Tóth, Beáta Bugyi. Activities of Flightless-I in the organisation of the actin cytoskeleton. UNIA Workshop, „Current trends in biomedicine", Baeza, Spain, November 11-13th 2019

Bukovics Péter, Gaszler Péter, Rauan Sakenov, **Pintér Réka**, Huber Tamás, Bugyi Beáta. Szerkezet-funkció koordináció gelsolin homológ fehérjékben. Magyar Biofizikai Társaság XXVII. Kongresszusa, Szeged, 2019. augustus 26-29. (Conference talk)

Péter Gaszler, Andrea Teréz Vig, **Réka Pintér**, Tamás Huber, Beata Bugyi. Activities of Flightless-I (Fli I) in the organisation of actin cytoskeleton. Molekuláris Élettudományi Konferencia, Eger, 2019. március 29-31.

Péter Gaszler, Péter Bukovics, Rauan Sakenov, **Réka Pintér**, Tamás Huber, Beáta Bugyi. Structural differences between Gelsolin and Flightless-I proteins and their behaviour in the presence and absence of Ca^{2+}. Molekuláris Élettudományi Konferencia, Eger, 2019. március 29-31.

Réka Pintér, Péter Gaszler, Tamás Huber, Andrea Teréz Vig, Mónika Ágnes Tóth, Beáta Bugyi. The role of Flightless-I (Fli-I) in the organisation of actin cytoskeleton. Medical Conference for PhD Students and Experts of Clinical Science, Pécs, Hungary, Oktober 27th 2018

Réka Pintér, Péter Gaszler, Tamás Huber, Andrea Teréz Vig, Mónika Ágnes Tóth, Beáta Bugyi. The role of Flightless-I (Fli-I) in the organisation of actin cytoskeleton. Regional Biophysics Conference, Zreče, Slovenia, May 16th - 20th 2018

Fórizs Judit Viktória, **Pintér Réka**, Huber Tamás, Vig Andrea Teréz, Tóth Mónika Ágnes és Bugyi Beáta. Flightless I fehérje szerepe az aktin sejtváz szerveződésében. MBFT Konferencia, Szeged, 2017. augusztus 22-25.

Publications not related to the dissertation

Dávid Szatmári, Beáta Bugyi, **Réka Pintér**, Dénes Lőrinczy. Cyclophosphamide treatment modifies the thermal stability of profiling bound monomeric and leiomodin 2 bound filamentous actin. Journal of Thermal Analysis and Calorimetry. 2022; https://doi.org/10.1007/s10973-022-11668-y
Impact factor: 4.755
Total citations/Independent citations: 0/0

Pintér R, Madai M, Horváth G, Németh V, Oldal M, Kemenesi G, Dallos B, Bányai K, Jakab F. Molecular detection and phylogenetic analysis of tick-borne encephalitis virus in rodents captured in the transdanubian region of Hungary. Vector Borne Zoonotic Dis 2014;14(8):621-624.
Impact factor: 2.298, Q2
Total citations/Independent citations: 8/7

Oldal M, Németh V, Madai M, **Pintér R**, Kemenesi G, Dallos B, Kutas A, Sebők J, Horváth G, Bányai K, Jakab F. Serosurvey of pathogenic hantaviruses among forestry workers in Hungary. Int J Occup Med Environ Health. 2014; 27(5):766-773.
Impact factor: 1.365, Q3
Total citations/Independent citations: 9/6

Pintér R, Madai M, Vadkerti E, Németh V, Oldal M, Kemenesi G, Dallos B, Gyuranecz M, Kiss G, Bányai K, Jakab F. Identification of tick-borne encephalitis virus in ticks collected in southeastern Hungary. Ticks Tick Borne Dis 2013; 4:427:431.
Impact factor: 2.878, Q1
Total citations/Independent citations: 11/10

Conference presentations not related to the dissertation

Péter Gaszler, Péter Bukovics, Rauan Sakenov, **Réka Pintér**, Tamás Huber, Beáta Bugyi. Structural differences between gelsolin and Flightless-I proteins and their behavior in the presence and absence of Ca^{2+} ion. Medical Conference for PhD Students and Experts of Clinical Science, Pécs, Hungary, Oktober 16-17th 2020

Réka Pintér, Judit Viktória Fórizs, Péter Gaszler, Beáta Bugyi. Activities of actin-binding proteins: principles and approaches. „New directions in biocomputation" Workshop, Dresden, Germany, September 12th -13th 2017

Pintér Réka, Fórizs Judit Viktória, Huber Tamás, Vig Andrea Teréz és Bugyi Beáta. A Disheveled-Associated Activator of Morphogenesis (DAAM) formin szerepe az aktin dinamikájában. MBFT Konferencia, Szeged, 2017. augusztus 22-25.

Pintér Réka, Fórizs Judit Viktória, Huber Tamás, Vig Andrea Teréz, Tóth Mónika Ágnes, Kalmár Lajos és Bugyi Beáta. SALS, egy rendezetlen fehérje szerepe a szarkomerogenezis során. MBFT Konferencia, Szeged, 2017. augusztus 22-25.

Fórizs Judit Viktória, **Pintér Réka**, Vig Andrea Teréz, Huber Tamás és Bugyi Beáta. A DAAM (Disheveled-Associated Activator of Morphogenesis) formin az aktin-mikrotubulus dinamika koordinációjában. MBFT Konferencia, Szeged, 2017. augusztus 22-25.

Gaszler P, Fórizs V.J, Vig A, Huber T, **Pintér R,** Bugyi B. The activities of the disheveled-associated activator of morphogenesis (DAAM) formin in actin dynamics. Molekuláris Élettudományi Konferencia, Eger, 2017. március 31 - április 2.

M. Madai, V. Németh, M. Oldal, G. Horváth, R. Herczeg, **R. Pintér**, A. Kutas, B. Dallos, K. Bányai, F. Jakab. Serological survey of hantavirus infection among rodents in Hungary. Int J Infect Dis. 2016; 53:127. (Abstract)
Impact factor: 2.532, Q1

Oldal M, Német V, Madai M, **Pintér R**, Kemenesi g, Dallos B, Kutas A, Sebők J, Horváth Gy, Bányai K, Jakab F. Hantavirus seroprevalence among forestry workers in Hungary. International Meeting on Emerging Diseases and Surveillance, Bécs, Ausztria, 2014. október 31-november 3.

Overall impact factor of publications: 28,92
Total number of citations: 44
Total number of independent citations: 27

frontiers in Molecular Biosciences

ORIGINAL RESEARCH
published: 08 September 2020
doi: 10.3389/fmolb.2020.575077

The Activities of the Gelsolin Homology Domains of Flightless-I in Actin Dynamics

*Réka Pintér[1], Tamás Huber[1], Péter Bukovics[1], Péter Gaszler[1], Andrea Teréz Vig[1], Mónika Ágnes Tóth[1], Gabriella Gazsó-Gerhát[2,3], Dávid Farkas[2], Ede Migh[2], József Mihály[2] and Beáta Bugyi[1,4]**

[1] Department of Biophysics, Medical School, University of Pécs, Pécs, Hungary, [2] Biological Research Centre Szeged, Institute of Genetics, Szeged, Hungary, [3] Faculty of Science and Informatics, Doctoral School in Biology, University of Szeged, Szeged, Hungary, [4] Szentágothai Research Center, Pécs, Hungary

OPEN ACCESS

Edited by:
Nikolaos E. Labrou, Agricultural University of Athens, Greece

Reviewed by:
Erika Anne Taylor, Wesleyan University, United States
Kamlendra Singh, Karolinska Institute, Sweden

***Correspondence:**
Beáta Bugyi
beata.bugyi@aok.pte.hu

Specialty section:
This article was submitted to Protein Chemistry and Enzymology, a section of the journal Frontiers in Molecular Biosciences

Received: *22 June 2020*
Accepted: *14 August 2020*
Published: *08 September 2020*

Citation:
Pintér R, Huber T, Bukovics P, Gaszler P, Vig AT, Tóth MÁ, Gazsó-Gerhát G, Farkas D, Migh E, Mihály J and Bugyi B (2020) The Activities of the Gelsolin Homology Domains of Flightless-I in Actin Dynamics. Front. Mol. Biosci. 7:575077. doi: 10.3389/fmolb.2020.575077

Flightless-I is a unique member of the gelsolin superfamily alloying six gelsolin homology domains and leucine-rich repeats. Flightless-I is an established regulator of the actin cytoskeleton, however, its biochemical activities in actin dynamics are still largely elusive. To better understand the biological functioning of Flightless-I we studied the actin activities of *Drosophila* Flightless-I by *in vitro* bulk fluorescence spectroscopy and single filament fluorescence microscopy, as well as *in vivo* genetic approaches. Flightless-I was found to interact with actin and affects actin dynamics in a calcium-independent fashion *in vitro*. Our work identifies the first three gelsolin homology domains (1–3) of Flightless-I as the main actin-binding site; neither the other three gelsolin homology domains (4–6) nor the leucine-rich repeats bind actin. Flightless-I inhibits polymerization by high-affinity (∼nM) filament barbed end capping, moderately facilitates nucleation by low-affinity (∼μM) monomer binding, and does not sever actin filaments. Our work reveals that in the presence of profilin Flightless-I is only able to cap actin filament barbed ends but fails to promote actin assembly. In line with the *in vitro* data, while gelsolin homology domains 4–6 have no effect on *in vivo* actin polymerization, overexpression of gelsolin homology domains 1–3 prevents the formation of various types of actin cables in the developing *Drosophila* egg chambers. We also show that the gelsolin homology domains 4–6 of Flightless-I interact with the C-terminus of *Drosophila* Disheveled-associated activator of morphogenesis formin and negatively regulates its actin assembly activity.

Keywords: actin, gelsolin homology, Flightless-I, *Drosophila*, fluorescence

Abbreviations: C, C-terminus; CapG, macrophage capping protein; CC, coiled-coil; D, Diaphanous autoregulatory domain; DAAM, Disheveled-associated activator of morphogenesis; DD, dimerization domain; DID, Diaphanous inhibitory domain; FH, formin homology domain; Fli-I, Flightless-I; G, GTPase binding domain; GH gelsolin homology domain; GSN, gelsolin; Lmod, Leiomodin; LRR, leucine-rich repeat; SALS-WH2, Wiskott-Aldrich Syndrome Homology 2 domains of Sarcomere Length Short; TIRFM, total internal reflection fluorescence microscopy.

INTRODUCTION

The gelsolin (GSN) superfamily comprises actin-remodeling proteins including gelsolin, Flightless-I (Fli-I), villin, adseverin, macrophage capping protein (CapG), advillin and supervillin that regulate diverse aspects of the actin cytoskeleton (reviewed in Burtnick et al., 2001; Silacci et al., 2004; Ghoshdastider et al., 2013; Nag et al., 2013). The eponymous member; gelsolin with six gelsolin domains (**Figure 1**) is a Ca^{2+}-regulated multifunctional protein; it interacts with both filamentous and monomeric actin and possesses barbed end capping, severing and nucleation activities *in vitro* (Burtnick et al., 2001; Silacci et al., 2004; Nag et al., 2013).

Fli-I was originally characterized in *Drosophila melanogaster* as a protein product of the *flightless-I* gene associated with developmental processes including cellularization and organization of indirect flight muscle (Perrimon et al., 1989; Campbell et al., 1993). Disruption of *fli-I* can cause lethality in early embryogenesis and defects in actin-associated processes in mouse, *Drosophila* and *C. elegans* indicating the essential role of the protein in embryonic development (Campbell et al., 1993; Campbell et al., 2002; Deng et al., 2007; Lu et al., 2008). In contrast, homozygous null gelsolin (Witke et al., 1995), CapG (Witke et al., 2001) or villin (Pinson et al., 1998; Ferrary et al., 1999) mutant mice are viable and fertile. The vital role of Fli-I is further supported by its tissue distribution that is the most widespread amongst GSN family proteins; it is abundantly expressed in skeletal and heart muscles, as well as in nerve cells (Campbell et al., 1993; Campbell et al., 1997; Davy et al., 2000; Nag et al., 2013). Fli-I is a well-established negative regulator of wound healing and tissue regeneration (Cowin et al., 2007; Cameron et al., 2016). The human protein is implicated in epidermolysis bullosa and Smith-Magenis syndrome causing developmental and behavioral abnormalities (Chen et al., 1995; Kopecki et al., 2011).

Fli-I alloys domains from two protein families that endows it with unique structural characteristics (**Figure 1**). The N-terminal region is composed of tandem leucine-rich repeats (LRRs) forming a protein-protein interaction domain. The C-terminal half of the protein possesses six gelsolin homology (GH) domains analogously to gelsolin. The LRR region of Fli-I has diverse interaction partners and may participate in interconnecting signaling and cytoskeletal reorganization events (Liu and Yin, 1998; Fong and de Couet, 1999; Goshima et al., 1999; Davy et al., 2000), while the C-terminal GH domains are thought to serve as a platform for actin interactions. Notably, the actin-binding ability of Fli-I of human, mouse and *C. elegans* origin has been demonstrated *in vitro* by pull-down and sedimentation approaches in cell extracts, as well as with purified proteins (Liu and Yin, 1998; Goshima et al., 1999; Li et al., 2008; Mohammad et al., 2012). The association of Fli-I to actin-based structures was confirmed in various cell lines and also in animal models (mouse, *Drosophila, C. elegans*) (Davy et al., 2000, 2001; Campbell et al., 2002; Deng et al., 2007; Li et al., 2008; Lu et al., 2008; Mohammad et al., 2012). The binding of Fli-I to both G-actin and F-actin was suggested (Liu and Yin, 1998; Goshima et al., 1999; Mohammad et al., 2012). The respective contribution of the GH domains of Fli-I to actin-binding has not been investigated, also its binding strengths to G-, and F-actin are not known.

The actin interactions and activities of Fli-I do not seem to rely on calcium *in vitro*, suggesting its different mode of regulation comparing against the calcium-dependent activation of gelsolin (Goshima et al., 1999; Mohammad et al., 2012). Biochemical analysis revealed that Fli-I retards actin assembly in bulk pyrenyl polymerization experiments and increases the amount of unassembled actin at steady-state, leading to the suggestion that Fli-I acts as a capping protein (Mohammad et al., 2012; Arora et al., 2015). The filament severing activity of Fli-I was proposed based on the appearance of short actin filaments in electron microscopy images in the presence of Fli-I (Goshima et al., 1999). Actively promoting F-actin disassembly by severing is expected to accelerate filament disassembly kinetics in dilution induced bulk depolymerization experiments (Coue and Korn, 1985; Kinosian et al., 1998; Toth et al., 2016). In contrast, Fli-I failed to enhance the rate of filament disassembly in such assays (Mohammad et al., 2012). Thus, albeit several studies have already been performed regarding the effects of Fli-I on actin dynamics, conflicting data exist in the literature; the actin activities of Fli-I and the underlying mechanisms are still largely elusive. To get further insights into the biological functioning of Fli-I we aimed to analyze the biochemical activities of recombinantly produced *Drosophila* proteins including the gelsolin homology domains, as well as the leucine-rich repeat segment. We took advantage of the combination of bulk fluorescence spectroscopy and individual filament total internal reflection fluorescence microscopy (TIRFM) approaches to dissect the activities of different regions of Fli-I in the regulation of actin dynamics. We also investigated the influence of Fli-I on actin cytoskeleton in developing *Drosophila* egg chambers by *in vivo* genetic approaches.

RESULTS

The Gelsolin Homology Domains of Fli-I Interact With Actin and Affect Actin Dynamics in a Calcium-Independent Manner

Calcium-binding of full-length gelsolin is a prerequisite for the activation of its actin interactions and activities (Burtnick et al., 2001; Silacci et al., 2004; Nag et al., 2013; Feldt et al., 2019). Proteolytic cleavage of the protein at the caspase 3 site results in a Ca^{2+}-independent N-terminal (GH13) and a Ca^{2+} dependent C-terminal (GH46) halves (**Figure 1**) (Pope et al., 1991; Kothakota et al., 1997; Silacci et al., 2004; Nag et al., 2013). Comparative sequence analysis of gelsolin and Fli-I reveals that most of the sequence elements responsible for the Ca^{2+}-induced activation of gelsolin (C-terminal helical latch, type 1 and type 2 Ca^{2+}-binding sites) are not conserved in Fli-I (**Figure 2**; Goshima et al., 1999; Nag et al., 2013). Previous work did not find any effect of Ca^{2+} on the actin interactions of Fli-I proteins from mouse and *C. elegans*, supporting that the actin activities of Fli-I do not rely on Ca^{2+}-binding (Goshima et al., 1999;

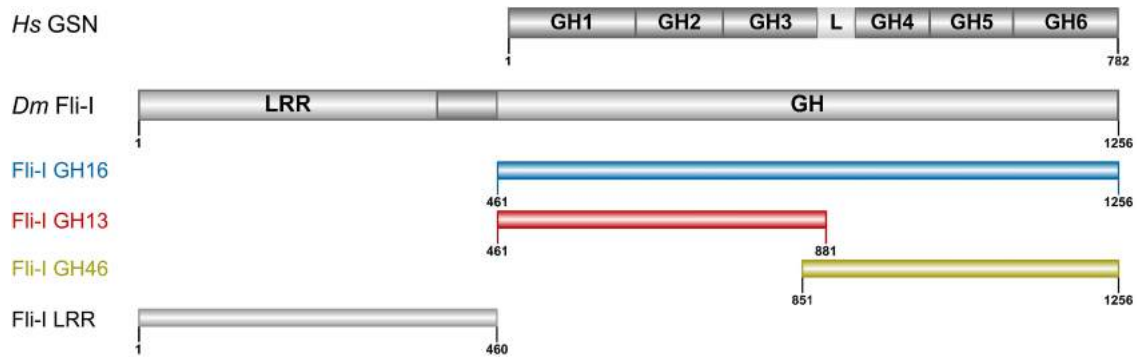

FIGURE 1 | Domain organization of gelsolin and Flightless-I. Domain organization of gelsolin (GSN: 1–782 aa) and the Flightless-I constructs used in our study (Fli-I GH16: 461–1256 aa, GH13: 461–881 aa, GH46: 851–1256 aa, LRR: 1–460 aa). The Figure was made by IBS 1.0.2 (Liu et al., 2015). *Hs, Homo sapiens; Dm, Drosophila melanogaster*; GSN, gelsolin; Fli-I, Flightless-I; GH, gelsolin homology; L, GH3-GH4 linker region; LRR, leucine-rich repeat.

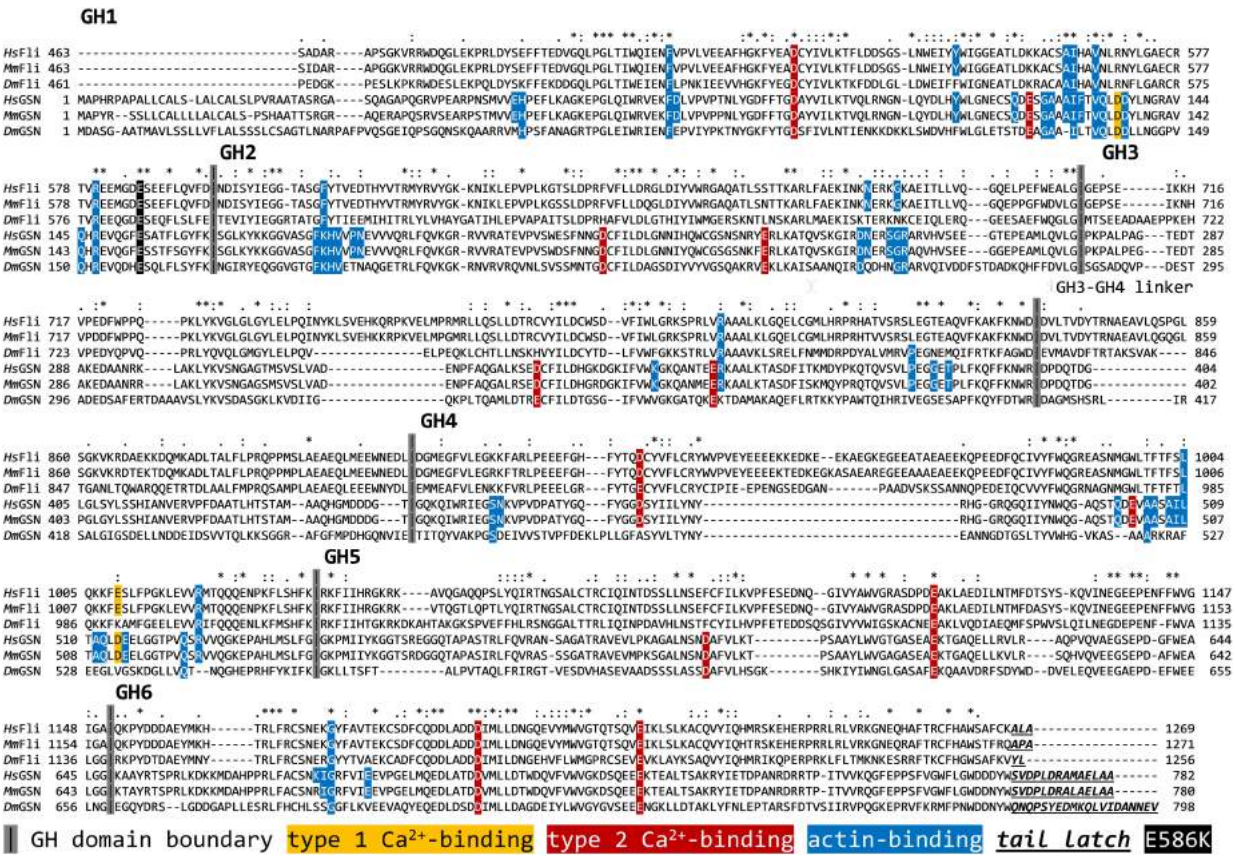

FIGURE 2 | Comparative sequence analysis of the gelsolin homology domains of Fli-I and gelsolin from different species. UniProt IDs: Q13045 (*Hs* Fli-I), Q9JJ28 (*Mm* Fli-I), Q24020 (*Dm* Fli-I), P06396 (*Hs* GSN), P13020 (*Mm* GSN), Q07171 (*Dm* GSN). The analysis was performed by ClustalX. *Hs, Homo sapiens; Mm, Mus musculus; Dm, Drosophila melanogaster*; FliI, Flightless-I; GSN, gelsolin; GH, gelsolin homology.

Mohammad et al., 2012). Based on the above, first we investigated the actin interactions and activities of *Drosophila* Fli-I in the absence and presence of calcium ions (**Figure 3**). A fragment of Fli-I encompassing all the six gelsolin homology domains (GST-GH16) was produced recombinantly as a GST fusion protein, similar to previous approaches (Goshima et al., 1999; Li et al., 2008; Mohammad et al., 2012; **Figure 1**). To dissect the activities of the different regions of the protein, an N- (GST-GH13), and a C-terminal (GST-GH46) GST-tagged segment corresponding to the caspase 3 proteolytic fragments of gelsolin, as well as the isolated leucine-rich repeat region (GST-LRR) were investigated (**Figure 1**).

Gelsolin is known to bind monomeric actin and forms a GA_2 (1 GSN:2 G-actin) complex in a Ca^{2+}-dependent fashion (Coue and Korn, 1985; Selden et al., 1998; Nag et al., 2013). Consistently, by monitoring the steady-state anisotropy of fluorescently labeled G-actin (0.2 μM Alexa488NHS-G-actin) we found that GSN binds weakly to monomeric actin in the absence of Ca^{2+} (1 mM EGTA condition), while the addition of $CaCl_2$ (1 mM) profoundly strengthens the interaction (**Figure 3A**). The break-point titration is consistent with the 1 GSN:2 G-actin stoichiometry, as well as with the high-affinity of the complex. The addition of Fli-I GST-GH16 to monomeric actin, even in the absence of $CaCl_2$ (1 mM EGTA condition) resulted in a significant increase in anisotropy from ∼0.136 (in the absence of GST-GH16) to ∼0.150 (in the presence of ∼1 μM GST-GH16; the maximum amount of protein that could be tested in these experiments) (**Figure 3B**). This result suggests a direct binding between the gelsolin homology domains of Fli-I and G-actin in agreement with previous reports (Liu and Yin, 1998; Goshima et al., 1999; Mohammad et al., 2012). A similar response in a broader concentration range could be detected in the case of Fli-I GST-GH13 (**Figure 3B**). The fit of the anisotropy data gave a dissociation equilibrium constant of $K_{D(Fli-I\ GST-GH13)}$ = 576 ± 182 nM of the Fli-I GST-GH13:G-actin complex (**Figure 3B**, Eq. 3). Analysis of the [GST-Fli-I] dependence of the anisotropy measured in the presence of $CaCl_2$ (1 mM) revealed a similar binding trend and affinity as detected in the absence of the divalent cation, indicating that the interaction of Fli-I with G-actin is not affected by the presence of Ca^{2+} ($K_{D(Fli-I\ GST-GH13)}$ = 638 ± 152 nM, **Figure 3C**). No significant change in anisotropy was found when Fli-I GST-GH46 (∼2 μM) was added to G-actin; either in EGTA or $CaCl_2$ conditions suggesting the lack of actin interaction of this region (**Figures 3B,C**).

Subsequently, the calcium-response of the effects of Fli-I on actin assembly was monitored in pyrenyl polymerization experiments (**Figures 3D–F**). In control measurements, we

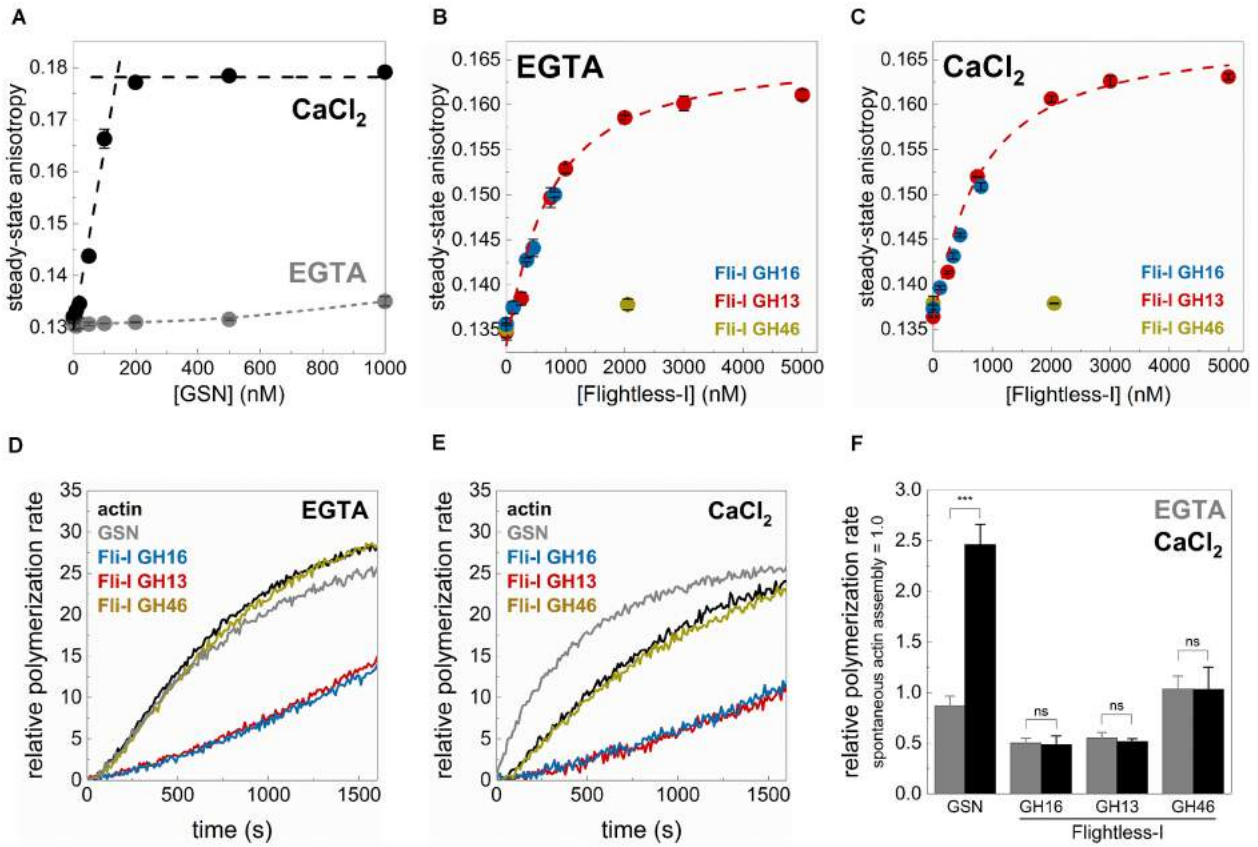

FIGURE 3 | The gelsolin homology domains of Flightless-I influence actin dynamics in a Ca^{2+}-independent manner. **(A)** Steady-state anisotropy of Alexa488NHS-G-actin (0.2 μM) as a function of [GSN] in the presence of 1 mM EGTA (Ca^{2+}-free condition) or 1 mM $CaCl_2$. Black dashed lines show the linear fits to the data measured at low and high [GSN]. The breakpoint was found at [GSN] = 140.05 nM indicating a ∼1 GSN:2 G-actin stoichiometry. Data are shown as mean ± SD, n = 3. **(B,C)** Steady-state anisotropy of Alexa488NHS-G-actin (0.2 μM) as a function of [GST-Fli-I] in the presence of 1 mM EGTA (Ca^{2+}-free condition) **(B)** or 1 mM $CaCl_2$ **(C)**. Red dashed lines show the fit of the data according to Eq. 3. The fit gave the following dissociation equilibrium constants: $K_{D(Fli-I\ GST-GH13)}$ = 576 ± 182 nM (1 mM EGTA), $K_{D(Fli-I\ GST-GH13)}$ = 638 ± 152 nM (1 mM $CaCl_2$). Data are shown as mean ± SD, n = 3. **(D,E)** Representative pyrenyl emission kinetics recorded in the absence or presence of GST-Fli-I (5 nM) or GSN (5 nM) and in the presence of 1 mM EGTA **(D)** or 1 mM $CaCl_2$ **(E)**. Conditions: 2.5 μM actin (5% pyrenyl labeled). **(F)** Relative polymerization rates derived from pyrenyl transients shown on panels **(D,E)**. Data are shown as mean ± SD, n = 2–4. ***$p < 0.001$.

found that gelsolin (5 nM) does not significantly affect actin polymerization in a Ca^{2+}-free environment (1 mM EGTA condition), while it accelerates actin assembly kinetics in the presence of $CaCl_2$ (1 mM) (2.46 ± 0.19-fold increase, n = 2–3, p = 0.001) (**Figures 3D–F**; Yin and Stossel, 1979; Coue and Korn, 1985; Kis-Bicskei et al., 2018). In contrast to the calcium-dependent polymerization promoting effect of GSN, Fli-I GST-GH16 (5 nM) inhibited actin assembly to the same extent both in the absence and presence of Ca^{2+} (n = 2–3, p = 0.554) (**Figures 3D–F**). The inhibitory effect of Fli-I on the rate of actin polymer formation is in agreement with previous reports (Mohammad et al., 2012). Qualitatively and quantitatively the same response was detected for Fli-I GST-GH13 (5 nM) (**Figures 3D–F**). Whereas Fli-I GST-GH46 (5 nM) did not have any effect on actin assembly, independently from the presence of calcium (n = 3, p = 0.976) (**Figures 3D–F**).

Altogether, these observations support that in contrast to gelsolin, the actin-related activities of Fli-I are not regulated by Ca^{2+}-binding. On the other hand, it is important to note that the GH13 region of Fli-I seems to be responsible for the G-actin interaction and the actin assembly inhibition activities of the gelsolin homology domains of the protein.

The Gelsolin Homology Domains of Fli-I Affect Actin Assembly From Free G-Actin That Relies on the GH13 Regions

To address the biochemical activities of Fli-I in actin dynamics, the effects of Fli-I on actin assembly kinetics from free G-actin were further investigated in bulk pyrenyl polymerization experiments (**Figure 4**). The data revealed that the effects of Fli-I GST-GH16 on polymer formation from free G-actin follow a biphasic concentration-response. At lower concentrations (<∼10 nM) it inhibits actin polymerization; in contrast, at higher concentrations of Fli-I GST-GH16 (>∼25 nM) the inhibition was less pronounced (**Figures 4A,E**). We found that Fli-I GST-GH13 can influence actin dynamics in a qualitatively and quantitatively similar manner as Fli-I GST-GH16 (**Figures 4B,E**). Larger concentrations of GST-GH13 (>∼100 nM) even accelerates polymerization above the spontaneous rate (**Figures 4B,E**). Based on the tendency; this behavior would be expected of GST-GH16 if higher concentrations could be tested in the experiments. In contrast, the GST-GH46 region does not affect actin polymerization in the concentration range in which the two other fragments of Fli-I were tested (**Figures 4C,E**). These results are consistent with our previous data and demonstrate that the actin activities of Fli-I GST-GH16 are reconstituted by the GST-GH13 segment, while the GST-GH46 region is not able to interact with actin. Moreover, the biphasic nature of the effect of Fli-I GST-GH13/GST-GH16 on polymerization kinetics suggests multiple activities in actin dynamics.

We also tested whether the isolated leucine-rich repeat of Fli-I interacts with actin. In steady-state anisotropy measurements, no significant change was detected upon titration of G-actin (0.2 μM Alexa488NHS-G-actin) with Fli-I GST-LRR (r = 0.130 ± 0.001 in the absence of GST-LRR and r = 0.130 ± 0.001 in the presence of 800 nM GST-LRR). Also, Fli-I GST-LRR does not affect actin assembly in bulk pyrenyl polymerization experiments (**Figures 4D,E**). These observations indicate that similarly to GH46, the isolated LRR does not interact with actin (Liu and Yin, 1998).

The Gelsolin Homology Domains of Fli-I Inhibit Actin Filament Growth by Barbed End Capping

The polymerization inhibition that we observe at low nM concentrations of Fli-I reflects high-affinity interactions and can result from the prevention of subunit addition to filament ends. This can be manifested by capping through filament end interactions, but also by sequestration upon binding to monomeric actin. On the other hand, some proteins by interacting with fluorescently labeled actin (e.g., by pyrene, IAEDANS) can modify its structural properties resulting in a change in the spectral characteristics of the actin-bound fluorophore (e.g., Leiomodin (Lmod), Wiskott-Aldrich Syndrome Homology 2 domains of Sarcomere Length Short (SALS-WH2) (Toth et al., 2016; Szatmari et al., 2017). This effect could result in an apparent change in pyrenyl kinetics even in the absence of any functional effects on actin polymerization.

To elaborate on the mechanisms underlying the polymerization inhibition activity of Fli-I, actin assembly was visualized at the level of individual polymers by using total internal reflection fluorescence microscopy (**Figures 5A,B**). In control samples, polymers were nucleated spontaneously and elongated at a rate of v = 4.61 ± 0.36 subunit × s^{-1} (n = 23) that corresponds to the well-established barbed end association rate constant of free G-actin (k_+ = 11.53 ± 0.90 $\mu M^{-1}s^{-1}$; Pollard, 2007; Bugyi and Carlier, 2010). Addition of Fli-I GST-GH16 (10 nM) to actin resulted in almost complete inhibition of polymer growth (0.24 ± 0.10 subunit × s^{-1}, n = 39, $p \leq 0.0001$). Consistently with the observations made in the fluorescence spectroscopy experiments, the effects of Fli-I GST-GH16 on polymer assembly can be recapitulated by Fli-I GST-GH13; as 10 nM GST-GH13 resulted in a similar inhibition as observed for 10 nM GST-GH16 (v = 0.28 ± 0.12 subunit × s^{-1}, n = 33, p = 0.158). Also, we found that Fli-I GST-GH46 does not have significant effect on polymer growth rate in TIRFM assays (v = 4.56 ± 0.30 subunit × s^{-1}, n = 20, p = 0.589). Altogether, the TIRFM data support the results obtained from pyrenyl fluorescence experiments: low amounts of Fli-I inhibits actin assembly and this activity relies on the GH13 segment of the protein.

Based on the experimental conditions in our TIRFM assays (0.5 μM free G-actin; below the pointed end critical concentration), actin polymer growth is dominated by barbed end assembly. Considering the dissociation equilibrium constant of the GST-Fli-I:G-actin interaction derived from anisotropy measurements (**Figures 3B,C**), 10 nM Fli-I – which causes polymer growth inhibition in TIRFM experiments – is expected to bind to ∼1% of the G-actin; i.e., ∼5 nM. This would result in a negligible reduction (∼1.4%) in the polymer growth rate as predicted by Eq. 4. Thus, G-actin sequestration that relies on monomer binding by Fli-I does not explain the marked polymerization inhibition observed at nanomolar

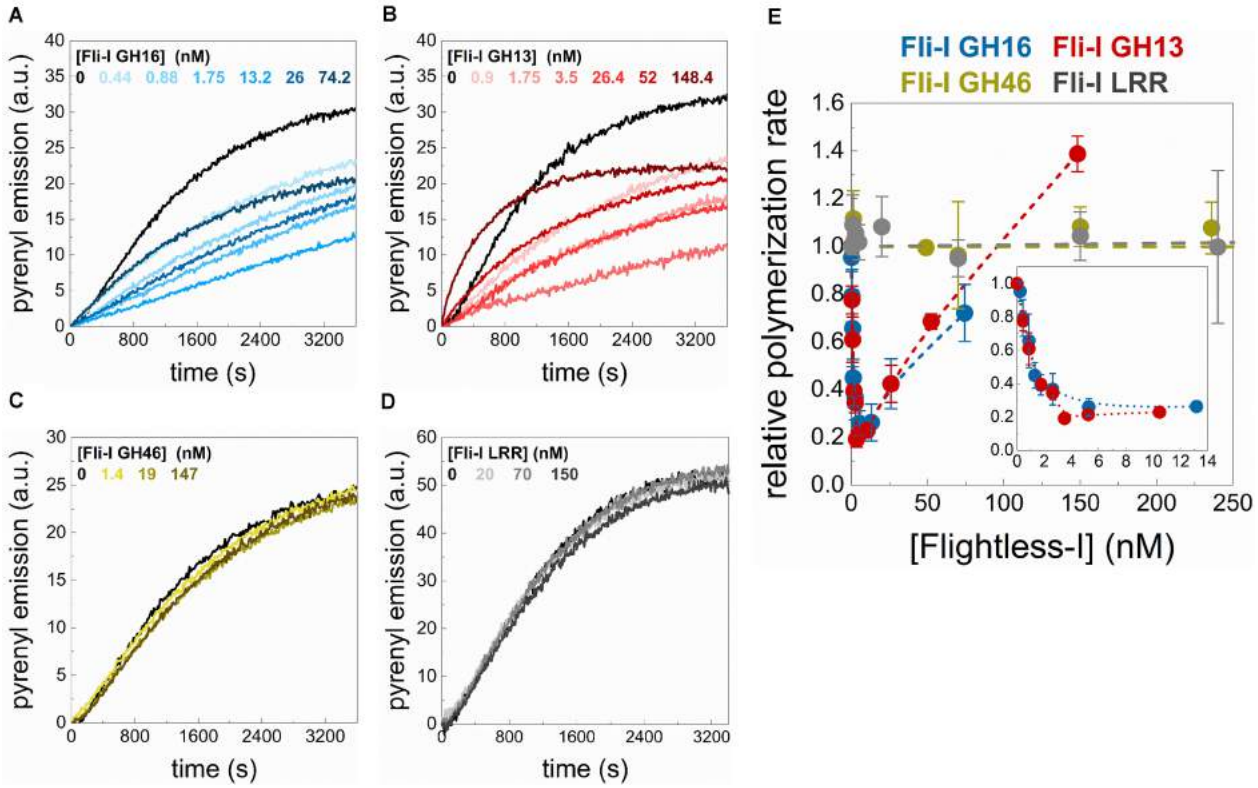

FIGURE 4 | The gelsolin homology domains of Flightless-I affect actin assembly that relies on its GH13 domains. **(A–D)** Representative pyrenyl fluorescence emission kinetics recorded in the absence or presence of different concentrations of GST-Fli-I constructs. Conditions: 2.5 μM actin (5% pyrenyl labeled). **(E)** Relative polymerization rate as a function of [GST-Fli-I]. Data are shown as mean ± SD, n = 2–7. Inset: enlarged view of the data corresponding to low [GST-Fli-I] (<14 nM).

protein concentrations. Consequently, our data point toward barbed end related activities. To experimentally address this issue, the end-to-end annealing of preformed, mechanically fragmented filaments was monitored by dual-color TIRFM (**Figures 5C,D**). In the absence of Fli-I the spontaneous lengthwise association, i.e., annealing of the actin filament fragments was supported by the increase in filament length with time, as well as by the appearance of spectrally inhomogeneous filaments. In the presence of either Fli-I GST-GH16 or GST-GH13 (120 nM) the filaments remained short and were characterized by homogeneous fluorescence emission indicating that annealing is inhibited by these constructs. No such inhibitory effect was detected when Fli-I GST-GH46 was added to actin, in agreement with our previous observations.

Collectively, these data show that Fli-I possesses a filament end capping activity and support that the inhibition of actin assembly by Fli-I results from the prevention of actin incorporation at the barbed ends.

The Gelsolin Homology Domains of Fli-I Do Not Sever Filaments but Facilitate the Formation of Nucleation Intermediates

Pyrenyl polymerization experiments revealed that the addition of larger amounts of Fli-I resulted in facilitated polymerization (**Figures 4A,B,E**) that might result from cutting of the actin filaments thereby generating more ends for elongation (severing) and/or enhanced nucleation. To test the severing ability of Fli-I, dilution-induced bulk disassembly kinetics measurements were performed (**Figures 6A,B**). In control experiments we found that the spontaneous disassembly of actin filaments is relatively slow, in contrast, gelsolin (5 nM, in the presence of 1 mM $CaCl_2$) accelerated disassembly kinetics by ∼50-fold consistently with its severing activity (**Figures 6A,B**; Kinosian et al., 1998; Nag et al., 2013; Toth et al., 2016). In the presence of GST-Fli-I at a concentration that can enhance actin polymerization in pyrenyl fluorescence experiments (105 nM, **Figure 4E**) no significant increase in the rate of filament disassembly was observed as compared to spontaneous depolymerization, neither in the absence (*data not shown*) nor in the presence of 1 mM $CaCl_2$ (**Figures 6A,B**). As an alternative approach, the disassembly efficiency of gelsolin and GST-Fli-I was also visualized in TIRFM experiments by adding the proteins to preassembled filaments (**Figures 6C,D**). The disassembly activity was quantified by measuring the area covered by filamentous actin after 5 min following gelsolin or GST-Fli-I addition. The presence of gelsolin (0.5 nM, in the presence of 1 mM $CaCl_2$) resulted in a marked decrease in the filament area as compared to the control (A_{actin} = 337.47 ± 84.92 μm^2, n = 10, A_{GSN} = 165.95 ± 49.05 μm^2, n = 12, $p \leq 0.0001$). In contrast,

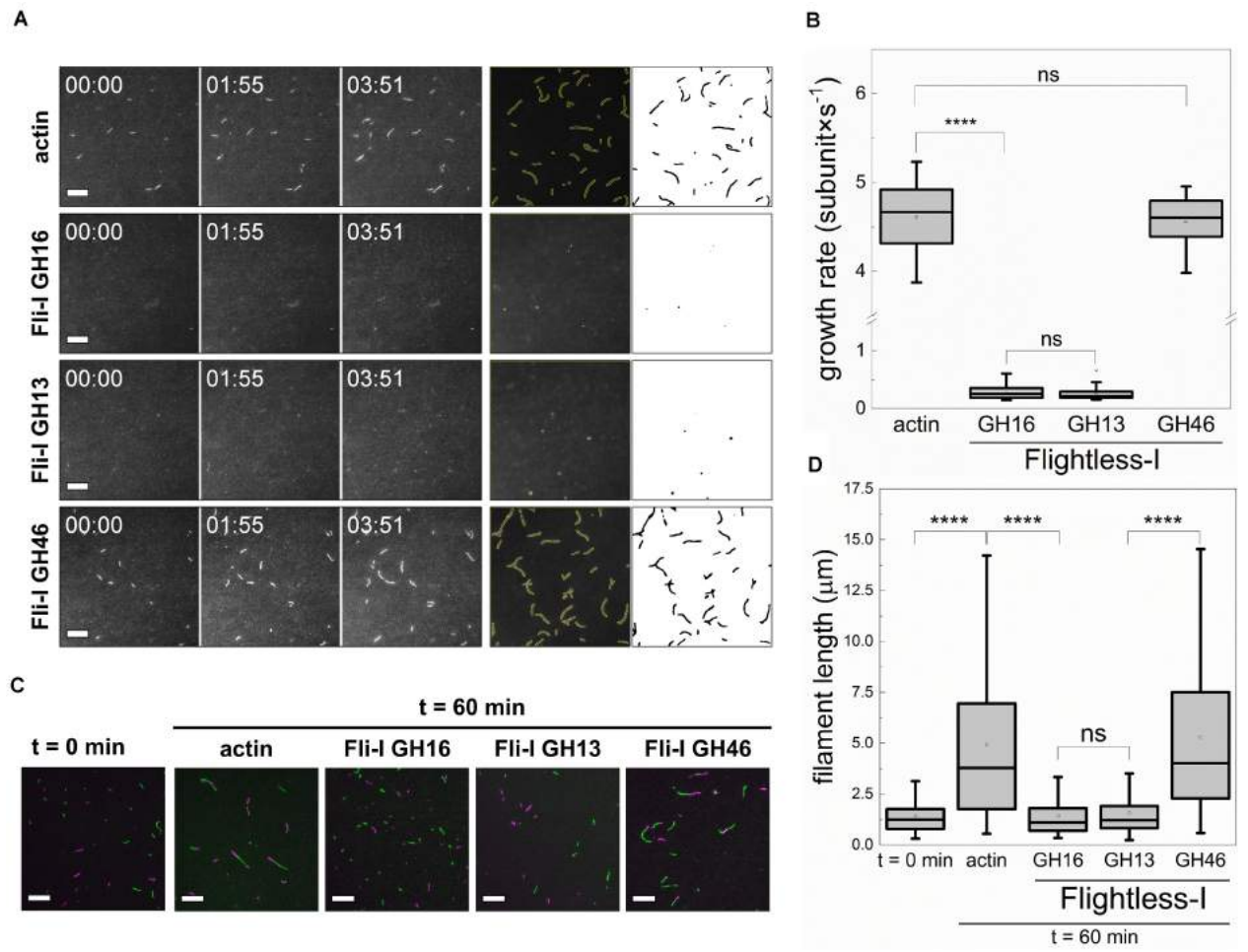

FIGURE 5 | The gelsolin homology domains of Flightless-I inhibit actin filament growth by barbed end capping. **(A)** Left panels: Representative montages of actin assembly followed by TIRFM in the absence or presence of GST-Fli-I. Right panels: Representative skeletonized TIRFM images used for analysis showing the field of view of a 66 × 66 μm^2 region in the absence or presence of GST-Fli-I. Conditions: [actin] = 0.5 μM (10% Alexa488NHS labeled), [Fli-I GST-GH16] = 10 nM, [Fli-I GST-GH13] = 10 nM, [Fli-I GST-GH46] = 100 nM. Scale bar = 10 μm, time = min:s. **(B)** Filament growth rate from G-actin in the absence or presence of different GST-Fli-I constructs derived from time-lapse TIRFM images shown on **(A)**, n = 20–60. **(C)** Representative montage of actin filament end-to-end annealing followed by TIRFM in the absence or presence of different GST-Fli-I constructs. The t = 0 min corresponds to the initial fragmentation of filaments, while t = 60 min indicates the time interval after fragmentation. Conditions: [actin] = 0.5 μM (10% Alexa488NHS and 10% Alexa568NHS labeled), [GST-Fli-I] = 120 nM. Scale bar = 10 μm. **(D)** Filament length at t = 0 min and 60 min in the absence or presence of GST-Fli-I, derived from TIRFM images shown on **(C)**, $n_{samples}$ = 3–9, $n_{Filaments}$ = 136–174. $^{****}p < 0.0001$.

addition of either the GST-GH16 or GST-GH13 fragments of Fli-I (105 nM) did not influence significantly this parameter ($A_{Fli-I\ GST-GH16}$ = 373.44 ± 38.458 μm^2, n = 14, p = 0.224, $A_{Fli-I\ GST-GH13}$ = 370.31 ± 54.58 μm^2, n = 12, p = 0.373). Based on these results, we conclude that, in contrast to gelsolin, the gelsolin homology domains of Fli-I do not possess actin filament severing activity.

Considering the monomer binding ability of Fli-I revealed by anisotropy measurements, we hypothesized that the assembly promoting activity of Fli-I results from its ability to *de novo* nucleate actin filaments, similarly to gelsolin (Burtnick et al., 2001; Nag et al., 2013; Kis-Bicskei et al., 2018). To test the nucleation ability of Fli-I the number of actin filaments formed in the absence or presence of Fli-I GST-GH16 was measured at steady-state by TIRFM (**Figures 6E,F**). For this purpose, actin filaments were allowed to form spontaneously or in the presence of a relatively high concentration of Fli-I GST-GH16 (800 nM) overnight, followed by phalloidin stabilization and dilution. In the absence of Fli-I GST-GH16, the number of actin filaments was found to be N = 11.78 ± 5.12, while Fli-I GST-GH16 increased this parameter significantly by ∼4-fold (N = 49.06 ± 15.20, $p \leq 0.0001$) (**Figure 6F**). On the other hand, the steady-state filament length was markedly reduced in the presence of Fli-I GST-GH16 as compared to the control, further supporting the polymerization inhibitory activity of Fli-I (**Figure 6G**). Due to the inhibited lengthening of the filaments by Fli-I, the size of some filaments may be under the resolution limit of the microscope, therefore filament number is expected

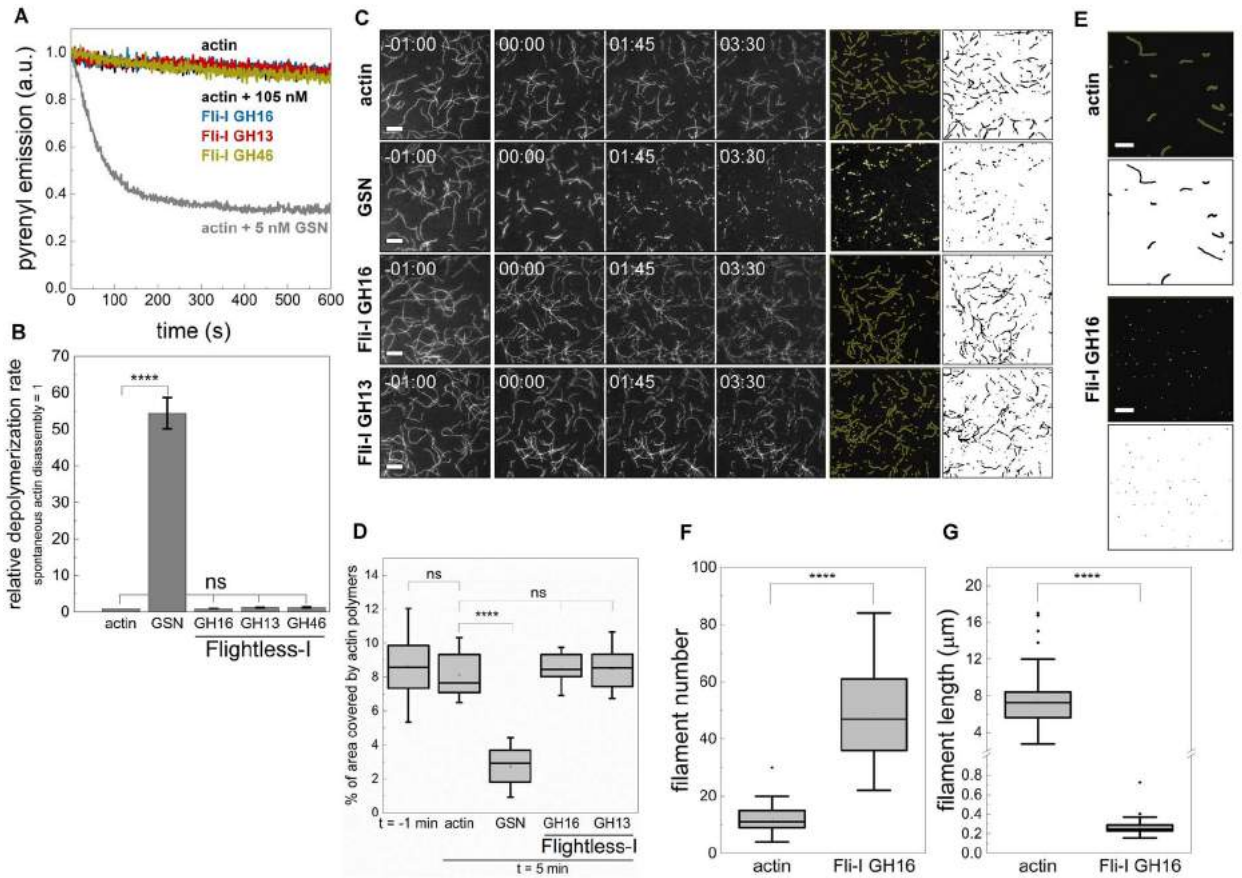

FIGURE 6 | The gelsolin homology domains of Flightless-I do not sever filaments but facilitate the formation of nucleation intermediates. **(A)** Kinetics of actin polymer disassembly as followed by the decrease in pyrenyl fluorescence emission in the absence or presence of GST-Fli-I or GSN. Conditions: [actin] = 50 nM (50% pyrenyl labeled), [GSN] = 5 nM, [GST-Fli-I] = 105 nM, [$CaCl_2$] = 1 mM. Note that the depolymerization of F-actin in the absence (actin; black line) and presence of different GST-Fli-I constructs (105 nM; blue, red and yellow traces, as indicated) follow similar kinetics; the pyrenyl traces largely overlap. While that of recorded in the presence of GSN (5 nM; gray) differs significantly. **(B)** Relative depolymerization rate derived from the pyrenyl transients shown on panel **(A)**, n = 2–3. **(C)** Left panels: Representative montages of actin disassembly followed by TIRFM in the absence or presence of GST-Fli-I or GSN. The frames labeled by -01:00 and 00:00 show the field of view just before and right after the addition of GSN or GST-Fli-I, respectively. Right panels: Representative skeletonized TIRFM images used for filament area analysis showing the field of view of a 66 × 66 μm^2 region in the absence or presence of GSN or GST-Fli-I. Conditions: [actin] = 0.5 μM (10% Alexa488NHS labeled), [GSN] = 0.5 nM, [GST-Fli-I] = 105 nM. Scale bar = 10 μm, time = min:s. **(D)** Percent of the area covered by actin filaments 5 min after the addition of GSN or GST-Fli-I derived from TIRFM images shown on **(C)**, n = 12–51. **(E)** Representative skeletonized TIRFM images used for filament number and length analysis showing the field of view of a 66 × 66 μm^2 region in the absence or presence of Fli-I GST-GH16. Conditions: [actin] = 2 μM (10% Alexa488NHS labeled), [Fli-I GST-GH16] = 800 nM. Scale bar = 10 μm. **(F)** Number of filaments assembled from G-actin either spontaneously or in the presence of Fli-I GST-GH16 derived from TIRFM images shown on **(E)**, n = 69–73. **(G)** Filament length assembled from G-actin either spontaneously or in the presence of Fli-I GST-GH16 derived from TIRFM images shown on **(E)**, n = 69–73. ****$p < 0.0001$.

to be underestimated in our experiments. Thus, it appears that when present at relatively high concentrations, Fli-I can promote actin assembly at a moderate level by facilitating the *de novo* formation of nucleation intermediates that is attributed to its relatively low-affinity monomer binding.

Profilin Supports Barbed End Capping but Interferes With Monomer Binding of Fli-I

Cellular actin structures are built from profilin:G-actin (PA), therefore we aimed to investigate whether the presence of profilin influences the actin assembly activities of Fli-I. In pyrenyl polymerization experiments, we found that both Fli-I GST-GH16 and GST-GH13 inhibit the assembly of profilin:G-actin at subnanomolar concentrations (**Figures 7A–D**). However, in contrast to their effects on the assembly of free G-actin, they failed to increase the bulk polymerization rate of profilin:G-actin at higher concentrations. The analysis of the GST-Fli-I concentration dependence of the bulk polymerization rate gave half-inhibitory concentration values of $IC_{50(\text{Fli}-\text{I GST}-\text{GH16})}$ = 0.93 ± 0.12 nM and $IC_{50(\text{Fli}-\text{I GST}-\text{GH13})}$ = 0.13 ± 0.01 nM (**Figure 7D**, Eq. 1). These data indicate that Fli-I prevents the assembly of profilin:G-actin with high-affinity barbed end capping. Similar to the lack of the effect of Fli-I GST-GH46 on actin assembly from free

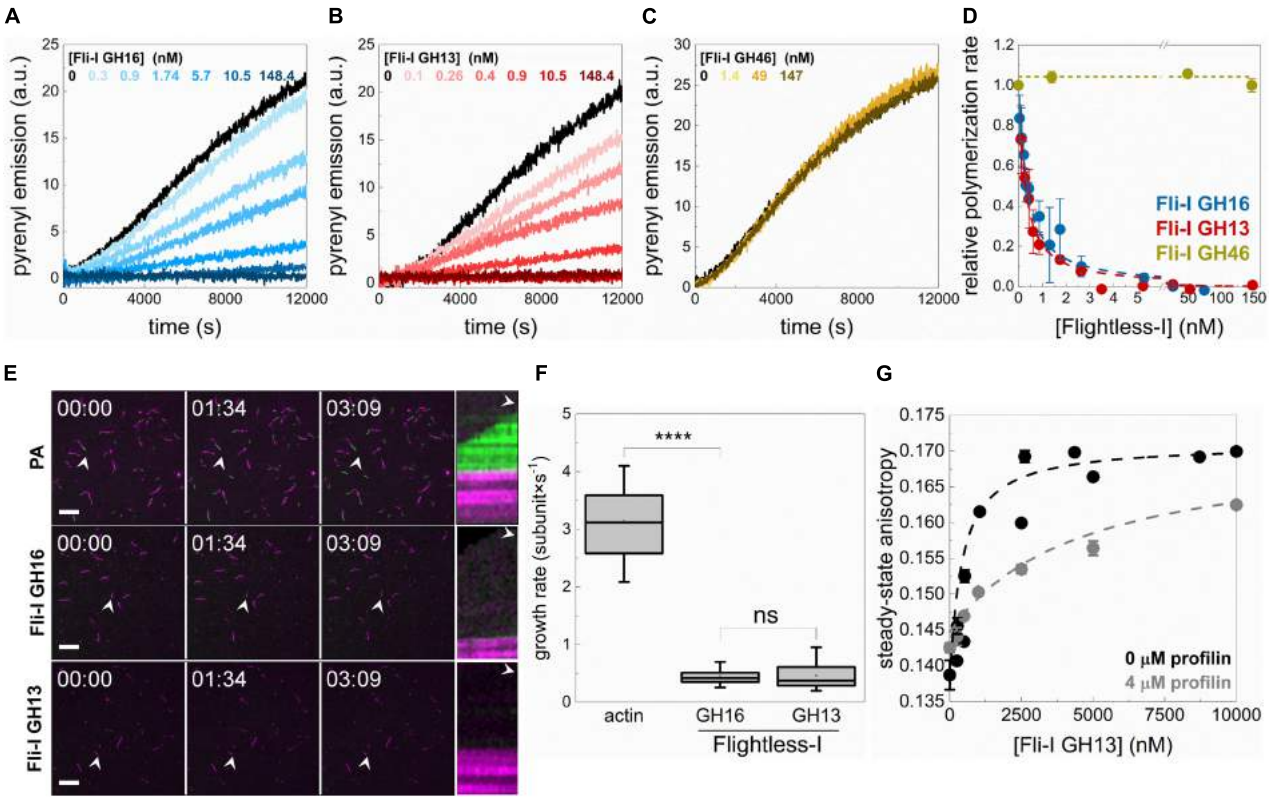

FIGURE 7 | Profilin supports barbed end capping but interferes with the monomer binding activity of Flightless-I. **(A–C)** Polymerization kinetics of profilin:G-actin (PA) followed by the change in pyrenyl emission in the absence or presence of different concentrations of GST-Fli-I. Conditions: [actin] = 2.5 μM (2% pyrenyl labeled), [profilin] = 6 μM. **(D)** Relative polymerization rate as a function of [GST-Fli-I]. Data are shown as mean ± SD, n = 2–7. Blue and red dashed lines show the fit to the data (Eq. 1). The fit gave $IC_{50(Fli\text{-}I\ GST\text{-}GH16)}$ = 0.93 ± 0.12 nM and $IC_{50(Fli\text{-}I\ GST\text{-}GH13)}$ = 0.13 ± 0.01 nM. **(E)** Representative montages of profilin:actin (PA) assembly (green) from preformed F-actin seeds (magenta) followed by TIRFM in the absence or presence of GST-Fli-I. Arrowheads highlight the filaments that were tracked for kymographs. Conditions: [actin] = 0.5 μM (10% Alexa488NHS or Alexa568NHS labeled), [profilin] = 2 μM, [GST-Fli-I] = 10 nM. Scale bar = 10 μm, time = min:s. **(F)** Filament growth rate from profilin:actin in the absence or presence of GST-Fli-I derived from time-lapse TIRFM images shown on **(E)**, n = 37–62. **(G)** Steady-state anisotropy of Alexa488NHS-G-actin (0.2 μM) in complex with profilin (4 μM) as a function of [GST-Fli-I]. Data are shown as mean ± SD, n = 2–3. Dashed lines in the corresponding color show the fit of the data according to Eq. 3. The fit gave dissociation equilibrium constants of $K_{D(Fli\text{-}I\ GST\text{-}GH13)}$ = 411.43 ± 22.69 nM (in the absence of profilin) and $K_{D(Fli\text{-}I\ GST\text{-}GH13)}$ = 4511.6 ± 631.92 nM (in the presence of profilin). ****$p < 0.0001$.

G-actin, this construct failed to influence the polymerization of profilin:G-actin (**Figures 7C,D**).

Dual-color TIRFM experiments performed to study profilin:G-actin assembly corroborated our observations made in spectroscopic assays (**Figures 7E,F**). Polymer growth (**Figure 7E**, green portion) was observed from preformed F-actin seeds (**Figure 7E**, magenta portion) both in the absence and presence of Fli-I. In control samples, profilin:G-actin assembled at the barbed ends of preformed F-actin actin seeds at a rate of v_{PA} = 3.14 ± 0.58 subunit × s^{-1} (n = 37) that is consistent with the slightly reduced association rate constant of profilin:G-actin to the barbed ends as compared to free G-actin (k_+ = 7.86 ± 1.45 subunit × s^{-1}; Barko et al., 2010; Toth et al., 2016; Vig et al., 2017; **Figure 7F**). In the presence of Fli-I GST-GH16 (10 nM) or GST-GH13 (10 nM) the number of elongating barbed ends, as well as the rate of profilin:G-actin association to F-actin seeds was severely reduced [$v_{Fli-I\ GST-GH16}$ = 0.45 ± 0.14 subunit × s^{-1} (n = 62, $p \leq 0.0001$), $v_{Fli-I\ GST-GH13}$ = 0.46 ± 0.23 subunit × s^{-1} (n = 57)] (**Figures 7E,F**).

The lack of the polymerization promoting effect that we detect in the presence of profilin indicates that the interaction of Fli-I with monomeric actin is modulated by profilin. To test this, the steady-state anisotropy of fluorescently labeled actin (0.2 μM Alexa488NHS-G-actin) in complex with profilin (4 μM) was measured upon titration with Fli-I GST-GH13 (**Figure 7G**). The analysis revealed that the binding strength of Fli-I GST-GH13 to profilin:G-actin is markedly reduced ($K_{D(Fli-I\ GST-GH13)}$ > 4 μM) as compared to that of free G-actin ($K_{D(Fli-I\ GST-GH13)}$ ~500–600 nM, **Figures 3B,C**, **7G**). These observations are consistent with the ability of profilin to inhibit Fli-I:G-actin interaction and suggest that Fli-I and profilin bind to monomeric actin in a competitive fashion.

The Influence of the GST Fusion on the Actin Activities of Fli-I

Although previous studies (Goshima et al., 1999; Li et al., 2008; Mohammad et al., 2012), as well as our initial set

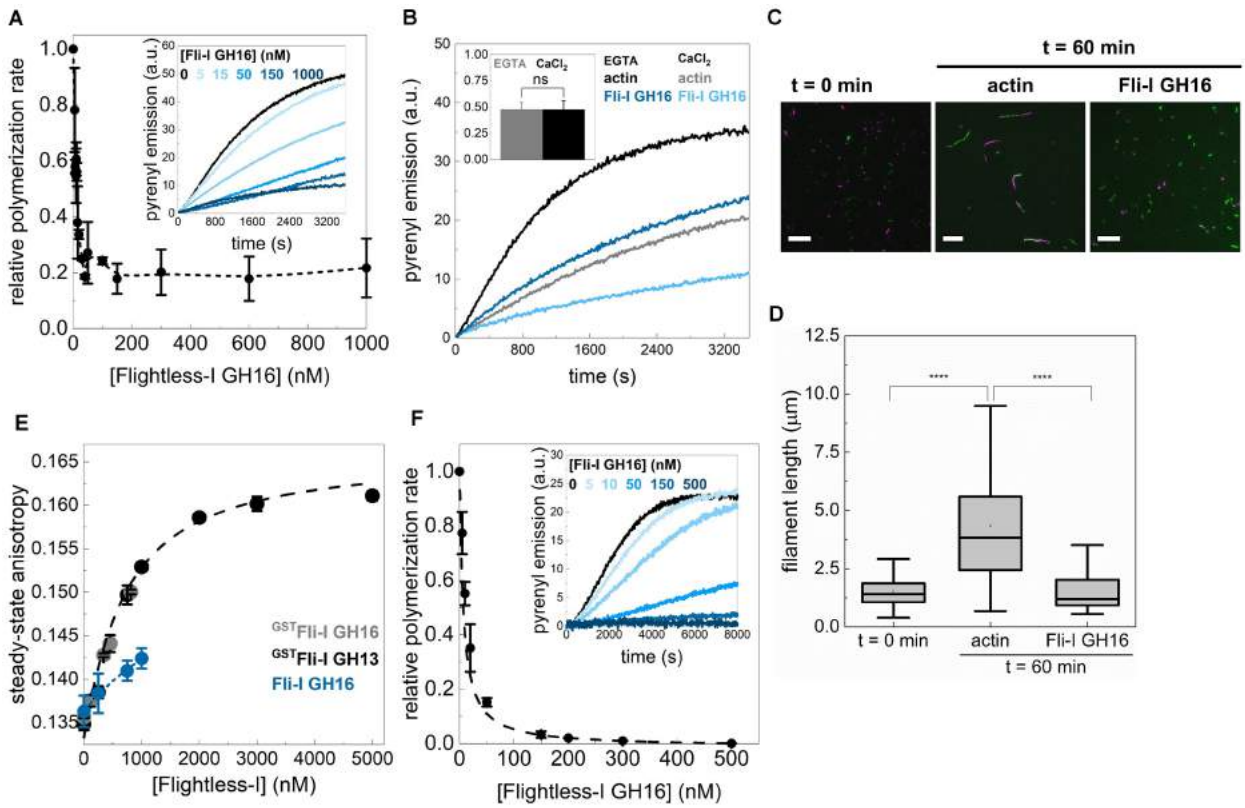

FIGURE 8 | The influence of the GST fusion on the actin activities of Flightless-I. **(A)** Relative polymerization rate as a function of [Fli-I GH16]. Data are shown as mean ± SD, n = 2–7. Inset: representative pyrenyl fluorescence emission kinetics recorded in the absence or presence of different concentrations of Fli-I GH16. Conditions: 2.5 μM actin (5% pyrenyl labeled). **(B)** Representative pyrenyl emission kinetics recorded in the absence or presence of Fli-I GH16 (14 nM) and in the presence of 1 mM EGTA or 1 mM $CaCl_2$. Conditions: 2.5 μM actin (5% pyrenyl labeled). Inset: Relative polymerization rates derived from pyrenyl transients. Data are shown as mean ± SD, n = 2–4. **(C)** Representative montage of actin filament end-to-end annealing followed by TIRFM in the absence or presence of Fli-I GH16. The t = 0 min corresponds to the initial fragmentation of filaments, while t = 60 min indicates the time interval after fragmentation. Conditions: [actin] = 0.5 μM (10% Alexa488NHS and 10% Alexa568NHS labeled), [Fli-I GH16] = 100 nM. Scale bar = 10 μm. **(D)** Filament length at t = 0 min and 60 min in the absence or presence of Fli-I GH16, derived from TIRFM images shown on **(C)**, $n_{samples}$ = 5–10, $n_{Filaments}$ = 100–292. **(E)** Steady-state anisotropy of Alexa488NHS-G-actin (0.2 μM) as a function of [Fli-I GH16] in the presence of 1 mM EGTA. The datasets shown in black and gray are shown for comparison and the same as presented in **Figure 3B**. Data are shown as mean ± SD, n = 3. **(F)** Relative polymerization rate of profilin:G-actin as a function of [Fli-I GH16]. Data are shown as mean ± SD, n = 2–4. Inset: representative pyrenyl fluorescence emission kinetics recorded in the absence or presence of different concentrations of Fli-I GH16. Conditions: 2.5 μM actin (5% pyrenyl labeled), [profilin] = 6 μM. Dashed line shows the fit to the data (Eq. 1). The fit gave $IC_{50(Fli\text{-}IGH16)}$ = 6.92 ± 0.03 nM. ****$p < 0.0001$.

of experiments, were carried out by using GST-tagged Fli-I proteins, as an additional control, we wanted to check the potential of GST to influence the activities of Fli-I on actin dynamics (**Figure 8**). We found that Fli-I GH16 lacking the GST-tag inhibits actin assembly kinetics in a calcium-independent fashion, and also the end-to-end annealing of actin filaments at nM concentrations (**Figures 8A–D**). This is nearly identical to our results with the GST fusion construct, and therefore these observations corroborate the high-affinity barbed end capping of the native gelsolin homology domains of Fli-I. However, higher concentrations of the tag-free Fli-I GH16 (∼1 μM, the maximum amount that could be tested in the experiments) only modestly increased the rate of pyrenyl actin assembly (**Figure 8A**, inset dark blue curve), which is weaker than the apparent polymerization promoting effect observed for Fli-I GST-GH16 (**Figures 4A,E**). Although no complete assembly inhibition was observed, the polymerization rate was decreased to ∼20% by the cleaved construct (**Figure 8A**). A similar residual ∼20% polymerization activity was detected in the interim regime (∼5–10 nM) in the presence of Fli-I GST-GH16 (**Figure 4E**, *inset*). To test for G-actin interaction directly, we performed steady-state anisotropy measurements and revealed that, similar to Fli-I GST-GH16, Fli-I GH16 can bind to G-actin, but the removal of the GST-tag attenuates the interaction (**Figure 8E**). Due to the limitation of applying higher protein concentrations, we could not record enough data points for reliable quantitative analysis. Nevertheless, we estimate that the interaction is characterized by an affinity in the few μM range. We also found that the tag-free Fli-I GH16 inhibits completely the assembly of profilin:G-actin (**Figure 8F**). The half-inhibitory concentration was found to be $IC_{50(Fli-IGH16)}$ = 6.92 ± 0.03 nM (**Figure 8F**, Eq. 1). This value is somewhat larger than that of Fli-I GST-GH16; still, it is important to emphasize that it reflects a high-affinity barbed end interaction.

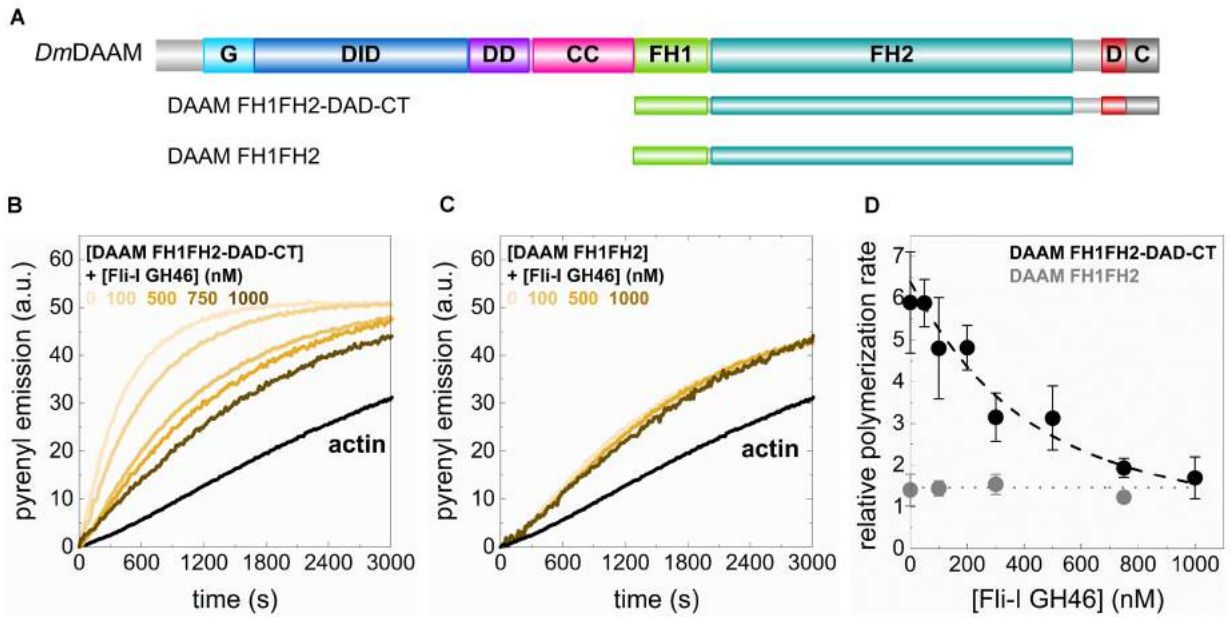

FIGURE 9 | The GH46 domains of Flightless-I interact with the C-terminus of DAAM and negatively regulate its actin assembly activities. **(A)** Domain organization of the DAAM constructs used in our study (DAAM FH1FH2: 552–1054 aa, DAAM FH1FH2-DAD-CT: 552–1153 aa). G, GTPase binding domain; DID, Diaphanous inhibitory domain; DD, dimerization domain; CC, coiled-coil; FH, formin homology domain; D, Diaphanous autoregulatory domain; C, C-terminus. **(B,C)** Representative pyrenyl emission kinetics recorded in the absence or presence of DAAM FH1FH2-DAD-CT or DAAM FH1FH2 at different concentrations of Fli-I GST-GH46. Conditions: 2.5 μM actin (5% pyrenyl labeled), [DAAM] = 250 nM. **(D)** Relative polymerization rates as a function of [Fli-I GST-GH46]. Black dashed line shows the fit of the data according to Eq. 2. The fit gave dissociation equilibrium constant of K_D = 255 ± 189 nM.

These results indicate that caution is highly recommended when interpreting data gathered with GST-tagged proteins. Whereas no qualitative difference was found, it appears that the quantitative nature of the *in vitro* G-actin and filament end interactions of Fli-I are influenced by the GST tag. This effect might be explained by GST-mediated stabilization of the protein structure or GST-facilitated dimerization (Gould et al., 2011; Bell et al., 2013; Zhao et al., 2013). Nonetheless, based on the above comparison of the *in vitro* properties of the GST-tagged versus GST-cleaved versions of Fli-I GH16 we conclude that the calcium-independent high-affinity barbed end capping activity and the lower-affinity monomer binding ability of the gelsolin homology domains are retained in the native, GST cleaved state, and for this reason, our major conclusions do not require modifications.

The GH46 Domains of Fli-I Interact With the C-Terminus of DAAM and Negatively Regulate Its Actin Assembly Activities

In the above experiments, we did not detect any direct actin interactions or activities of the GH46 domains of Fli-I. Previously, the GH46 region of the human Fli-I protein was shown to interact with the C-terminal Diaphanous autoinhibitory domain (DAD) of human mDia1 and Disheveled-associated activator of morphogenesis (Daam) 1 formins *in vitro*, and proposed to enhance their actin assembly promoting activities (Higashi et al., 2010). The interaction was found to be specific to Fli-I since the binding was not detected for the GH46 domains of gelsolin. Based on this we sought to investigate the effects of Fli-I GST-GH46 on *Drosophila* DAAM catalyzed actin assembly. An N-terminally truncated, constitutively active DAAM construct comprising the formin homology (FH) domains, FH1 and FH2 and the C-terminal DAD-CT regions (FH1FH2-DAD-CT), as well as the isolated DAAM FH1FH2 domains, were studied in pyrenyl polymerization experiments (**Figure 9A**; Matusek et al., 2008; Barko et al., 2010; Vig et al., 2017). Our previous work showed that the FH1FH2-DAD-CT of DAAM is more potent in promoting actin assembly as compared to FH1FH2 due to the presence of the DAD-CT region (Vig et al., 2017; **Figures 9B,C**). We found that while Fli-I GST-GH46 does not influence FH1FH2-mediated actin polymerization, it inhibits the DAAM FH1FH2-DAD-CT-catalyzed actin assembly in a concentration-dependent fashion (**Figures 9B,C**). At maximum saturation, the assembly rate corresponded to that of characteristic to DAAM FH1FH2 (**Figure 9D**). Analysis of the data gave the dissociation equilibrium constant of the Fli-I GST-GH46:DAAM interaction of K_D = 255 ± 189 nM (Eq. 2).

These results indicate that Fli-I GST-GH46 binds to DAAM through the DAD-CT region, which is in agreement with previous findings (Higashi et al., 2010) and reveal that the interaction is conserved from fruitfly to human. On the other hand, our data suggest that the binding of Fli-I to DAAM inhibits the contribution of DAD-CT to the actin assembly promoting

activity of FH1FH2 (Vig et al., 2017) and thereby negatively regulates the effect of DAAM on actin polymerization.

Fli-I GH13 Disrupts the Actin Cytoskeleton *in vivo*

To assess the *in vivo* significance of our *in vitro* findings, we tested the effect of Fli-I overexpression in developing *Drosophila* egg chambers. A wild type egg chamber is composed of 16 germ cells (the oocyte and 15 nurse cells) surrounded by the somatic follicle cells forming a single cell layer around the oocyte and the nurse cells (**Figures 10A,A'**). Stage 10B egg chambers contain various types of actin-rich structures such as a prominent cortical actin network, ring canals and a nuclear positioning stress fiber-like system in the nurse cells (**Figures 10A,A'**). Because Fli-I is not known to contribute to the formation of these actin structures (Perrimon et al., 1989; Campbell et al., 1993), the egg chamber appeared as a suitable model system to study the consequences of ectopic expression of Fli-I in an *in vivo* system. To this end, we created transgenic lines for Fli-I GH16, GH13 and GH46 under UAS control and expressed the proteins with *mat-tub4-Gal4* in the germline cells of the ovary. Overexpression of a UAS-LacZ control line had no effect on actin organization of the egg chambers (n = 45) (**Figures 10B,B'**), whereas that of GH16 (n = 39) and GH13 (n = 42) caused a severe disruption of the cortical actin network of the nurse cells in every egg chamber examined, often resulting in giant nurse cells with multiple nuclei due to fusion of their cytoplasm (**Figures 10C–D'**). In addition, we observed markedly reduced actin accumulation around the ring canals and largely reduced levels of the nuclear positioning actin cables (**Figures 10C–D'**). By contrast, expression of GH46 did not influence actin organization in the nurse cells or the oocyte (n = 43) (**Figures 10E,E'**). These observations suggest that the presence of GH13 interferes with the formation of various types of actin cables, while GH46 has no such an effect. This effect of GH13 is entirely consistent with the *in vitro* barbed end capping activity of GH13 that provides a plausible molecular mechanism for the *in vivo* effect. Thus, we conclude that our *in vitro* and *in vivo* data both support that of the truncated Fli-I GH domains GH13 is a potent inhibitor of actin polymerization whereas GH46 does not contribute to actin interaction.

DISCUSSION

We have analyzed the activities of *Drosophila* Fli-I in actin dynamics *in vitro* by using a combination of bulk fluorescence and individual filament approaches. We found that the gelsolin homology domains of Fli-I possess calcium-independent activities in the regulation of actin dynamics, in agreement with previous reports (**Figure 3**; Goshima et al., 1999; Mohammad et al., 2012). The experimental data agree well with the bioinformatics analysis that predicts the lack of the conservation of structural elements in Fli-I essential for the calcium-dependent regulation of gelsolin (Goshima et al., 1999; Mohammad et al., 2012; Nag et al., 2013; **Figure 2**). The calcium insensitivity of the Fli-I:actin interaction suggests that the gelsolin homology domains of Fli-I adopt a conformation different from that of gelsolin, in which the actin-binding interface is constitutively exposed.

We showed that gelsolin homology domains of Fli-I interact directly with both actin filaments and monomers (**Figures 3–6**; Liu and Yin, 1998; Goshima et al., 1999; Mohammad et al., 2012). Importantly, our work reveals that the F-actin and G-actin binding of Fli-I is characterized by markedly different affinities in the ∼nM and ∼μM range, respectively. The magnitude of the actin affinities of Fli-I agrees well with the preferential association of the protein to F-actin against G-actin detected in 3T3 and 293T cell lysates (Li et al., 2008; Mohammad et al., 2012). The binding strength but not the qualitative nature of the interaction between Fli-I GH16 and actin is influenced by the GST fusion of the protein (**Figure 8**). This indicates that GST may influence the folding of the protein and/or promote the ability of Fli-I to dimerize (Gould et al., 2011; Bell et al., 2013; Zhao et al., 2013). Our work identifies the GH13 domains as the main actin interacting region of Fli-I, since neither the C-terminal GH46 domains nor the leucine-rich repeat region at the N terminus associates to actin (**Figures 3–6**). Bioinformatics analysis predicts that residues responsible for gelsolin:actin interactions show a rather weak similarity in Fli-I, with the highest conservation in the GH1 domain (**Figure 2**). In agreement with our observations, previous investigations found that the GH1 truncated human Fli-I, GH26 did not influence the level of steady-state pyrenyl fluorescence suggesting the critical importance of GH1 in actin interaction (Arora et al., 2015). Also, the human Fli-I protein carrying the E586K mutation in the GH1 domain failed to coimmunoprecipitate with actin in 293T cells (He et al., 2018). Based on these considerations the GH1 domain of Fli-I is likely to be the main actin-binding site of the protein.

Our work suggests that the multifunctional nature of gelsolin is not characteristic of Fli-I. The analysis of the activities of Fli-I at the level of individual filaments demonstrates that, as a functional consequence of the high-affinity actin interaction, Fli-GH16 inhibits actin filament elongation by efficiently capping filament barbed ends (**Figure 5**). Although *C. elegans* Fli-I was proposed to possess filament severing activity based on the appearance of short actin oligomers on electron microscopy images (Goshima et al., 1999), we have not found any evidence for an actin filament severing by Fli-I (**Figure 6**). As an alternative explanation barbed end capping and limited filament elongation would also result in short actin filaments as we observed in TIRFM experiments (**Figures 5**, **6**). Severing by gelsolin requires the concerted targeting of both its GH1 and GH4 domains to subunit:subunit interfaces at the opposite sides of the actin filament that imposes simultaneous steric clashes competing off the intersubunit interactions (Nag et al., 2013). Besides, the type 1 calcium binding sites of gelsolin may also contribute to severing by disrupting the intersubunit cation binding site (Glu167) of actin (Nag et al., 2013). From this aspect, the lack of actin binding by GH46 and conservation of the type 1 calcium binding sites in Fli-I already predicts that this protein is very unlikely to possess a severing activity, and this is entirely confirmed by our experimental results. We observed that Fli-I can moderately facilitate the formation of nucleation intermediates due to its low-affinity binding to monomeric actin (**Figure 6**). Importantly,

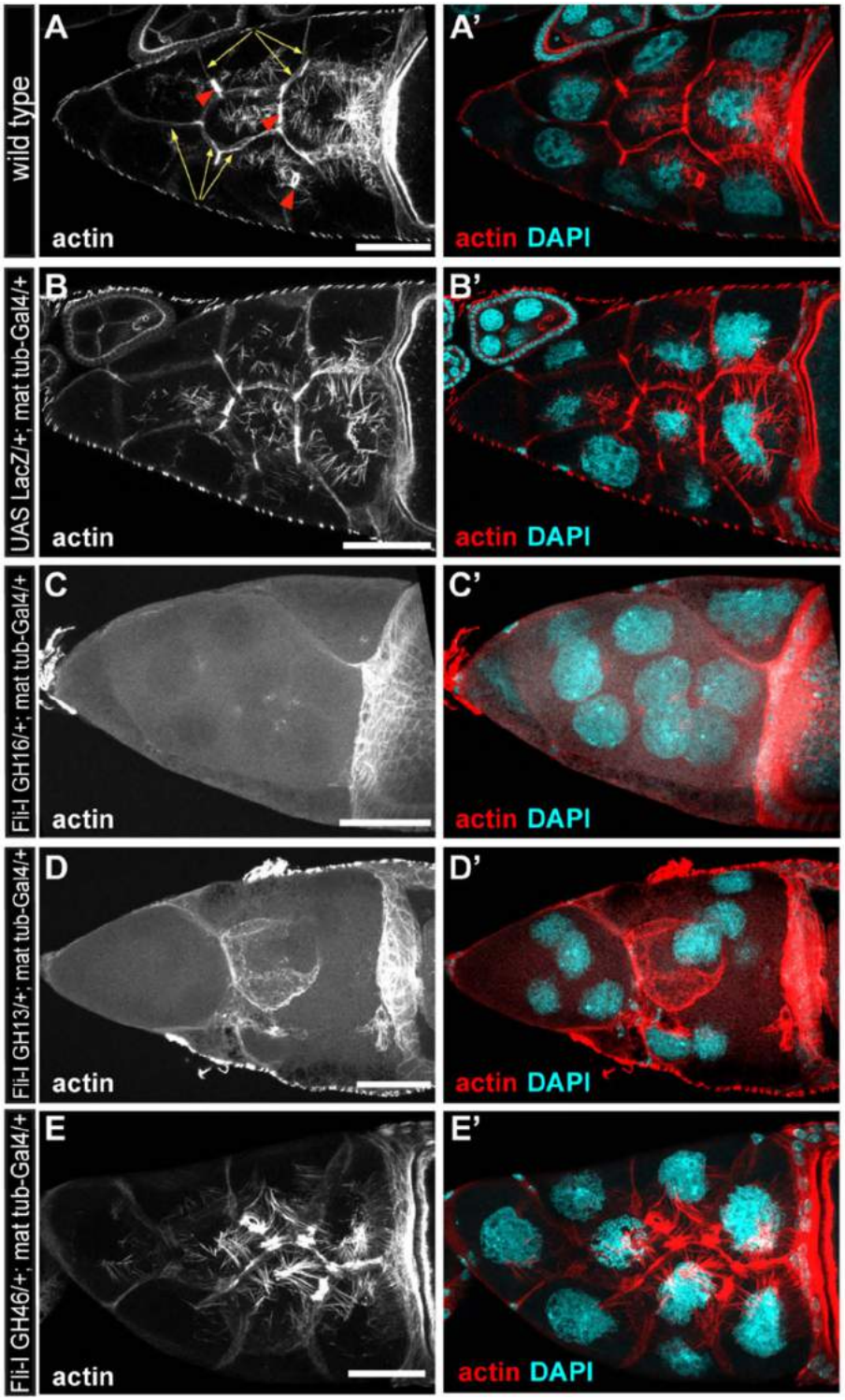

FIGURE 10 | The effect of the gelsolin homology domains of Fli-I on actin organization in *Drosophila* egg chambers. **(A,A')** Actin organization in nurse cells of a wild type *Drosophila* egg chamber in stage 10B is characterized by the presence of cortical actin (yellow arrows), ring canals (red arrowheads) and cytoplasmic actin cables growing from the plasma membrane to the nucleus. Actin is shown in **(A)** in grayscale, an overlay of DAPI (in cyan) and actin (in red) are shown in **(A')**. **(B,B')** Maternal expression of a UAS-lacZ control does not affect actin organization in the nurse cells. **(C–D')** Maternal expression of UAS-Fli-I GH16 **(C,C')** or UAS-Fli-I GH13 **(D,D')** severely impairs cytokinesis in the nurse cells resulting in fused cells with reduced cortical actin level, ring canals are not evident and the nuclear positioning cytoplasmic actin cables are also missing. **(E,E')** By contrast, in UAS-Fli-I GH46 expressing egg chambers actin organization is not altered as compared to wild type. Anterior edge of the oocyte is visible on the right side of each panel; anterior is on the left, posterior is on the right. Scale bar = 50 μm.

profilin interferes with the monomer binding of Fli-I; therefore in the presence of profilin Fli-I is only able to cap actin filament barbed ends but fails to promote actin assembly from profilin:actin (**Figure 7**). The negative influence of profilin on the Fli-I:G-actin interaction indicates that the actin-binding sites of profilin and Fli-I are likely to overlap. High-resolution structural analysis showed that the GH1 of gelsolin binds in the barbed end groove of actin subdomains 1 and 3 at a site that is shared by profilin (Schutt et al., 1993; Burtnick et al., 2004; Nag et al., 2009). Hence, these data suggest that the GH1 region of Fli-I adopts a similar binding mode to actin as gelsolin. Collectively, our biochemical analyses indicate that the most prominent actin interaction of Fli-I is the high-affinity filament end binding that endows the protein with barbed end capping activity. In accordance with this, while GH46 has no effect on *in vivo* actin polymerization, as expected from the excess of a barbed end capping protein, overexpression of GH13 prevents the formation of various types of actin cables in the developing *Drosophila* egg chambers (**Figure 10**).

Although Fli-I GH46 does not interact with actin, we found that it influences formin-mediated actin assembly *in vitro* (**Figure 9**). Fli-I GH46 inhibits actin assembly catalyzed by DAAM FH1FH2-DAD-CT but does not affect that of mediated by DAAM FH1FH2. These observations indicate that Fli-I GH46 interacts with the C-terminal DAD-CT region of DAAM, corroborating previous studies (Higashi et al., 2010). Our work reveals that the binding strength of the interaction falls in the submicromolar range. The functional consequence of this interaction remains to be elucidated. DAD is involved in the RhoGTPase-dependent regulation of the activities of DAAM through its association to the N-terminal Diaphanous inhibitory domain (DID) (Liu et al., 2008; Vig et al., 2017). This led to the proposal that the Fli-I:DAAM interaction may interfere with this autoinhibitory mechanism and thereby promotes the activation of DAAM (Higashi et al., 2010). Contrasting to this prediction, in our *in vitro* system Fli-I had an inhibitory effect. DAD-CT is involved in the interaction of DAAM with both actin monomers and filament ends and positively regulates the nucleation and elongation activities of the protein *in vitro* (Vig et al., 2017). This can provide a plausible explanation for our *in vitro* observations. Because *in vitro* in the absence of the DID domain the Fli-I/DAD-CT interaction might be more stable than the presumably transient interaction *in vivo*, further investigations are needed to resolve this issue. Nevertheless, other functional alternatives can also be considered. We have formerly shown that the DAD-CT region is important in microtubule interaction, as well as in the actin filament:microtubule coalignment activity of DAAM (Szikora et al., 2017). Based on this, one can hypothesize that the Fli-I:DAAM interaction has a role in the regulation of the microtubule cytoskeleton or the actin:microtubule cross-talk. In support of this, Fli-I was localized to both actin and microtubule-based structures in Swiss 3T3 fibroblasts (Davy et al., 2001). Thus, besides its activities directly targeting actin, the GH46:DAAM interaction can provide an indirect way for Fli-I to regulate actin dynamics and/or to extend its activities toward the microtubule cytoskeleton through a formin-mediated pathway.

MATERIALS AND METHODS

Protein Expression and Purification

The cDNAs of *Drosophila melanogaster* Flightless-I subfragments were cloned into pGEX-6P1 vector (GH1-6: 461–1256 aa) and into pGEX-2T vector (GH1-3: 461–881, GH4-6: 851–1256, LRR: 1–460). Flightless-I constructs were expressed as glutathione S-transferase (GST) fusion proteins in *Escherichia coli* BL21(DE3)pLysS strain (Novagen). The transformed bacteria were grown at 37°C in Luria Broth (Lennox) EZMix^{TM} powder microbial growth medium (Sigma-Aldrich) overnight. Protein expression was induced with 0.5 mM isopropyl β-D-1-thiogalactopyranoside (IPTG) at OD_{600} ∼0.6–0.8. After overnight expression at 20°C the bacterial pellet was collected by centrifugation (Hermle Z326K; 10,000 g, 10 min, 4°C) and stored at –20°C until use. For protein purification the bacterial pellet was lysed by sonication in Lysis buffer [20 mM Tris-HCl pH 8.0, 1 M NaCl, 5 mM $CaCl_2$, 1 mM ATP, 0.5% Triton X-100, 1% sucrose, 2 mM DTT, 5% glycerol supplemented with 0.1 mM PMSF and Protease Inhibitor Cocktail (Sigma-Aldrich, P8465)]. The cell lysate was centrifuged (Hitachi CP 80NX; 10,000 g, 25 min, 4°C) and the supernatant was gently stirred with 0.8% (m/v) polyethyleneimine solution (pH 7.9, PEI, Sigma-Aldrich) on ice to precipitate nucleic acids. Subsequently, the solution was centrifuged (Hitachi CP 80NX; 17,300 g, 10 min, 4°C) and solid, fine powdered ammonium sulfate (AS, Sigma-Aldrich) was added to the supernatant to 60% saturation by gently stirring it for 30–45 min to precipitate the proteins. The precipitate was collected by centrifugation (Hitachi CP 80NX; 21.700 g, 25 min, 4°C). The pellet was resuspended in Lysis buffer and precipitated repeatedly by adding a 60% saturated AS solution to remove the redundant PEI. After centrifugation (Hitachi CP 80NX; 21.700 g, 25 min, 4°C), the pellet was resuspended in Low salt buffer (20 mM TRIS pH 7.9, 50 mM NaCl, 1% sucrose, 5% glycerol, 1 mM DTT). The solution was incubated with Glutathione Sepharose 4B resin (Sigma-Aldrich) at 4°C overnight. Subsequently, it was loaded onto a column and washed with Low salt buffer. The GST-tagged proteins were eluted with 50 mM glutathione dissolved in Low salt buffer (Glutathione Reduced, Sigma-Aldrich). Alternatively, the GST tag from Fli-I G16 was cleaved by PreScission Protease on column (4°C, 15 min) and the cleaved protein was collected as flowthrough. Fli-I proteins were concentrated with Amicon-Ultra 50 kDa tube (Merck Millipore) by centrifugation (Hermle Z326K; 3000 g, 5 min, 4°C). The concentrate was loaded onto a PD10 column (GE Healthcare) for buffer exchange into Low salt buffer. Before flash freezing in liquid nitrogen the constructs were clarified by ultracentrifugation (Beckman Coulter; 300,000 g, 30 min, 4°C) and stored at –80°C until use. Control experiments showed that a freeze/thaw cycle does not affect the functionality of the constructs (*data are not shown*). The concentrations were measured spectrophotometrically using the extinction coefficients derived from the amino acid sequence (ExPAsy ProtParam tool)[1]. The purity of the protein was checked by

[1]http://web.expasy.org/protparam/

UV-VIS absorption photometry by calculating the A_{280}/A_{260} ratio (Manchester, 1995), which was found to be >1.7. We found that such a labor-intensive method was essential for the efficient removal of nucleic acid contamination from recombinantly produced Flightless-I. Of note, that difficulty in isolation of soluble recombinant Flightless-I protein were reported (Liu and Yin, 1998). Rabbit skeletal muscle actin (actin) was purified, gel filtered on Superdex 200 (GE Healthcare) and stored in G-buffer (4 mM TRIS, pH 7.8, 0.1 mM $CaCl_2$, 0.2 mM ATP, 0.5 mM DTT) as described previously (Spudich and Watt, 1971; Toth et al., 2016; Vig et al., 2017). The actin bound calcium was replaced to magnesium before the measurements by adding 200 μM EGTA and 50 μM $MgCl_2$. Actin was labeled at Lys^{328} by Alexa Fluor® 488 carboxylic acid succinimidyl ester (Alexa488NHS, Invitrogen), Alexa Fluor® 568 carboxylic acid succinimidyl ester (Alexa568NHS, Invitrogen) or at Cys^{374} by N-(1-pyrene)iodoacetamide (pyrene, Thermo Fisher Scientific) according to standard protocols (Toth et al., 2016; Vig et al., 2017). Mouse profilin 1 (profilin), human gelsolin (GSN) and fragments of *Drosophila* Disheveled-associated activator of morphogenesis (DAAM) formin were obtained as described previously (Toth et al., 2016; Szikora et al., 2017; Vig et al., 2017).

Fluorescence Spectroscopy

Bulk Actin Assembly/Disassembly Measurements

Pyrene-actin assembly assay was performed using gel-filtered actin (2.5 μM, containing 2 or 5% pyrene labeled actin in the presence and absence of profilin, respectively). The polymerization of magnesium-actin was initiated by the addition of 1 mM $MgCl_2$ and 50 mM KCl in the absence and presence of different concentrations of Fli-I proteins. To address the effect of Ca^{2+} on the actin activities of Fli-I or GSN measurements were performed either in the presence of 1 mM EGTA (Ca^{2+}-free condition) or 1 mM $CaCl_2$. In measurements when profilin was present the profilin concentration was 6 μM. Considering the dissociation equilibrium constant of profilin:G-actin to be K_D ~0.2 μM, ~95% of the monomeric actin was bound to profilin under these experimental conditions. Pyrene fluorescence emission was monitored by a Safas Xenius FLX spectrofluorimeter (λ_{ex} = 365 nm, λ_{em} = 407 nm). For quantitative analysis, the *polymerization rate* was derived as the slope of the linear part of the pyrene trace at each condition. The relative polymerization rate was calculated as the ratio of polymerization rates obtained in the presence and absence of Fli-I proteins. The relative polymerization rate ($v_{relative}$) of profilin:actin as a function of [Fli-I] (F_0) was fit by the following equation:

$$v_{relative} = 1 - \frac{1 - \frac{v_{min}}{v_0}}{1 + \frac{IC_{50}}{F_0}} \quad (1)$$

where v_0 and v_{min} are the relative polymerization rates in the absence and presence of saturating amount of Fli-I, respectively and IC_{50} is the Fli-I concentration corresponding to 50% inhibition.

The Fli-I dependence of the rate of DAAM FH1FH2-DAD-CT catalyzed actin assembly (v) was fit by the following equation:

$$\frac{v - v_{max}}{v_{min} - v_{max}} = \frac{A_0 + F_0 + K_D - \sqrt{(A_0 + F_0 + K_D)^2 - 4A_0F_0}}{2F_0} \quad (2)$$

where v_{min} and v_{max} are the polymerization rates in the absence and presence of saturating amount of [Fli-I]; A_0 and F_0 are the total DAAM FH1FH2-DAD-CT and Fli-I concentration, respectively, K_D is the dissociation equilibrium constant of the DAAM:Fli-I complex.

Steady-State Anisotropy Measurements

To study the Fli-I:G-actin interaction the steady-state anisotropy (anisotropy) of Alexa488NHS-Mg^{2+}-ATP-G-actin (Alexa488NHS-G-actin) was measured. Alexa488NHS-G-actin (0.2 μM) was incubated with Latrunculin A (LatA, 4 μM) for 15 min at room temperature. Then Fli-I constructs were added at different concentrations and the samples were further incubated for 1 h at 22°C either in the presence of 1 mM EGTA (Ca^{2+}-free condition) or 1 mM $CaCl_2$. In measurements when profilin was present profilin (4 μM) was added to actin after the incubation with LatA and the samples were further incubated for 1 h at 22°C before the addition of Fli-I constructs. Similarly, to the kinetic analysis, the anisotropy measurements were performed in the presence of 1 mM $MgCl_2$ and 50 mM KCl/NaCl. Since the presence of LatA prevents actin polymerization, thus the increase in steady-state anisotropy could not result from filament formation, it solely reflects the binding of Fli-I to actin. Anisotropy was measured using a Horiba Jobin Yvon Fluorolog-3 spectrofluorometer (λ_{ex} = 488 nm, λ_{em} = 516 nm) excitation and emission slits were both set to 5 nm. For quantitative analysis the Fli-I concentration dependence of the steady-state anisotropy (r) measured either in the absence or presence of profilin was fit by the following equation:

$$\frac{r - r_A}{r_{AF} - r_A} = \frac{A_0 + F_0 + K_D - \sqrt{(A_0 + F_0 + K_D)^2 - 4A_0F_0}}{2F_0} \quad (3)$$

where A_0 and F_0 are the total G-actin and Fli-I concentration, respectively, r_A is the steady-state anisotropy of Alexa488NHS-G-actin, r_{AF} is the steady-state anisotropy of Alexa488NHS-G-actin at saturating amount of Fli-I and K_D is the dissociation equilibrium constant of the G-actin:Fli-I complex.

Total Internal Reflection Fluorescence Microscopy

Actin Assembly/Disassembly Measurements

The effects of Fli-I on the assembly/disassembly of individual actin filaments were studied by total internal reflection fluorescence microscopy (TIRFM). Glass flow cells were incubated with 1 volume of N-ethylmaleimide myosin for 1 min, washed extensively with 2 volumes of myosin buffer (F buffer supplemented with 0.5 M KCl; F buffer = G buffer supplemented with 1 mM $MgCl_2$ and 50 mM KCl) and 1 volume of 1% (m/v) BSA (dissolved in F buffer) and equilibrated with 2 volumes of TIRF buffer (0.5% (m/v) methylcellulose, 0.5% (m/v) BSA,

10 mM 1,4-diazabicyclo[2,2,2]octane (DABCO), 100 mM DTT dissolved in F buffer). The polymerization of magnesium-actin (0.5 μM, 10% Alexa488NHS labeled) was initiated by the addition of 1 mM $MgCl_2$ and 50 mM KCl in the absence or presence of different concentrations of Fli-I constructs. Dual-color TIRF experiments were performed to follow the assembly of G-actin in the absence or presence of Fli-I and profilin. G-actin (0.5 μM, 10% Alexa568NHS labeled) was polymerized in the flow cell for 10 min to form "magenta" actin filaments, then unpolymerized actin was washed out by 1 volume of TIRF buffer. A mixture of G-actin (0.5 μM, 10% Alexa488NHS labeled), profilin (2 μM) and Fli-I in TIRF buffer was transferred into the flow cell. Time-lapse images of actin assembly were captured every 10.5 s with an Olympus IX81 microscope (laser lines: 491 nm and 561 nm, APON TIRF 60x NA1.45 oil immersion objective, Hamamatsu CCD camera). In assembly assays, to derive the elongation rate of actin filaments time-lapse images were analyzed by either the MultipleKymograph plugin of Fiji or by manually measuring filament lengthening. The elongation rate of actin filaments (v) was related to the critical concentration of actin assembly ($c_c \sim 0.1$ μM; Pollard, 2007; Bugyi and Carlier, 2010), to the association rate constant of actin monomers to filament barbed ends (k_+) and to the total actin concentration ($[G_0]$) by the following equation:

$$v = k_+ ([G_0] - c_c) \quad (4)$$

In disassembly assays actin (0.5 μM, 10% Alexa488NHS labeled) was allowed to polymerize for 35 min in the flow cell, then buffer conditions were changed to TIRF buffer supplemented with Fli-I (105 nM) or gelsolin (5 nM). Time-lapse images of actin disassembly were captured every 10.5 s with an Olympus IX81 microscope (laser lines: 491 and 561 nm, APON TIRF 60x NA1.45 oil immersion objective, Hamamatsu CCD camera). The percent area covered by actin filaments 5 min after the initiation of actin disassembly was derived from a 66 × 66 μm^2 region of the images by using Fiji.

Annealing Experiments

To study the end-to-end annealing of actin filaments (1 μM, containing either 10% Alexa488NHS or 10% Alexa568NHS labeled actin) were allowed to polymerize 1 h at room temperature and stabilized by phalloidin (1:1 molar ratio) overnight. Filaments with different spectral properties were mixed either in the absence or presence of Fli-I and subsequently fragmented by a 26G syringe (10×). Samples were diluted to 2 nM actin by TIRF buffer and were processed for microscopy analysis. Images were captured immediately after fragmentation (t = 0 min) and after 60 min (t = 60 min) with an Olympus IX81 microscope (laser lines: 491 and 561 nm, APON TIRF 60x NA1.45 oil immersion objective, Hamamatsu CCD camera). The length of the actin filaments was derived by using Fiji.

Steady-State Measurements of Actin Filament Number

Actin filaments (2 μM) were allowed to polymerize overnight either in the absence or presence of Fli-I GH16 (800 nM). Filaments were stabilized by AlexaFluor^{TM}488 Phalloidin (Thermo Fischer Scientific; 1:1 molar ratio), diluted to 5 nM into TIRF buffer and were processed for microscopy analysis. Images were captured with an Olympus IX81 microscope (laser line: 491 nm, APON TIRF 60x NA1.45 oil immersion objective, Hamamatsu CCD camera). The number and length of actin filaments were derived from a 66 × 66 μm^2 region of the images by using Fiji.

Fly Work and Immunohistochemistry

Fly-strains were raised under standard laboratory conditions at 25°C. As wild type, we used an isogenized w^{1118} stock. For germline expression of the UAS transgenes, we used *matα4 Tub-Gal4* (BDSC#7063). Adult ovaries were dissected in cold PBS, fixed in 4% paraformaldehyde (diluted in PBS) at room temperature for 20 min. After fixation, the samples were washed three times for 20 min in PBS containing 0.1% TritonX-100 (PBST) and blocked in PBST with 1% BSA, 0.02% NaN_3 and 5% FBS (PBT-N) for 2 h. The antibodies were diluted in PBT-N and incubated overnight at 4°C. Actin was labeled with AlexaFluor^{TM}546 Phalloidin (Thermo Fischer Scientific, 1:100), nurse cell nuclei were labeled with DAPI (Sigma-Aldrich, 1:500). Samples were mounted in ProLong Gold (Thermo Fisher Scientific). Each staining was repeated twice, and we examined 10–15 egg chambers from each. Confocal images were captured on a Zeiss LSM 800 confocal microscope. Images were edited with ImageJ/Fiji software and Adobe Illustrator CS6.

Statistical Analysis

The data presented were derived from at least two independent experiments. Values are displayed as mean ± SD. The number of independent experiments is given in the figure legends. Statistical analysis (Student's t-test) was performed by Microsoft Excel ($^{ns}p \geq 0.05$, $^{*}p < 0.05$, $^{**}p < 0.01$, $^{***}p < 0.001$, $^{****}p < 0.0001$). The significance levels are given in the text and on the corresponding figures.

DATA AVAILABILITY STATEMENT

All datasets presented in this study are included in the article/supplementary material.

AUTHOR CONTRIBUTIONS

JM and BB: conceptualization, supervision, and writing – review and editing. GG-G, RP, PB, PG, and BB: formal analysis and visualization. JM, BB, and TH: funding acquisition. GG-G, DF, EM, RP, TH, PB, PG, AV, MT, and BB: investigation. JM, BB, and RP: writing – original draft. All authors contributed to the article and approved the submitted version.

FUNDING

This work was supported by the GINOP-2.3.2-15-2016-00049, GINOP-2.3.2-15-2016-00001, GINOP-2.3.2-15-2016-00032,

EFOP-3.6.2-16-2017-00006, and OTKA K132782 grants. The work was supported by the ÚNKP-19-3-II New National Excellence Program of the Ministry for Innovation and Technology (PG). Supported by PTE ÁOK-KA 2019-50 (TH).

ACKNOWLEDGMENTS

We are grateful to Robert C. Robinson for providing us the plasmid of human gelsolin.

REFERENCES

Arora, P. D., Wang, Y., Bresnick, A., Janmey, P. A., and McCulloch, C. A. (2015). Flightless I interacts with NMMIIA to promote cell extension formation, which enables collagen remodeling. *Mol. Biol. Cell* 26, 2279–2297. doi: 10.1091/mbc.E14-11-1536

Barko, S., Bugyi, B., Carlier, M. F., Gombos, R., Matusek, T., Mihaly, J., et al. (2010). Characterization of the biochemical properties and biological function of the formin homology domains of Drosophila DAAM. *J. Biol. Chem.* 285, 13154–13169. doi: 10.1074/jbc.m109.093914

Bell, M. R., Engleka, M. J., Malik, A., and Strickler, J. E. (2013). To fuse or not to fuse: what is your purpose? *Protein Sci.* 22, 1466–1477. doi: 10.1002/pro.2356

Bugyi, B., and Carlier, M. F. (2010). Control of actin filament treadmilling in cell motility. *Annu. Rev. Biophys.* 39, 449–470. doi: 10.1146/annurev-biophys-051309-103849

Burtnick, L. D., Robinson, R. C., and Choe, S. (2001). "Structure and Function of Gelsolin," in *Molecular Interactions of Actin: Actin Structure and Actin-Binding Proteins*, eds C. G. dos Remedios and D. D. Thomas (Berlin: Springer Berlin Heidelberg), 201–211.

Burtnick, L. D., Urosev, D., Irobi, E., Narayan, K., and Robinson, R. C. (2004). Structure of the N-terminal half of gelsolin bound to actin: roles in severing, apoptosis and FAF. *EMBO J.* 23, 2713–2722. doi: 10.1038/sj.emboj.7600280

Cameron, A. M., Turner, C. T., Adams, D. H., Jackson, J. E., Melville, E., Arkell, R. M., et al. (2016). Flightless I is a key regulator of the fibroproliferative process in hypertrophic scarring and a target for a novel antiscarring therapy. *Br. J. Dermatol.* 174, 786–794. doi: 10.1111/bjd.14263

Campbell, H. D., Fountain, S., McLennan, I. S., Berven, L. A., Crouch, M. F., Davy, D. A., et al. (2002). Fliih, a gelsolin-related cytoskeletal regulator essential for early mammalian embryonic development. *Mol. Cell. Biol.* 22, 3518–3526. doi: 10.1128/mcb.22.10.3518-3526.2002

Campbell, H. D., Fountain, S., Young, I. G., Claudianos, C., Hoheisel, J. D., Chen, K. S., et al. (1997). Genomic structure, evolution, and expression of human FLII, a gelsolin and leucine-rich-repeat family member: overlap with LLGL. *Genomics* 42, 46–54. doi: 10.1006/geno.1997.4709

Campbell, H. D., Schimansky, T., Claudianos, C., Ozsarac, N., Kasprzak, A. B., Cotsell, J. N., et al. (1993). The Drosophila melanogaster flightless-I gene involved in gastrulation and muscle degeneration encodes gelsolin-like and leucine-rich repeat domains and is conserved in Caenorhabditis elegans and humans. *Proc. Natl. Acad. Sci. U.S.A.* 90:11386. doi: 10.1073/pnas.90.23.11386

Chen, K. S., Gunaratne, P. H., Hoheisel, J. D., Young, I. G., Miklos, G. L., Greenberg, F., et al. (1995). The human homologue of the Drosophila melanogaster flightless-I gene (flil) maps within the Smith-Magenis microdeletion critical region in 17p11.2. *Am. J. Hum. Genet.* 56, 175–182.

Coue, M., and Korn, E. D. (1985). Interaction of plasma gelsolin with G-actin and F-actin in the presence and absence of calcium ions. *J. Biol. Chem.* 260, 15033–15041.

Cowin, A. J., Adams, D. H., Strudwick, X. L., Chan, H., Hooper, J. A., Sander, G. R., et al. (2007). Flightless I deficiency enhances wound repair by increasing cell migration and proliferation. *J. Pathol.* 211, 572–581. doi: 10.1002/path.2143

Davy, D. A., Ball, E. E., Matthaei, K. I., Campbell, H. D., and Crouch, M. F. (2000). The flightless I protein localizes to actin-based structures during embryonic development. *Immunol. Cell Biol.* 78, 423–429. doi: 10.1046/j.1440-1711.2000.00926.x

Davy, D. A., Campbell, H. D., Fountain, S., de Jong, D., and Crouch, M. F. (2001). The flightless I protein colocalizes with actin- and microtubule-based structures in motile Swiss 3T3 fibroblasts: evidence for the involvement of PI 3-kinase and Ras-related small GTPases. *J. Cell Sci.* 114(Pt 3), 549–562.

Deng, H., Xia, D., Fang, B., and Zhang, H. (2007). The Flightless I homolog, fli-1, regulates anterior/posterior polarity, asymmetric cell division and ovulation during Caenorhabditis elegans development. *Genetics* 177, 847–860. doi: 10.1534/genetics.107.078964

Feldt, J., Schicht, M., Garreis, F., Welss, J., Schneider, U. W., and Paulsen, F. (2019). Structure, regulation and related diseases of the actin-binding protein gelsolin. *Expert Rev. Mol. Med.* 20:e7. doi: 10.1017/erm.2018.7

Ferrary, E., Cohen-Tannoudji, M., Pehau-Arnaudet, G., Lapillonne, A., Athman, R., Ruiz, T., et al. (1999). In vivo, villin is required for Ca(2+)-dependent F-actin disruption in intestinal brush borders. *J. Cell. Biol.* 146, 819–830. doi: 10.1083/jcb.146.4.819

Fong, K. S., and de Couet, H. G. (1999). Novel proteins interacting with the leucine-rich repeat domain of human flightless-I identified by the yeast two-hybrid system. *Genomics* 58, 146–157. doi: 10.1006/geno.1999.5817

Ghoshdastider, U., Popp, D., Burtnick, L. D., and Robinson, R. C. (2013). The expanding superfamily of gelsolin homology domain proteins. *Cytoskeleton* 70, 775–795. doi: 10.1002/cm.21149

Goshima, M., Kariya, K.-I., Yamawaki-Kataoka, Y., Okada, T., Shibatohge, M., Shima, F., et al. (1999). Characterization of a Novel Ras-Binding Protein Ce-FLI-1 Comprising Leucine-Rich Repeats and Gelsolin-like Domains. *Biochem. Biophys. Res. Commun.* 257, 111–116. doi: 10.1006/bbrc.1999.0420

Gould, C. J., Maiti, S., Michelot, A., Graziano, B. R., Blanchoin, L., and Goode, B. L. (2011). The formin DAD domain plays dual roles in autoinhibition and actin nucleation. *Curr. Biol.* 21, 384–390. doi: 10.1016/j.cub.2011.01.047

He, J. P., Hou, P. P., Chen, Q. T., Wang, W. J., Sun, X. Y., Yang, P. B., et al. (2018). Flightless-I Blocks p62-Mediated Recognition of LC3 to Impede Selective Autophagy and Promote Breast Cancer Progression. *Cancer Res.* 78, 4853–4864. doi: 10.1158/0008-5472.can-17-3835

Higashi, T., Ikeda, T., Murakami, T., Shirakawa, R., Kawato, M., Okawa, K., et al. (2010). Flightless-I (Fli-I) Regulates the Actin Assembly Activity of Diaphanous-related Formins (DRFs) Daam1 and mDia1 in Cooperation with Active Rho GTPase. *J. Biol. Chem.* 285, 16231–16238. doi: 10.1074/jbc.M109.079236

Kinosian, H. J., Newman, J., Lincoln, B., Selden, L. A., Gershman, L. C., and Estes, J. E. (1998). Ca2+ regulation of gelsolin activity: binding and severing of F-actin. *Biophys. J.* 75, 3101–3109. doi: 10.1016/S0006-3495(98)77751-77753

Kis-Bicskei, N., Becsi, B., Erdodi, F., Robinson, R. C., Bugyi, B., Huber, T., et al. (2018). Tropomyosins Regulate the Severing Activity of Gelsolin in Isoform-Dependent and Independent Manners. *Biophys. J.* 114, 777–787. doi: 10.1016/j.bpj.2017.11.3812

Kopecki, Z., Arkell, R. M., Strudwick, X. L., Hirose, M., Ludwig, R. J., Kern, J. S., et al. (2011). Overexpression of the Flii gene increases dermal-epidermal blistering in an autoimmune ColVII mouse model of epidermolysis bullosa acquisita. *J. Pathol.* 225, 401–413. doi: 10.1002/path.2973

Kothakota, S., Azuma, T., Reinhard, C., Klippel, A., Tang, J., Chu, K., et al. (1997). Caspase-3-generated fragment of gelsolin: effector of morphological change in apoptosis. *Science* 278, 294–298. doi: 10.1126/science.278.5336.294

Li, J., Yin, H. L., and Yuan, J. (2008). Flightless-I regulates proinflammatory caspases by selectively modulating intracellular localization and caspase activity. *J. Cell Biol.* 181, 321–333. doi: 10.1083/jcb.200711082

Liu, W., Sato, A., Khadka, D., Bharti, R., Diaz, H., Runnels, L. W., et al. (2008). Mechanism of activation of the Formin protein Daam1. *Proc. Natl. Acad. Sci. U.S.A.* 105, 210–215. doi: 10.1073/pnas.0707277105

Liu, W., Xie, Y., Ma, J., Luo, X., Nie, P., Zuo, Z., et al. (2015). IBS: an illustrator for the presentation and visualization of biological sequences. *Bioinformatics* 31, 3359–3361. doi: 10.1093/bioinformatics/btv362

Liu, Y. T., and Yin, H. L. (1998). Identification of the binding partners for flightless I, A novel protein bridging the leucine-rich repeat and the gelsolin superfamilies. *J. Biol. Chem.* 273, 7920–7927. doi: 10.1074/jbc.273.14.7920

Lu, J., Dentler, W. L., and Lundquist, E. A. (2008). FLI-1 Flightless-1 and LET-60 Ras control germ line morphogenesis in C. elegans. *BMC Dev. Biol.* 8:54. doi: 10.1186/1471-213X-8-54

Manchester, K. L. (1995). Value of A260/A280 ratios for measurement of purity of nucleic acids. *Biotechniques* 19, 208–210.

Matusek, T., Gombos, R., Szecsenyi, A., Sanchez-Soriano, N., Czibula, A., Pataki, C., et al. (2008). Formin proteins of the DAAM subfamily play a role during axon growth. *J. Neurosci.* 28, 13310–13319. doi: 10.1523/JNEUROSCI.2727-08.2008

Mohammad, I., Arora, P. D., Naghibzadeh, Y., Wang, Y., Li, J., Mascarenhas, W., et al. (2012). Flightless I is a focal adhesion-associated actin-capping protein that regulates cell migration. *FASEB J.* 26, 3260–3272. doi: 10.1096/fj.11-202051

Nag, S., Larsson, M., Robinson, R. C., and Burtnick, L. D. (2013). Gelsolin: the tail of a molecular gymnast. *Cytoskeleton* 70, 360–384. doi: 10.1002/cm.21117

Nag, S., Ma, Q., Wang, H., Chumnarnsilpa, S., Lee, W. L., Larsson, M., et al. (2009). Ca2+ binding by domain 2 plays a critical role in the activation and stabilization of gelsolin. *Proc. Natl. Acad. Sci. U.S.A.* 106, 13713–13718. doi: 10.1073/pnas.0812374106

Perrimon, N., Smouse, D., and Miklos, G. L. (1989). Developmental genetics of loci at the base of the X chromosome of Drosophila melanogaster. *Genetics* 121, 313–331.

Pinson, K. I., Dunbar, L., Samuelson, L., and Gumucio, D. L. (1998). Targeted disruption of the mouse villin gene does not impair the morphogenesis of microvilli. *Dev. Dyn.* 211, 109–121. doi: 10.1002/(sici)1097-0177(199801)211:1<109::aid-aja10>3.0.co;2-7

Pollard, T. D. (2007). Regulation of actin filament assembly by Arp2/3 complex and formins. *Annu. Rev. Biophys. Biomol. Struct.* 36, 451–477. doi: 10.1146/annurev.biophys.35.040405.101936

Pope, B., Way, M., and Weeds, A. G. (1991). Two of the three actin-binding domains of gelsolin bind to the same subdomain of actin. Implications of capping and severing mechanisms. *FEBS Lett.* 280, 70–74. doi: 10.1016/0014-5793(91)80206-i

Schutt, C. E., Myslik, J. C., Rozycki, M. D., Goonesekere, N. C., and Lindberg, U. (1993). The structure of crystalline profilin-beta-actin. *Nature* 365, 810–816. doi: 10.1038/365810a0

Selden, L. A., Kinosian, H. J., Newman, J., Lincoln, B., Hurwitz, C., Gershman, L. C., et al. (1998). Severing of F-actin by the amino-terminal half of gelsolin suggests internal cooperativity in gelsolin. *Biophys. J.* 75, 3092–3100. doi: 10.1016/S0006-3495(98)77750-77751

Silacci, P., Mazzolai, L., Gauci, C., Stergiopulos, N., Yin, H. L., and Hayoz, D. (2004). Gelsolin superfamily proteins: key regulators of cellular functions. *Cell Mol. Life Sci.* 61, 2614–2623. doi: 10.1007/s00018-004-4225-4226

Spudich, J. A., and Watt, S. (1971). The regulation of rabbit skeletal muscle contraction. I. Biochemical studies of the interaction of the tropomyosin-troponin complex with actin and the proteolytic fragments of myosin. *J. Biol. Chem.* 246, 4866–4871.

Szatmari, D., Bugyi, B., Ujfalusi, Z., Grama, L., Dudas, R., and Nyitrai, M. (2017). Cardiac leiomodin2 binds to the sides of actin filaments and regulates the ATPase activity of myosin. *PLoS One* 12:e0186288. doi: 0.1371/journal.pone.0186288

Szikora, S., Foldi, I., Toth, K., Migh, E., Vig, A., Bugyi, B., et al. (2017). The formin DAAM is required for coordination of the actin and microtubule cytoskeleton in axonal growth cones. *J. Cell Sci.* 130, 2506–2519. doi: 10.1242/jcs.203455

Toth, M. A., Majoros, A. K., Vig, A. T., Migh, E., Nyitrai, M., Mihaly, J., et al. (2016). Biochemical Activities of the Wiskott-Aldrich Syndrome Homology Region 2 Domains of Sarcomere Length Short (SALS) Protein*. *J. Biol. Chem.* 291, 667–680. doi: 10.1074/jbc.m115.683904

Vig, A. T., Foldi, I., Szikora, S., Migh, E., Gombos, R., Toth, M. A., et al. (2017). The activities of the C-terminal regions of the formin protein disheveled-associated activator of morphogenesis (DAAM) in actin dynamics. *J. Biol. Chem.* 292, 13566–13583. doi: 10.1074/jbc.M117.799247

Witke, W., Li, W., Kwiatkowski, D. J., and Southwick, F. S. (2001). Comparisons of CapG and gelsolin-null macrophages: demonstration of a unique role for CapG in receptor-mediated ruffling, phagocytosis, and vesicle rocketing. *J. Cell Biol.* 154, 775–784. doi: 10.1083/jcb.200101113

Witke, W., Sharpe, A. H., Hartwig, J. H., Azuma, T., Stossel, T. P., and Kwiatkowski, D. J. (1995). Hemostatic, inflammatory, and fibroblast responses are blunted in mice lacking gelsolin. *Cell* 81, 41–51. doi: 10.1016/0092-8674(95)90369-0

Yin, H. L., and Stossel, T. P. (1979). Control of cytoplasmic actin gel-sol transformation by gelsolin, a calcium-dependent regulatory protein. *Nature* 281, 583–586. doi: 10.1038/281583a0

Zhao, X., Li, G., and Liang, S. (2013). Several affinity tags commonly used in chromatographic purification. *J. Anal. Methods Chem.* 2013:581093. doi: 10.1155/2013/581093

Conflict of Interest: The authors declare that the research was conducted in the absence of any commercial or financial relationships that could be construed as a potential conflict of interest.

The activities of the C-terminal regions of the formin protein disheveled-associated activator of morphogenesis (DAAM) in actin dynamics

Received for publication, May 29, 2017, and in revised form, June 20, 2017 Published, Papers in Press, June 22, 2017, DOI 10.1074/jbc.M117.799247

Andrea Teréz Vig[‡], István Földi[§], Szilárd Szikora[§], Ede Migh[§], Rita Gombos[§], Mónika Ágnes Tóth[‡], Tamás Huber[‡], Réka Pintér[‡], Gábor Csaba Talián[‡], József Mihály[§], and Beáta Bugyi[‡¶1]

From the [‡]Department of Biophysics, Medical School, University of Pécs, Szigeti Str. 12, Pécs H-7624, the [§]Biological Research Centre, Institute of Genetics, MTA-SZBK NAP B Axon Growth and Regeneration Group, Hungarian Academy of Sciences, Temesvári krt. 62, Szeged H-6726, and the [¶]Szentágothai Research Center, Ifjúság Str. 34, Pécs H-7624, Hungary

Edited by Velia M. Fowler

Disheveled-associated activator of morphogenesis (DAAM) is a diaphanous-related formin protein essential for the regulation of actin cytoskeleton dynamics in diverse biological processes. The conserved formin homology 1 and 2 (FH1–FH2) domains of DAAM catalyze actin nucleation and processively mediate filament elongation. These activities are indirectly regulated by the N- and C-terminal regions flanking the FH1–FH2 domains. Recently, the C-terminal diaphanous-autoregulatory domain (DAD) and the C terminus (CT) of formins have also been shown to regulate actin assembly by directly interacting with actin. Here, to better understand the biological activities of DAAM, we studied the role of DAD-CT regions of *Drosophila* DAAM in its interaction with actin with *in vitro* biochemical and *in vivo* genetic approaches. We found that the DAD-CT region binds actin *in vitro* and that its main actin-binding element is the CT region, which does not influence actin dynamics on its own. However, we also found that it can tune the nucleating activity and the filament end–interaction properties of DAAM in an FH2 domain-dependent manner. We also demonstrate that DAD-CT makes the FH2 domain more efficient in antagonizing with capping protein. Consistently, *in vivo* data suggested that the CT region contributes to DAAM-mediated filopodia formation and dynamics in primary neurons. In conclusion, our results demonstrate that the CT region of DAAM plays an important role in actin assembly regulation in a biological context.

Formins are actin assembly machineries playing essential roles in diverse biological processes. The core actin-interacting region is the conserved formin homology (FH)[2] 2 domain that catalyzes actin nucleation and mediates processive elongation of filament ends. The activities of the FH2 domain are assisted by the upstream formin homology 1 (FH1) domain that interacts with profilin–actin (1–5). The N- and C-terminal regions flanking the FH1–FH2 domains have diverse composition and functions among different formin families. Formins belonging to the Diaphanous-related formin (DRF) family, including Diaphanous (Dia), Disheveled-associated activator of morphogenesis (DAAM), formin-like protein (FMNL), FH1/FH2 domain-containing protein, and inverted formin2 (INF2) are characterized by the presence of an N-terminal Diaphanous inhibitory domain (DID) and a C-terminal Diaphanous autoregulatory domain (DAD). It is well established that the intramolecular contacts formed between these regions keep the FH2 in an inactive state by preventing its interaction with actin. The functions of the FH2 domain in actin assembly are activated upon Rho GTPase-dependent relief of the DID/DAD autoinhibitory interaction (5–11).

Recent studies showed that, besides autoregulation, the C-terminal regions of formins from yeast to mammals (such as mouse Dia1, FMNL3, INF2, *Drosophila* Capuccino, yeast Bni1 and Bnr1, and human Daam1) can also influence the active FH2 domain-mediated actin assembly (12–15). A common feature of the C-terminal regions studied so far is that they increase the efficiency of the FH2-catalyzed nucleation. Additionally, isolated C-terminal regions can directly interact with actin, independently of the FH2 domain. The C terminus of INF2 contains a Wiskott-Aldrich syndrome homology (WH2)-like DAD motif, which in its isolated form sequesters monomeric actin and severs actin filaments (12), whereas the WH2-DAD C-terminal region of FMNL3 nucleates actin and slows elongation in a dimeric form (14). Similarly, the isolated dimeric DAD from mDia1 seems to be sufficient to promote actin nucleation (13). In contrast, the tail region of Capuccino does not influence nucleation or elongation in the absence of FH2 (15). The bio-

This work was supported by Hungarian Science Foundation (OTKA) Grants K109689 (to B. B.) and K109330 (to J. M.); Hungarian Brain Research Program Grant KTIA_NAP_13-2-2014-0007 (to J. M.); National Research, Development, and Innovation Office Grant GINOP-2.3.2-15-2016-00001 (to J. M.); National Innovation Office "Baross Gábor" Program Grant REG-DD-09-1-2009-0009 Tirfm 09 (to B. B.); grants from the European Union and the State of Hungary, co-financed by the European Social Fund in the framework of TÁMOP 4.2.4.A/2-11-1-2012-0001 "National Excellence Program"; New National Excellence Program of the Ministry of Human Capacities (to B. B. and T. H.); and ÚNKP-16-4 New National Excellence Program of the Ministry of Human Capacities (to B. B.). The authors declare that they have no conflicts of interest with the contents of this article.
This article contains supplemental Movie S1.

[1] To whom correspondence should be addressed: Dept. of Biophysics, University of Pécs Medical School, Pécs, Szigeti Str. 12, H-7624, Hungary. Tel.: 36-72-536-265; E-mail: beata.bugyi@aok.pte.hu.

[2] The abbreviations used are: FH, formin homology; DRF, diaphanous-related formin family; DAAM, disheveled-associated activator of morphogenesis; DID, diaphanous inhibitory domain; DAD, diaphanous autoregulatory domain; WH2, Wiskott-Aldrich syndrome homology; TIRFM, total internal reflection fluorescence microscopy; aa, amino acid; CP, capping protein; CT, C terminus; LatA, latrunculin A.

chemical evidence suggests that the activities of the C-terminal regions vary among formins and raise the question how and which of the activities of the isolated C-terminal regions are transmitted to the functionality of each formin in the context of the FH1–FH2 domains. In addition, the *in vivo* significance of the direct interaction of the C-terminal regions of formins with actin and its role in actin cytoskeleton dynamics regulation are not well understood.

In this work, we investigated the *Drosophila* DAAM formin belonging to the DRF family. DAAM is involved in diverse morphogenetic processes mediated by the actin cytoskeleton. For example, DAAM plays a role in organizing apical actin cables that define the tracheal cuticle pattern (16). It is also required for axonal growth and guidance by promoting filopodia formation in the growth cone (17), and DAAM is essential for sarcomerogenesis (18–20). In our previous work, we described the physicochemical properties of the interaction of *Drosophila* DAAM FH1–FH2 and actin, and we showed that DAAM FH1–FH2 is a profilin-gated actin assembly factor (18, 21). To better understand the biological functioning of DAAM, we aimed to analyze the biochemical activities of recombinantly produced DAD-CT regions of DAAM in its isolated form, as well as in the context of the FH1–FH2 domains in the regulation of actin assembly. By dissecting the activities of the DAD and CT regions of DAAM, we aimed to reveal which of the reported activities of the C-terminal regions of formins are shared by the DAD-CT regions of *Drosophila* DAAM to influence FH1–FH2-assisted actin assembly. We also investigated how the DAD-CT region influences filopodia formation and FH2-mediated actin dynamics in primary neurons using *in vivo* genetic approaches.

Results

cDAAM is more efficient in catalyzing actin nucleation than the FH1–FH2 domains

To investigate the effects of the C-terminal regions of *Drosophila* DAAM on actin assembly, first we produced two recombinant proteins that either lack or possess the C-terminal DAD-CT regions, the FH1–FH2 and cDAAM proteins, respectively (Fig. 1*A*). To analyze the actin assembly efficiencies of these constructs, the polymerization kinetics of G-actin and profilin/G-actin were measured in pyrenyl polymerization experiments (Fig. 2, *A* and *B*). We found that both constructs can accelerate actin polymerization (Fig. 2*A*). However, cDAAM accelerates the overall polymerization rate of both free G-actin and profilin/G-actin ~36-fold more efficiently than the FH1–FH2 (which lacks the C-terminal DAD-CT regions) at all concentrations that were tested (Fig. 2*B*). This observation is consistent with the findings on the human Daam1 protein, suggesting that this feature is conserved between species (13).

Because the FH2 domain of some formins, such as Bni1 and mDia1, has low affinity to monomeric actin in the absence of the C-terminal regions (13, 22, 23), we wanted to examine whether the differences in the actin assembly promoting activities of FH1–FH2 and cDAAM can arise from different actin affinities. Therefore, the interactions of FH1–FH2 and cDAAM with G-actin and profilin/G-actin were investigated in steady-state fluorescence anisotropy experiments. To avoid artificial increase in anisotropy due to the presence of polymerizing agents, latrunculin A was used to keep actin in monomeric form (24, 25). We observed a similar concentration-dependent increase in the values of the steady-state anisotropy in the presence of both DAAM constructs (Fig. 2*C*). This reflects that FH1–FH2, as well as cDAAM, binds monomeric actin, and the complexes are characterized by similar affinities in the few tens of nanomolar range (Table 1). This result suggests that the lower polymerization activity of FH1–FH2 compared with cDAAM does not originate from their different affinities to monomeric actin.

The different polymerization efficiencies of FH1–FH2 and cDAAM can also arise from differences in their nucleation and/or elongation activities. Because bulk pyrenyl polymerization assays cannot distinguish these two activities, the assembly of individual actin filaments was investigated by total internal reflection fluorescence microscopy (TIRFM) (Fig. 2, *D–F*). In control experiments, we found that the number of actin filaments significantly decreased in the presence of profilin, compared with that of measured for free G-actin ($p < 0.0001$, Fig. 2, *D* and *E*), consistent with the nucleation-suppressing activity of profilin (26, 27). In the presence of FH1–FH2 and cDAAM, a dramatic increase in the number of filaments formed was observed as compared with the number of spontaneously formed filaments, which reflects the nucleation-promoting activity of these constructs (Fig. 2, *D* and *E*). Importantly, quantitative analysis of these data revealed that cDAAM nucleated significantly more filaments than FH1–FH2, suggesting that cDAAM is more efficient at promoting the initial nucleation phase of actin filament formation than FH1–FH2 (Fig. 2, *D* and *E*). This result demonstrates that the DAD-CT region makes the FH2 domain more efficient in catalyzing actin nucleation. Spontaneously growing actin filaments elongated at a rate of 4.30 ± 0.6 and 3.48 ± 0.4 subunits·s^{-1} in the absence and presence of profilin, respectively (Fig. 2*F*). These values are in agreement with the well-established barbed-end association rate constants of ATP-Mg^{2+}–G-actin (free G-actin, $k_+ = 10.23 \pm 1.5$ μM^{-1}·s^{-1}; profilin/G-actin, $k_+ = 8.29 \pm 0.9$ μM^{-1}·s^{-1}, see Equation 4 (21, 28, 29)). The analysis showed that both FH1–FH2 and cDAAM almost completely inhibit the elongation of free G-actin ($v_{FH1-FH2} = 0.36 \pm 0.2$ subunits·s^{-1} ($p < 0.0001$) and $v_{cDAAM} = 0.37 \pm 0.1$ subunits·s^{-1} ($p < 0.0001$), Fig. 2*F*). In contrast, in the presence of profilin the elongation rate is similar to that of the spontaneously growing actin filaments ($v_{FH1-FH2} = 3.44 \pm 0.3$ subunits·s^{-1} ($p = 0.45$) and $v_{cDAAM} = 3.49 \pm 0.4$ subunit·s^{-1} ($p = 0.44$), Fig. 2*F*). Thus, profilin by relieving the elongation inhibitory activity of the constructs contributes to effective filament growth. These observations, regarding the profilin-gated effect of FH1–FH2 on filament elongation are entirely consistent with our previously published data (21). The profilin-dependent regulation of filament elongation was also reported for the human Daam1 protein (30); however, the net effect was different. Daam1 did not affect filament growth significantly in the absence of profilin, although it accelerated elongation from profilin–actin ~4-fold as compared with the spontaneous rate (30). These differences may arise from different conditions, including the species-specific

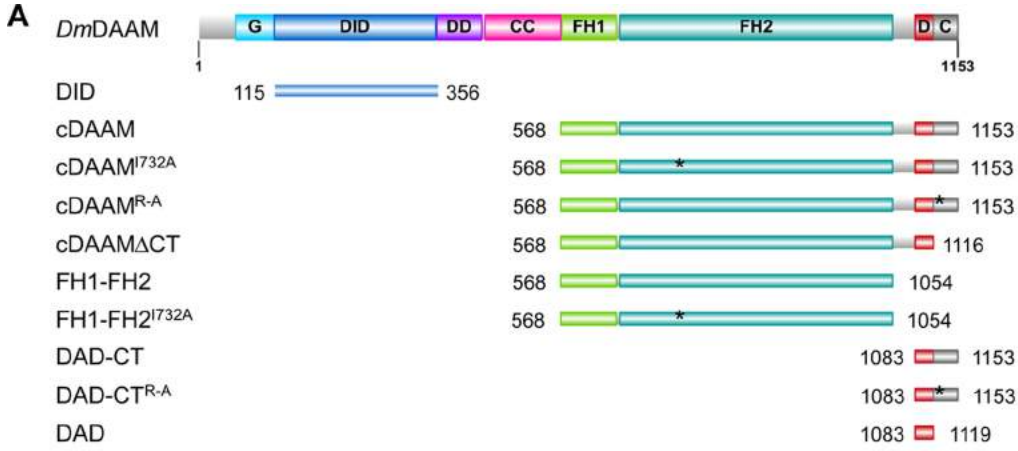

B FH2 domains

```
                                    .   .:.   ::   *       :    :   :   :
Dm DAAM    701  DGSYEDLRVTGKAAKQKVLSVIDGRRAQNCTILLSKLK-MSDMEISKAILSMDSNEQLQLD 760  (I732)
Hs DAAM1   669  ADAIDDTLSS--KLKVKELSVIDGRRAQNCNILLSRLK-LSNDEIKRAILTMDEQEDLPKD 726  (I698)
Hs DAAM2   654  LGSTEDIYLA--SRKVKELSVIDGRRAQNCIILLSKLK-LSNEEIRQAILKMDEQEDLAKD 711  (I683)
Hs Diaph1  831  DQEGGEEKKSVQKKKVKELKVLDSKTAQNLSIFLGSFR-MPYQEIKNVILEVNEA-VLTES 889  (I845)
Hs Diaph2  690  ALE--EKKTGPTKKKVKELRILDPKTAQNLSIFLGSYR-MPYEDIRNVILEVNED-MLSEA 746  (I720)
Hs Diaph3  698  DIE--EKKS--IKKKIKELKFLDSKIAQNLSIFLSSFR-VPYEEIRMMILEVDET-RLAES 752  (I705)
Hs Fmn1   1037  TYEK-------KNKVKKIIKLLDGKRSQTVGILISSLH-LEMKDIQQAIFNVDDS-VVDLE 1088 (I1061)
Hs Fmn2   1347  TIS--------KTKAKQVVKLLSNKRSQAVGILMSSLH-LDMKDIQHAVVNLDNS-VVDLE 1397 (I1208)
Hs FMNL1   689  SLDLSALKSKAAQKAPSKATLIEANRAKNLAITLRKGN-LGAERICQAIEAYDLQ-ALGLD 747  (I720)
Dm Capu    681  PKEL-------KVKRAKSIKVLDPERSRNVGIIWRSLH-VPSSEIEHAIYHIDTS-VVSLE 733  (I706)
Sc Bnr1    936  SSIALSSNNGKSSNELKKISFLSRDLAQQFGINLHMFSQLSDMEFVMKVLNCDNDIVQNVN 996  (I967)
Sc Bni1   1412  ------------KEDLQKITFLSRDISQQFGINLHMYSSLSVADLVKKILNCDRDFLQTPS 1460 (I1431)
```

C DAD | CT regions – WH2 domains

```
                          *:  ::
Dm DAAM   1084 GDNKGEFDDLISALRTGDVFGEDMAKFKRS- | RKARVLNGGGSSTGHTSPPRHGSLQREESGRERERTVRRQ--------- 1153
Hs WASP    430 -----GRGALLDQIRQG--IQLNKT------ | ------------------------------------------------ 447
Hs WAVE2   436 -----ARSDLLSAIRQG--FQLRRV------ | ------------------------------------------------ 453
Hs Lmod1   574 -----SRDQLLAAIRSSNLKQLKKV------ | ------------------------------------------------ 593
Hs Lmod2   521 -----AHENLMEAIRGSSIKQLKRV------ | ------------------------------------------------ 540
Hs Lmod3   534 -----PRDQLLNDIRHSSVAYLKPV------ | ------------------------------------------------ 553
Mm FMNL3   967 ------QQELIAELRRR---QAKEH------ | ------------------------------------------------ 982
Hs INF2    974 -------DALLADIRKG--FQLRKT------ | ------------------------------------------------ 989
Mm Diaph1 1194 -DETGVMDSLLEALQSGAAF-RRKRGPRQAN | RKAGCAVTSLLASELTKDDAMAAVPAKVSKNSETFPTILEEAKELVGRAS 1272
Dm Capu   1033                               | ---RRN-------VSTKVEKSGRISLKERMLMRRSKN------------ 1059
```

Figure 1. Domain organization and sequence alignments of DAAM. *A,* domain organization of full-length *Drosophila melanogaster* DAAM formin (*Dm DAAM*) and of the constructs investigated in this study. *G,* GTPase-binding domain; *DID,* diaphanous inhibitory domain; *DD,* dimerization domain; *CC,* coiled coil; *FH,* formin homology domain; *D,* diaphanous autoregulatory domain; *CT,* C-terminal sequence element. *Numbers* indicate the number of the first and the last residue in each construct. The positions of the mutated amino acids are highlighted by *asterisks*. The figure was made with Illustrator for Biological Sciences (57). *B,* sequence alignment of FH2 domains from different formins. The conserved Ile in the FH2 domain is highlighted in *red*, and its position in each formin is given in *parentheses* at the end of the sequences. The αD helix of the knob region is *underlined*. *C,* alignment of C-terminal regions from different formins and WH2 domain sequences. The hydrophobic amino acid triplet and the LKK(T/V) motif are shown by *bold* and *bold italics*, respectively. Positively charged Arg and Lys residues in the CT region are shown in *italics*. The Arg residues replaced by Ala in the DAAM DAD-CT$^{Arg-Ala}$ construct are highlighted in *red*. Residues that are shown to be important for actin interaction in mDia1, FMNL3, and Capuccino are *underlined* (13, 14, 47). UniProt accession numbers are as follows: *Dm DAAM*, Q8IRY0; *Hs DAAM1,* Q9Y4D1; *Hs DAAM2*, Q86T65; *Hs Diaph1*, O60610; *Hs Diaph2*, O60879; *Hs Diaph3*, Q9NSV4; *Hs* Fmn1, Q68DA7; *Hs Fmn2,* Q9NZ56; *Hs FMNL1*, O95466; *Dm Capu*, Q24120; *Sc Bnr1,* P40450; *Sc* Bni1, P41832; *Hs WASP*, P42768; *Hs WAVE2*, Q9Y6W5; *Hs Lmod1,* P29536; *Hs Lmod2*, Q6P5Q4; *Hs Lmod3*, Q0VAK6; *Mm FMNL3*, Q6ZPF4; *Hs INF2*, Q27J81. *Dm, D. melanogaster*; *Hs, Homo sapiens*; *Sc, Saccharomyces cerevisiae*; *Mm, Mus musculus*.

differences in activities, the expression system, the tag, the profilin isoform used, and/or the labeling of hDaam1.

In conclusion, the effects of the FH1–FH2 and cDAAM constructs on filament elongation from either free or profilin/G-actin are quantitatively the same; however, their nucleation efficiencies differ markedly. These observations clearly show that the more potent actin assembly activity of cDAAM as compared with FH1–FH2 arises from a difference in their nucleating efficiency, suggesting that the C-terminal regions contribute to the nucleating activity of the FH2 domain.

Main G-actin-binding site in DAD-CT is the CT region

To analyze the activities of the C-terminal regions of DAAM in more detail, recombinant fragments were produced containing both the DAD domain and the C-terminal end of the protein (DAD-CT) or only the isolated DAD domain (Fig. 1*A*). First, the interaction of DAD-CT and DAD with monomeric actin was investigated by measuring the steady-state anisotropy of fluorescently labeled actin. We found that DAD-CT can bind to G-actin, independently of the FH2 domain (Fig. 3*A*). How-

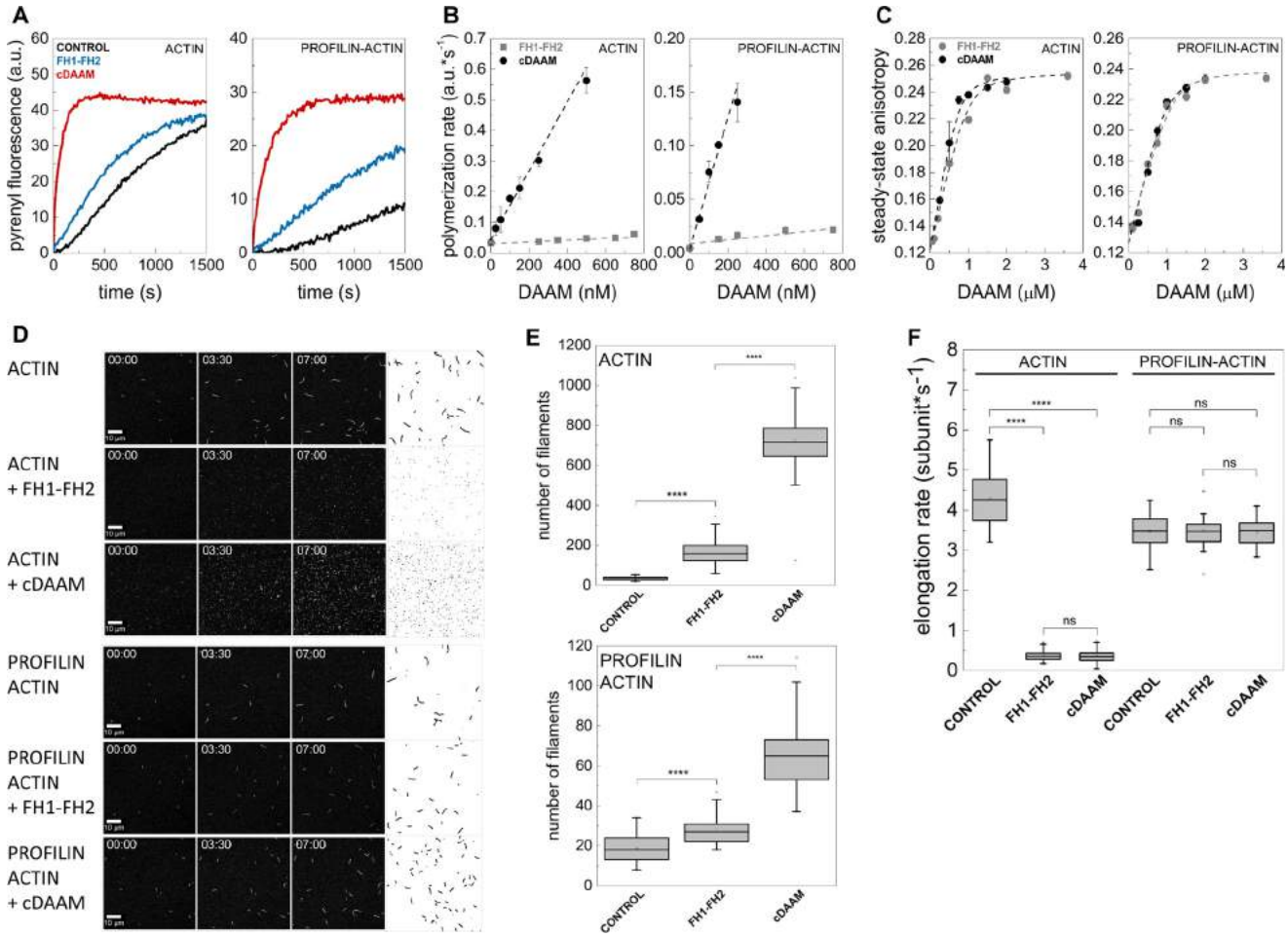

Figure 2. cDAAM is more efficient in catalyzing actin assembly than FH1–FH2. *A,* representative pyrenyl traces of spontaneous and FH1–FH2 or cDAAM catalyzed assembly of free G-actin and profilin/G-actin, as indicated. Final concentrations are as follows: [actin] = 2 μM; [profilin] = 6 μM; [FH1–FH2] = 200 nM; [cDAAM] = 200 nM. *B,* FH1–FH2 and cDAAM concentration dependence of the relative polymerization rate of free G-actin and profilin/G-actin, as indicated. *Error bars,* standard deviations, $n = 3–5$. *C,* steady-state anisotropy of Alexa488NHS–G-actin in the absence and presence of profilin as the function of DAAM concentration, as indicated. *Dashed lines* in the corresponding colors show the fits to the data according to Equation 3. Dissociation equilibrium constants are summarized in Table 1. *Error bars,* standard deviations, $n = 2–3$. Final concentrations are as follows: [actin] = 0.2 μM; [LatA] = 4 μM; [profilin] = 0.8 μM; [NaCl] = 5 mM. *D,* TIRFM montages of actin assembly and representative skeletonized images showing the field of view of actin assembly in the absence and presence of FH1–FH2 or cDAAM, as indicated. *Scale bar,* 10 μm, time = min/s. Final concentrations are as follows: [actin] = 0.5 μM; [profilin] = 2 μM; [FH1–FH2] = 100 nM; [cDAAM] = 100 nM. *E,* number of actin filaments nucleated spontaneously or in the presence of FH1–FH2 and cDAAM derived from skeletonized images. Final concentrations as in *D*, $n = 20–62$. *F,* elongation rate of individual actin filaments polymerized from free and profilin/G-actin in the absence and presence of FH1–FH2 or cDAAM. Final concentrations as in *D*, $n = 30–89$. *a.u.*, arbitrary units; *ns*, not significant.

Table 1

Dissociation equilibrium constants (K_D) of the DAAM/actin interactions

FL means fluorescently labeled protein; ND means not determined.

Construct	$K_D \pm$ S.D.[a] (μM)		
	G-actin	Profilin/G-actin^{FL}	Profilin^{FL}/G-actin
FH1-FH2	0.061 ± 0.02	0.056 ± 0.02	ND
cDAAM	0.052 ± 0.02	0.068 ± 0.02	ND
DAD-CT	3.87 ± 0.19	3.54 ± 0.22	4.71 ± 0.53
	9.71 ± 0.51 (17 mM NaCl)	ND	ND
	44.43 ± 2.85 (50 mM NaCl)	ND	ND
DAD	>100	>100	ND
DAD-CT$^{Arg-Ala}$	>500	>500	ND
FH1-FH2^{I732A}	6.78 ± 0.96	4.41 ± 0.76	ND
cDAAM^{I732A}	0.064 ± 0.02	0.093 ± 0.04	ND

[a] The values were derived in the presence of 5 mM NaCl, unless indicated otherwise.

ever, the increase in salt concentration (*i.e.* increase in the amount of NaCl) resulted in a gradual decrease in actin affinity, suggesting an ionic strength-dependent interaction (Fig. 3*A* and Table 1), which is similar to the salt-dependent interaction reported for the tail domain of Capuccino (15). DAD-CT interacts with profilin/G-actin equally well as with free G-actin indicating that profilin does not affect the binding (Fig. 3*A* and Table 1). In contrast to DAD-CT, the interaction of the DAD domain lacking the CT region with monomeric actin is extremely weak even at low ionic strength conditions (K_D >100 μM at 5 mM NaCl) (Fig. 3*A* and Table 1). To further analyze which regions are important in the interaction between DAD-CT and monomeric actin, we investigated a construct in which the basic arginine residues found in the CT region were replaced by alanines (DAD-CT$^{Arg-Ala}$) (Fig. 1, *A* and *C*). Our data did not show a detectable interaction between DAD-CT$^{Arg-Ala}$ and monomeric actin (K_D >500 μM at 5 mM NaCl) (Fig. 3*A* and Table 1).

To further elaborate on the binding mode of DAD-CT, the influence of different actin-binding proteins was tested on its interaction with G-actin. Profilin is known to interact with the

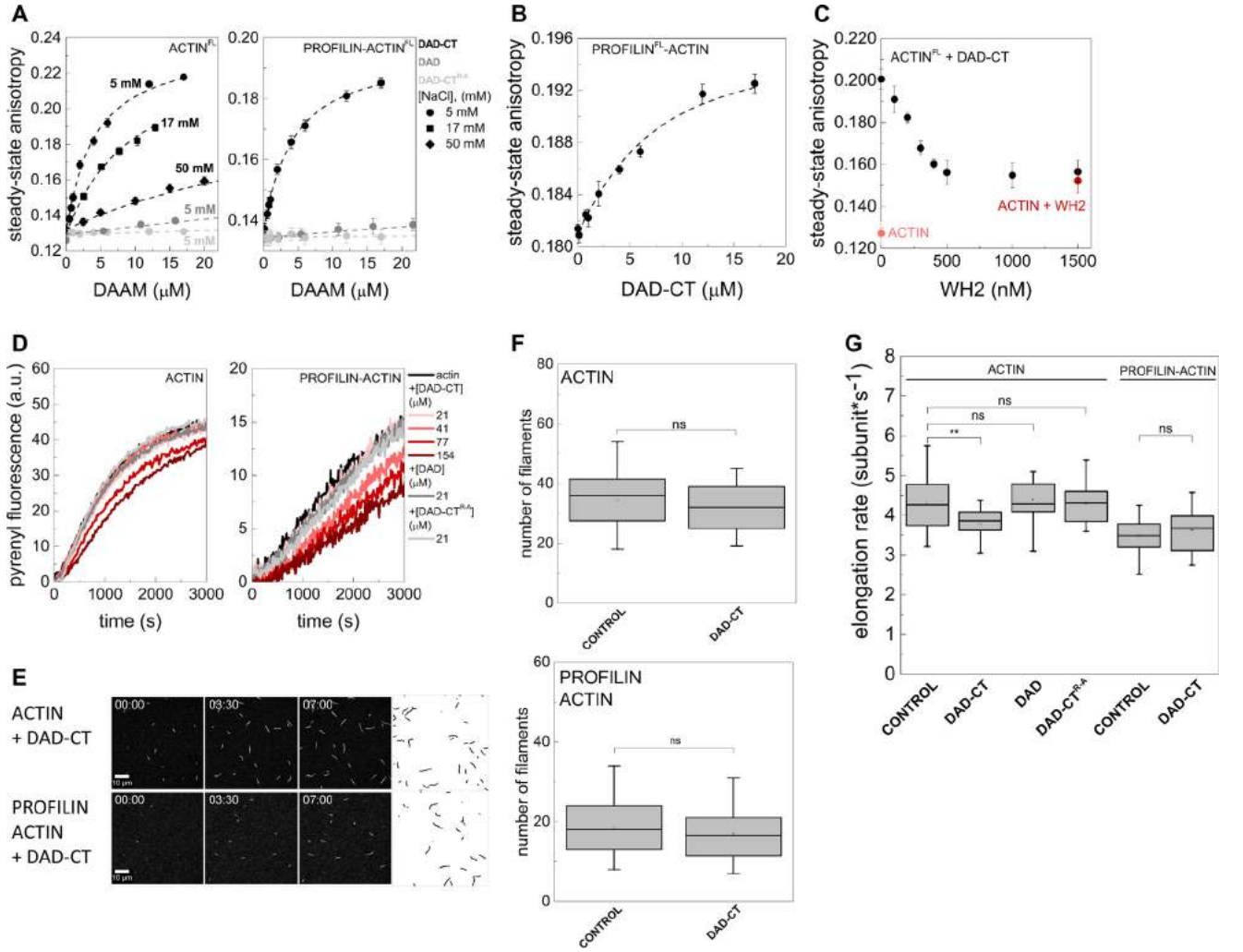

Figure 3. Interactions of DAD-CT and DAD with actin. *A,* steady-state anisotropy of Alexa488NHS-labeled G-actin in the absence and presence of profilin as the function of DAD-CT, DAD, and DAD-CT$^{Arg-Ala}$ concentrations, as indicated. *Dashed lines* in the corresponding colors show the fits to the data according to Equation 3. Dissociation equilibrium constants are summarized in Table 1. *Error bars,* standard deviations, $n = 2–4$. Final concentrations are as follows: [actin] = 0.2 μM; [LatA] = 4 μM; [profilin] = 0.8 μM; [NaCl] = 5 mM (*circles*); 17 mM (*squares*); 50 mM (*diamonds*). *FL,* fluorescently labeled protein. *B,* steady-state anisotropy of Alexa568NHS-labeled profilin in the presence of G-actin as the function of DAD-CT concentration, as indicated. *Dashed line* in the corresponding color shows the fit to the data according to Equation 3. Dissociation equilibrium constant is given in Table 1. *Error bars,* standard deviations, $n = 2–3$. Final concentrations are as follows: [actin] = 4 μM; [LatA] = 8 μM; [profilin] = 2 μM; [NaCl] = 5 mM. *FL,* fluorescently labeled protein. *C,* steady-state anisotropy of Alexa488NHS-labeled G-actin in complex with DAD-CT as a function of SALS-WH2 concentration. As controls, the steady-state anisotropies of G-actin in the absence of any binding proteins and G-actin saturated with SALS-WH2 (1.5 μM) are shown. Final concentrations are as follows: [actin] = 0.2 μM; [LatA] = 4 μM; [DAD-CT] = 20 μM; [NaCl] = 5 mM. *FL,* fluorescently labeled protein. *D,* representative polymerization kinetics of free G-actin and profilin/G-actin in the absence and presence of the C-terminal regions of DAAM, as indicated. Final concentrations are as follows: [actin] = 2 μM; [profilin] = 6 μM. *E,* TIRFM montages of actin assembly and representative skeletonized images showing the field of view of actin assembly in the absence and presence of DAD-CT, as indicated (for spontaneous actin assembly see Fig. 2*D*). *Scale bar* = 10 μm, time = min/s. Final concentrations are as follows: [actin] = 0.5 μM; [profilin] = 2 μM; [DAAM] = 42 μM. *F,* number of actin filaments nucleated spontaneously or in the presence of DAD-CT derived from skeletonized images. Final concentrations as in *E*, $n = 16–20$. *G,* elongation rate of individual actin filaments polymerized from free and profilin/G-actin in the absence and presence of DAD-CT (42 μM), DAD (42 μM), or DAD-CT$^{Arg-Ala}$ (42 μM). Final concentrations as in *E*, $n = 24–79$. *ns,* not significant.

hydrophobic cleft of monomeric actin (31). The steady-state anisotropy of fluorescently labeled profilin in complex with G-actin was measured in the presence of DAD-CT. We found that DAD-CT causes a concentration-dependent increase in the steady-state anisotropy of profilin bound to G-actin (Fig. 3*B* and Table 1). In case of competitive binding, one would expect the dissociation of fluorescent profilin from G-actin, which would result in a decrease in anisotropy. The opposite tendency that we observed suggests that a ternary complex is formed between monomeric actin, profilin, and DAD-CT, indicating that the core binding site of DAD-CT is different from that of profilin. Next, we tested how the interaction of DAD-CT is influenced by WH2 domain proteins, which N-terminally interact with the barbed face, while their C terminus binds along the ridge between the inner and outer domains of actin up to the pointed end (32–34). We used the WH2 domains of sarcomere length short protein (SALS-WH2), which have relatively long C-terminal extensions linked to the N-terminal α-helix (28). The steady-state anisotropy of the DAD-CT–G-actin complex was decreased upon addition of SALS-WH2 in a concentration-dependent manner (Fig. 3*C*). At a high SALS-WH2 concentration, the value of the anisotropy decreased to the value characteristic to the SALS-WH2–G-actin complex, suggesting that SALS-WH2 interferes with the G-actin binding

of DAD-CT. This indicates that the main binding site of DAD-CT overlaps with that of WH2.

Altogether, these observations indicate that the isolated C terminus of DAAM can interact with monomeric actin and that the core C-terminal actin-binding elements are located mainly in the CT region that is able to establish electrostatic interactions with actin.

DAD-CT does not influence actin dynamics in the absence of the FH2 domain

To test the functional consequences of monomer binding, the effects of isolated DAD-CT on actin dynamics were investigated. In fluorescence spectroscopy experiments we found that DAD-CT does not affect significantly the assembly of free G-actin and profilin/G-actin at lower concentrations (Fig. 3*D*). However, higher amounts of DAD-CT ($> \sim 40-50\ \mu$M) resulted in a concentration-dependent decrease in the pyrenyl fluorescence, similarly to what was observed for Capuccino tail (15). In agreement with the spectroscopic data, TIRFM experiments showed that DAD-CT cannot affect significantly actin nucleation (Fig. 3, *E* and *F*), and it does not affect the rate of elongation at lower concentrations either (data not shown). DAD-CT moderately slows elongation of free G-actin when it is present at higher amounts ($> \sim 40\ \mu$M) ($\nu_{\text{DAD-CT}} = 3.79 \pm 0.4$ subunit·s^{-1} ($p = 0.009$), Fig. 3*G*), but it does not influence elongation from profilin/G-actin ($\nu_{\text{DAD-CT}} = 3.64 \pm 0.6$ subunit·s^{-1} ($p = 0.47$), Fig. 3*G*). Also, DAD and DAD-CT$^{\text{Arg–Ala}}$ do not show any effect in the above experiments, consistent with their negligible interaction with monomeric actin (Fig. 3*G*).

In conclusion, in contrast to the DAD region of mDia1 (13), the isolated DAAM DAD-CT cannot influence significantly actin assembly in the absence of the FH2 domain, which suggests that the C-terminal region of DAAM possesses an FH2-dependent function in the regulation of actin dynamics.

Functional CT is required for the full nucleation promoting activity of DAAM

To further elaborate on the contribution of the DAD-CT region to the nucleation activity of the FH2 domain, we tested its effect in the presence of the FH2 domain. For this purpose, two C-terminally modified constructs were generated possessing the native FH2 but lacking a functional CT region, either by deleting the CT region (cDAAMΔCT) or by introducing the Arg–Ala mutation into the CT region (cDAAM$^{\text{Arg–Ala}}$) (Fig. 1*A*). The effects of the two constructs are indistinguishable from each other both in pyrenyl and TIRFM actin assembly assays, which support that the two modifications are equivalent (Fig. 4). However, neither cDAAMΔCT nor cDAAM$^{\text{Arg–Ala}}$ can retrieve the maximum nucleation-promoting activity of cDAAM. Both C-terminally modified constructs are ~6-fold more efficient in accelerating the overall rate of actin polymerization than FH1–FH2, but they are ~6-fold less effective than cDAAM possessing the native CT region (Fig. 4, *A* and *B*). Because they influence elongation in a similar manner as the wild-type constructs, the polymerization-promoting effect of cDAAMΔCT and cDAAM$^{\text{Arg–Ala}}$ originates from their actin nucleation activity, which is intermediate as compared with FH1–FH2 and cDAAM, as revealed by TIRFM measurements (Figs. 2*F* and 4, *C–E*).

These observations suggest that DAD contributes to the nucleation-promoting activity of cDAAM, but the presence of a functional CT region is absolutely necessary to reconstitute its full nucleation ability. Our data also indicate that the contribution of DAD and CT regions to actin nucleation is non-cooperative.

DAD-CT cannot compensate for loss-of function mutation-induced defects in the main activities of the FH2 domain

To better understand the role of DAD-CT in DAAM-mediated actin dynamics, the activities of this region were investigated in the presence of a mutant FH2 domain. The αD helix of the knob region of the FH2 domain contains a highly conserved Ile residue, which is essential for FH2-mediated polymerization (Fig. 1*B*) (13, 14, 23, 35, 36). By introducing the I732A mutation, we generated a cDAAM$^{\text{I732A}}$ construct that contains the DAD-CT region and an FH1–FH2$^{\text{I732A}}$ version that is devoid of the C-terminal domains (Fig. 1*A*). Steady-state anisotropy measurements revealed that the I732A mutation severely reduces the ability of the FH2 domain to bind both free and profilin/G-actin in the absence of DAD-CT (Fig. 5*A* and Table 1). However, we observed that cDAAM$^{\text{I732A}}$ can bind actin with similar affinity as cDAAM, which indicates that the presence of DAD-CT can compensate for the defects in monomer binding induced by the I732A mutation (Fig. 5*A* and Table 1).

In pyrenyl polymerization assays, we found that FH1–FH2$^{\text{I732A}}$ inhibits the overall polymerization of free G-actin, but the assembly rate of profilin/G-actin is not affected in the concentration range that we could test in these experiments (Fig. 5*B*). The cDAAM$^{\text{I732A}}$ mutant is more efficient in reducing the rate of actin assembly from both free G-actin and profilin/G-actin than FH1–FH2$^{\text{I732A}}$ (Fig. 5*B*). Importantly, the inhibition of the bulk polymerization rate by the constructs carrying the mutation is the opposite as to that observed for the wild-type FH2 domain (Fig. 2, *A* and *B*). These observations show that the I732A mutation impairs the proper actin assembly activities of DAAM FH2, which is consistent with previous data (36). To better understand the underlying effects, TIRFM experiments were performed. In contrast to the wild-type fragments (Fig. 2*E*), filament number was not changed significantly in the presence of either of the two mutant constructs (Fig. 5, *C* and *D*). This finding indicates that despite being able to interact with actin, the I732A mutation abolishes the nucleation activity of DAAM. Our data also suggest that the presence of the DAD-CT region is able to counteract the actin-binding defects of the FH2 domain induced by I732A; however, it cannot restore the proper functionality of the mutated FH2 domain in actin nucleation. The analysis of the effects on elongation revealed that FH1–FH2$^{\text{I732A}}$ only moderately affects filament growth from free G-actin in the concentration range in which the wild-type construct almost completely inhibits elongation ($\nu_{\text{FH1–FH2}}{}^{\text{I732A}} = 4.09 \pm 0.4$ subunit·s^{-1} ($p = 0.03$), Fig. 5*E*). Even higher amounts (20 μM FH1–FH2$^{\text{I732A}}$) resulted only in ~55% inhibition (Fig. 5*E*). In agreement with the pyrenyl polymerization experiments, FH1–FH2$^{\text{I732A}}$ does not affect significantly filament growth from profilin/G-actin at low concentrations

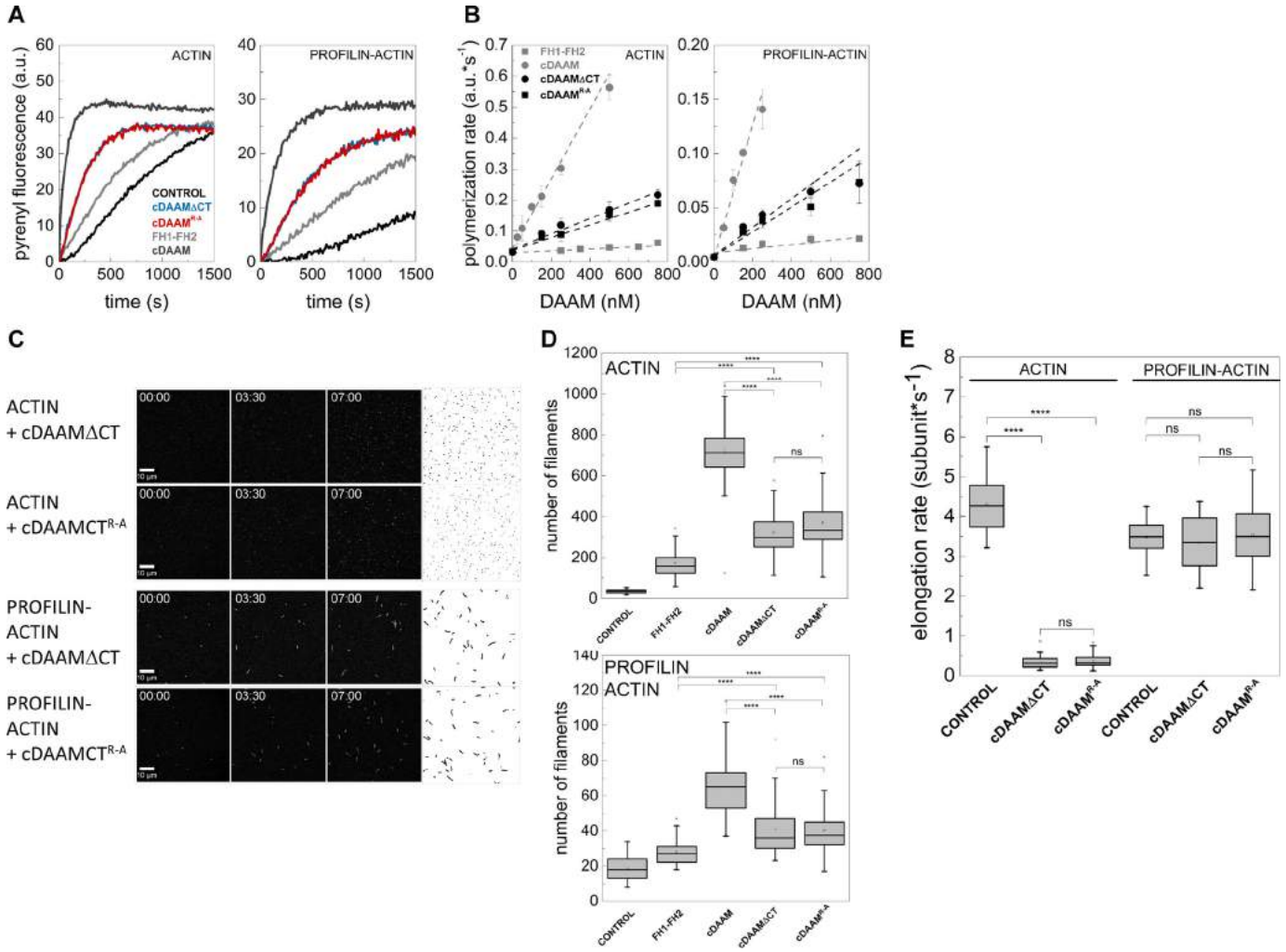

Figure 4. Effects of DAAM DAD and CT regions in the presence of the native FH2 domain. *A,* representative pyrenyl traces of spontaneous and cDAAM$^{Arg-Ala}$- or cDAAMΔCT-catalyzed assembly of free G-actin and profilin/G-actin, as indicated. The data for FH1–FH2 and cDAAM from Fig. 2*E* are shown here as controls. Final concentrations are as follows: [actin] = 2 μM; [profilin] = 6 μM; [cDAAM$^{Arg-Ala}$] = 200 nM; [cDAAMΔCT] = 200 nM. *B,* cDAAM$^{Arg-Ala}$ or cDAAMΔCT concentration dependence of the relative polymerization rate of free G-actin and profilin/G-actin, as indicated. *Error bars,* standard deviations, n = 3–4. Data obtained for FH1–FH2 and cDAAM from Fig. 2*B* are shown. *C,* TIRFM montages of actin assembly and representative skeletonized images showing the field of view of actin assembly in the absence and presence of cDAAM$^{Arg-Ala}$ or cDAAMΔCT, as indicated (for spontaneous actin assembly see Fig. 2*D*). *Scale bar,* 10 μm, time = min/s. Final concentrations are as follows: [actin] = 0.5 μM; [profilin] = 2 μM; [cDAAM$^{Arg-Ala}$] = 100 nM; [cDAAMΔCT] = 100 nM. *D,* number of actin filaments nucleated spontaneously or in the presence of cDAAM$^{Arg-Ala}$ or cDAAMΔCT derived from skeletonized images. Final concentrations as in *C*, n = 20–54. *E,* elongation rate of individual actin filaments polymerized from free and profilin/G-actin in the absence and presence of cDAAM$^{Arg-Ala}$ or cDAAMΔCT. Final concentrations as in *C*, n = 39–79. *a.u.*, arbitrary units; *ns*, not significant.

($v_{FH1-FH2}^{I732A}$ = 3.53 ± 0.4 subunit·s^{-1} (p = 0.30), Fig. 5*E*), although it moderately inhibits elongation when it is added at higher amounts ($v_{FH1-FH2}^{I732A}$ = 2.09 ± 0.1 subunit·s^{-1} ($p <$ 0.0001), Fig. 5*E*). cDAAM^{I732A} moderately slows filament elongation when it is added at the same amount as cDAAM (v_{cDAAM}^{I732A} = 3.97 ± 0.3 subunit·s^{-1} (p = 0.00014), Fig. 5*E*). At relatively high concentrations (2 μM), it largely slows down the elongation from free G-actin, similarly to the wild-type protein (v_{cDAAM}^{I732A} = 0.15 ± 0.02 subunit·s^{-1} ($p < 0.0001$), Fig. 5*E*). However, unlike cDAAM that maintains elongation in the presence of profilin (Fig. 2*F*), cDAAM^{I732A} functions oppositely, it hinders profilin/G-actin association to barbed ends in a concentration-dependent manner (Fig. 5*E*).

The reduced filament growth rate observed in the presence of cDAAM^{I732A} can result from the altered barbed-end rate constants of monomers due to capping-like function and/or a decrease in assembly-competent G-actin due to sequestration. To test these possibilities, the influence of cDAAM^{I732A} on the amount of unassembled actin was measured at steady-state ($J(c)$ plot, Fig. 5*F*). In the case of spontaneous actin assembly, the steady-state amount of unassembled free G-actin (critical concentration) is reflected by the breaking point of the $J(c)$ plot (Fig. 5*F*). In the absence of DAAM, the breaking point appeared at ~100 nM, in agreement with the well-established value of the barbed-end critical concentration (Fig. 5*F*) (1, 2). The $J(c)$ plot recorded in the presence of cDAAM^{I732A} was parallel to the plot obtained for actin, and the breaking point was not affected significantly (Fig. 5*F*). The complete and permanent blocking of barbed ends by classic barbed-end capping proteins, such as CapG, would result in a shift of the breaking point up to the value characteristic to the critical concentration of pointed ends (~600 nM) (1–3, 28). The unaffected breaking point indicates that the filament ends are not strongly capped by cDAAM^{I732A}, and monomer-polymer exchanges at barbed

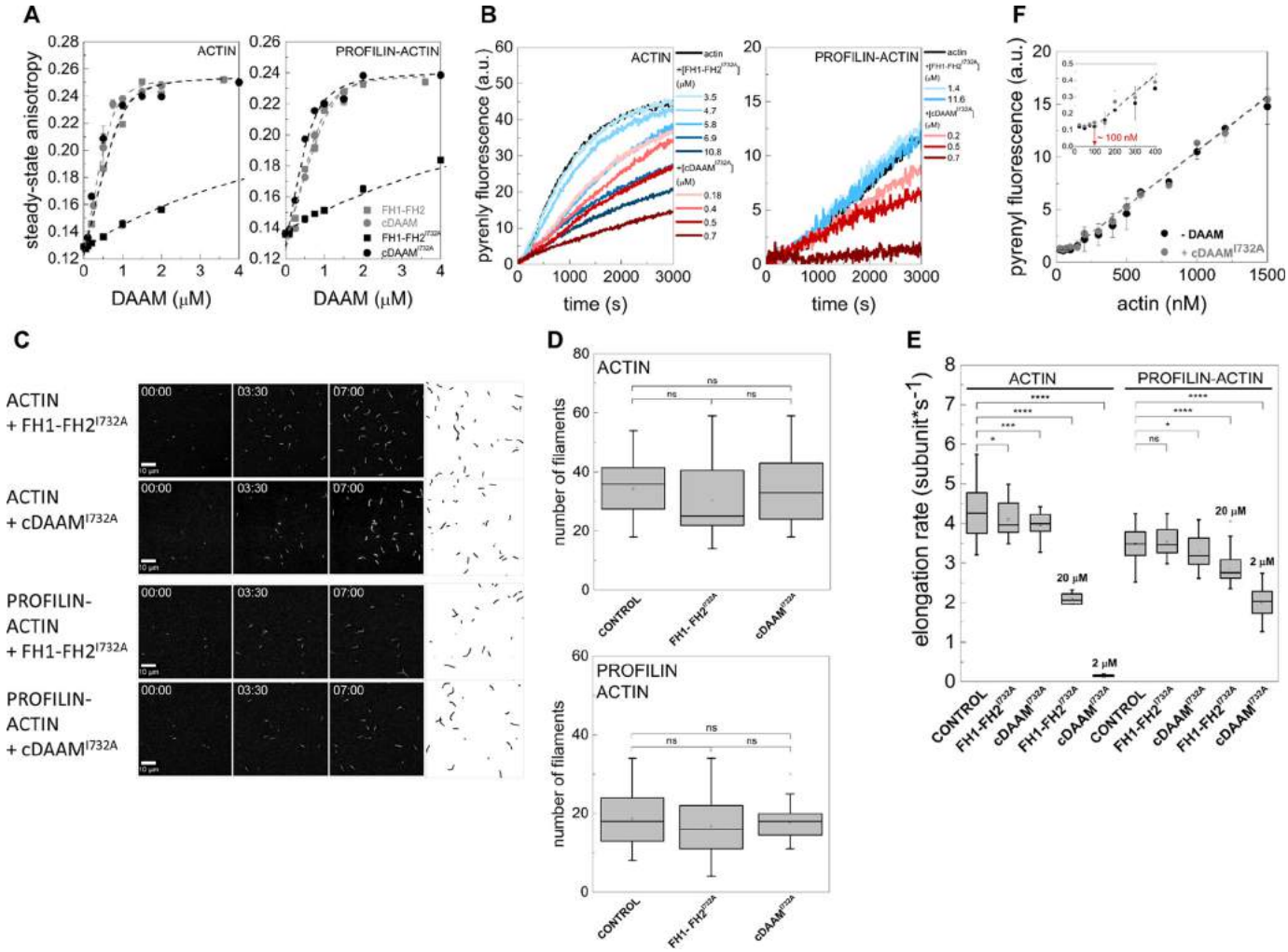

Figure 5. Effects of DAAM DAD and CT regions on the loss-of-function mutation of FH2. *A,* steady-state anisotropy of Alexa488NHS-labeled G-actin in the absence and presence of profilin as the function of DAAM concentration, as indicated. The data for FH1–FH2 and cDAAM from Fig. 2*C* are shown here as controls. *Dashed lines* in the corresponding colors show the fits to the data according to Equation 3. Dissociation equilibrium constants are summarized in Table 1. *Error bars,* standard deviations, $n = 2–3$. Final concentrations are as follows: [actin] = 0.2 μM; [LatA] = 4 μM; [profilin] = 0.8 μM; [NaCl] = 5 mM. *B,* representative polymerization kinetics of free G-actin and profilin/G-actin in the absence and presence of different regions of DAAM, as indicated. Final concentrations are as follows: [actin] = 2 μM; [profilin] = 6 μM. *C,* TIRFM montages of actin assembly and representative skeletonized images showing the field of view of actin assembly in the absence and presence of FH1–FH2^{I732A} and cDAAM^{I732A}, as indicated (for spontaneous actin assembly see Fig. 2*D*). *Scale bar,* 10 μm, time = min/s. Final concentrations are as follows: [actin] = 0.5 μM; [profilin] = 2 μM; [FH1–FH2^{I732A}] = 100 nM; [cDAAM^{I732A}] = 100 nM. *D,* number of actin filaments nucleated spontaneously or in the presence of FH1–FH2^{I732A} and cDAAM^{I732A} derived from skeletonized images. Final concentrations as in *C*, $n = 20–50$. *E,* elongation rate of individual actin filaments polymerized from free and profilin/G-actin in the absence and presence of FH1–FH2^{I732A} and cDAAM^{I732A}. Final concentrations as in *C*. 20 and 2 μM indicate the data obtained in the presence of higher concentrations of FH1–FH2^{I732A} and cDAAM^{I732A}, respectively, $n = 15–79$. *F,* critical concentration ($J(c)$) plots of actin assembly in the absence and presence of cDAAM^{I732A} (1 μM), as indicated. *Inset,* enlarged view of the initial part of the $J(c)$ plot, *red arrow* highlights the breaking points corresponding to the unassembled actin at steady-state. *Dashed lines* in the corresponding colors show the fit to the linear part of the data. *Error bars,* standard deviations, $n = 3$. *a.u.*, arbitrary units; *ns*, not significant.

ends can occur. We made a similar observation for other DAAM constructs (21). In the case of sequestration, considering the dissociation equilibrium constant of the cDAAM^{I732A}/G-actin interaction (Table 1), the critical concentration of actin assembly (Fig. 5*F*), and the concentration of cDAAM^{I732A} used in this experiment (1 μM), one would expect an increase of ~500 nM in the amount of unassembled actin due to sequestration, which would result in a significant shift in the breaking point to ~600 nM (28). In contrast, in the case of sequestration, the number of actin filaments is expected to be decreased (28); however, in TIRFM experiments we found that cDAAM^{I732A} does not change filament number (Fig. 5*D*), which further supports the lack of sequestering activity. Therefore, these data support that cDAAM^{I732A} neither sequesters G-actin nor blocks completely and permanently monomer-polymer exchange at barbed ends as a classic capping protein. To explain the large but not complete inhibition of elongation by cDAAM^{I732A}, one can assume that it slows filament elongation at barbed ends by influencing the rate constants of subunit association and/or dissociation.

Consistently with the importance of the conserved Ile residue in actin interaction (37), the mutation impairs not only the nucleation ability of the FH2 domain but also diminishes its interaction with the barbed end of the filaments. The combination of these two effects results in a decreased bulk polymerization rate, detected in the pyrenyl polymerization assays (Fig. 5*B*). At high concentration, DAAM FH2^{I732A} can maintain some interactions with filament ends similarly to other formins

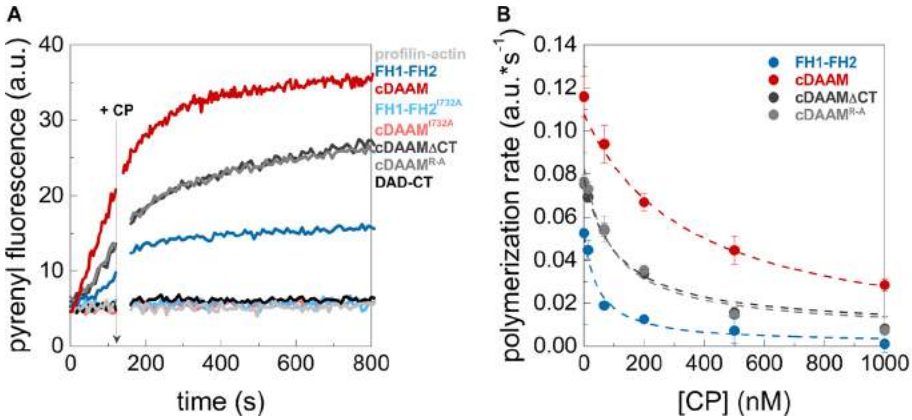

Figure 6. Antagonism between DAAM and CP. *A,* polymerization of profilin/G-actin initiated in the absence and presence of DAAM constructs, as indicated. The addition of CP after 120 s is indicated by an *arrow*. Final concentrations are as follows: [actin] = 2 μM; [profilin] = 6 μM; [CP] = 68 nM; [DAAM] = 200 nM. *B,* polymerization rates before ([CP] = 0 nM) and after addition of CP at different concentrations derived from pyrenyl traces. *Dashed lines* in the corresponding color show the fit of the data using Equation 2. The fit gave IC_{50} values of IC_{50}(cDAAM) = 345.9 ± 27.60 nM; IC_{50}(FH1–FH2) = 47.7 ± 16.97 nM; IC_{50}(cDAAMΔCT) = 108.6 ± 19.35 nM; and IC_{50}($cDAAM^{Arg-Ala}$) = 93.7 ± 19.06 nM for CP inhibition. *Error bars,* standard deviations, n = 2–4. *a.u.*, arbitrary units.

(*e.g.* mDia1 (13)). Even if such high concentration is physiologically not relevant, this approach allowed us to address the effects of DAD-CT on the interaction of FH2 with barbed ends. Our data indicate that besides the key Ile residue, other residues/binding sites in the FH2 domain also contribute to barbed-end interactions of DAAM, albeit with much lower affinities. Comparative structural analysis of DAAM FH2 with other formins reveals that residues in the knob region near the Ile^{732}, as well as the lasso/post interface, can contribute to actin binding (36). Based on our data, the coordination between these different binding sites is crucial for functional barbed-end interaction. Importantly, our observations that the magnitude of the effect of the $FH2^{I732A}$ mutant on filament elongation is more pronounced in the presence of DAD-CT than in the absence of it suggests that the C-terminal regions are important for filament end interaction.

DAD-CT contributes to the antagonism with capping proteins

We found that $cDAAM^{I732A}$ affects filament end dynamics more efficiently than the $FH1–FH2^{I732A}$ (Fig. 5, *B* and *E*), which suggests that besides nucleation, DAD-CT is also important for filament end interaction. We studied the effect of these domains in the presence of capping protein (CP) to further analyze the potential role of DAD-CT in the formin/barbed-end interaction. CP is well known for its ability to bind to filament barbed ends and block their elongation (Fig. 6) (38, 39). Formins were shown to be able to antagonize the effect of CPs at barbed ends to sustain processive growth of actin filaments (40–44). Thus, we investigated whether DAAM can compete with CP for barbed-end binding and, if it does so, which regions are important for this activity. Actin assembly was initiated in the absence or presence of different DAAM constructs, and the CP in increasing amounts was added to the polymerization mixtures after ~120 s (Fig. 6*A*) (40). CP inhibits both the rate and the extent of DAAM-mediated actin assembly for all constructs, however with different efficiencies (Fig. 6). Quantitative analysis revealed that cDAAM is more efficient than FH1–FH2 in protecting filament ends (IC_{50} = 345.9 ± 27.60 nM and IC_{50} = 47.7 ± 16.97 nM, respectively). Mutations in the CT region (cDAAMΔCT and $cDAAM^{Arg-Ala}$) partially reduce the ability of DAAM to compete with CP (IC_{50} = 108.6 ± 19.35 nM for cDAAMΔCT and IC_{50} = 93.7 ± 19.06 nM for $cDAAM^{Arg-Ala}$ Fig. 6). $FH1–FH2^{I732A}$ and $cDAAM^{I732A}$ failed to antagonize the capping effect when added at the same concentration as the wild-type constructs, in agreement with the importance of Ile^{732} in barbed-end interaction (Fig. 6*A*) (37). Because $FH1–FH2^{I732A}$ and $cDAAM^{I732A}$ do not show any difference in this assay, we conclude that the DAD-CT region is unable to compete for barbed-end binding in the absence of a functional FH2 domain (Fig. 6*A*). Consistent with this, we found that the isolated DAD-CT cannot uncap CP-bound barbed ends (Fig. 6*A*). These observations corroborate the role of the C-terminal regions of DAAM in filament-end interaction. Importantly, our data clearly demonstrate that although the FH2 domain is necessary for uncapping of CP, the DAD-CT regions can contribute to this antagonistic activity by tuning the filament end protection ability of FH2.

Role of DAD-CT in FH2-mediated F-actin interaction

Previously, we showed that both *Drosophila* DAAM FH2 and FH1–FH2 possess actin filament binding and bundling activities (21). This activity is characteristic for the human Daam1 protein, as well (30, 45). Based on this and to further extend our studies on the role of DAD-CT in actin interaction, we investigated whether the DAD-CT region can interact with F-actin in high-speed co-sedimentation experiments (Fig. 7*A*). The amount of DAD-CT sedimented with F-actin increased in a concentration-dependent manner, which indicates that DAD-CT can bind to the sides of filamentous actin with a dissociation equilibrium constant of K_D(DAD-CT) = 38.9 ± 3.2 μM (Fig. 7*A*). This suggests less efficient interaction than that of the FH2 domain, which is characterized by K_D in the low micromolar range (21). Removal of the CT significantly reduces the binding strength of the C terminus (K_D(DAD) >100 μM), whereas the binding of the $DAD-CT^{Arg-Ala}$ mutant to F-actin is negligible (Fig. 7*A*). To test the functional consequences of side binding, the bundling activity of DAAM was studied in low-speed centrifugation assays. We found that FH1–FH2, as well as cDAAM bundle actin filaments with approximately the same efficiency, and the I723A mutation does not affect the bundling

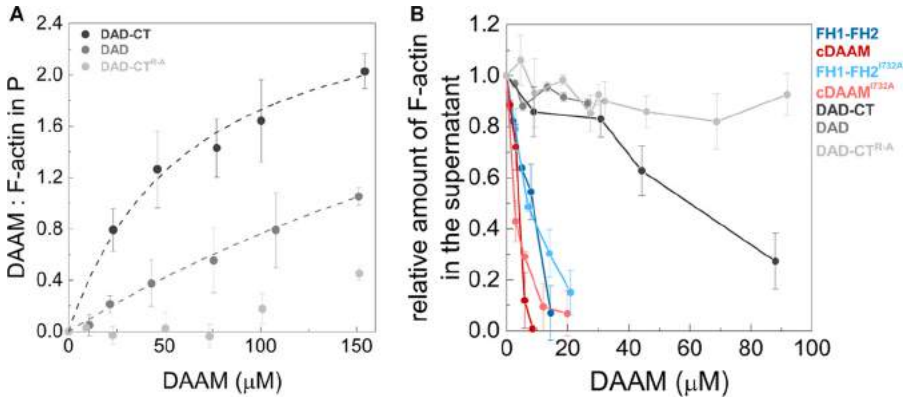

Figure 7. Interaction of DAD-CT with actin filaments. *A,* DAAM/F-actin ratio in the pellet (*P*) derived from the analysis of SDS-polyacrylamide gels. *Dashed lines* correspond to the fit of the data (21, 35); the fit gave K_D values of K_D(DAD-CT) = 38.9 ± 3.2 μM, K_D(DAD) > 100 μM. [F-actin] = 2.5 μM. *Error bars,* standard deviations, n = 2–4. *B,* bundling activity of different regions of DAAM. The relative amount of actin filaments in the supernatant as the function of DAAM concentration, determined from the quantification of SDS-PAGE analysis of the samples. Final concentrations are as follows: [F-actin] = 1 μM. *Error bars,* standard deviations, n = 2–3.

activity of FH2 (Fig. 7*B*). Our results revealed that the DAD-CT region can also bundle F-actin, independently of the FH2 domain; however, its efficiency is extremely low (Fig. 7*B*). Neither DAD nor DAD-CT$^{Arg-Ala}$ show significant activity at the concentrations we could test in the experiments (Fig. 7*B*).

Altogether, these results show that the isolated DAD-CT can interact with the sides of actin filaments and also suggest that the FH2 domain of DAAM is the core actin filament side-binding/bundling element, whereas the C-terminal region appears to have a minor contribution to this activity. Consistently with the G-actin interaction, these data further support that the main C-terminal actin-binding element is the CT region.

Actin assembly promoting activity of the FH2 domain of DAAM is regulated through an autoinhibitory interaction

The DRF formin subfamily proteins are regulated by intramolecular autoinhibitory interactions mediated by the N-terminal DID and the C-terminal DAD domains. DAAM possesses the N- and C-terminal sequence elements characteristic for these regulatory domains (Fig. 1*A*). Consistently, our previous investigations showed that *Drosophila* DAAM constructs lacking either one of the DID or DAD regions behave as constitutively active forms of the protein in *in vivo* assays (17). To address this issue biochemically, the effects of the recombinant DID fragment on FH1–FH2 (lacking the C-terminal DAD-CT region) and cDAAM (possessing the C-terminal DAD-CT region)-mediated actin assembly were investigated in pyrenyl polymerization experiments (Fig. 8*A*). We found that DID does not affect the spontaneous actin polymerization or the actin assembly promoting activity of FH1–FH2 (Fig. 8*A*). In contrast, it inhibits the cDAAM-mediated actin polymerization in a concentration-dependent manner (Fig. 8). At saturating DID concentrations, the polymerization rate was reduced to the value characteristic of spontaneous actin assembly (Fig. 8). For quantitative analysis, the relative polymerization rates from the slopes of the pyrenyl traces at half-maximum polymerization were derived and plotted as the function of DID concentration (Fig. 8*B*). The fit gave a dissociation equilibrium constant of ~30 nM, consistent with a tight interaction between the DID and the DAD-CT domains (see Equation 1).

These results support that the interaction of the FH2 domain of DAAM with actin is regulated by intramolecular interactions between the DID and the C-terminal regions (46). Thus, although the DAD-CT domain might be able to bind actin very weakly (Fig. 3*A*), similar to other DRFs, its major function is likely related to DID binding through which it shades the actin assembly activity of the FH2 domain.

In vivo activity of the CT region

To further assess the functional importance of the actin-interacting domains of DAAM, *Drosophila* primary neuronal cultures were used to analyze the *in vivo* effect of FH2 and CT on actin assembly. We took advantage of the fact that growth cone filopodia are primarily actin-based structures, and we previously showed that overexpression of a constitutively active form of dDAAM, lacking the DAD domain (ΔDAD-dDAAM), induces a significant increase in the filopodia number in primary neurons (17). To exploit this effect, CT-truncated and/or FH2^{I732A}-mutated ΔDAD-dDAAM constructs were expressed in *Drosophila* embryos (Fig. 9*A*). In accordance with our former results, the pan-neuronal expression of ΔDAD-dDAAM induced a significant increase of axonal filopodia formation as compared with control cells (9.9 ± 0.60 *versus* 6.9 ± 0.37) (Fig. 9, *B* and *C*). In contrast to it, overexpression of ΔDAD-CT-dDAAM induced only a moderate increase in filopodia number (7.8 ± 0.60) (Fig. 9, *B* and *C*). Thus, the constitutively active form of dDAAM was more effective in the presence of the CT region. Contribution of the FH2 domain was analyzed by expression of ΔDAD-dDAAM^{I732A}, which was also able to induce a moderate increase in filopodia number (7.9 ± 0.54), comparable with that of ΔDAD-CT-dDAAM (Fig. 9, *B* and *C*). These results reveal that, despite the huge differences in their *in vitro* actin assembly activity, the FH2 and CT domains display some requirements during filopodia formation in cultured neurons. In agreement with a partly redundant role, the filopodia number of cells expressing ΔDAD-CT-dDAAM^{I732A} was comparable with that of control cells (6.9 ± 0.52) (Fig. 9, *B* and *C*); thus, the lack of CT combined with the I732A mutation abolished completely the actin assembly activity of dDAAM.

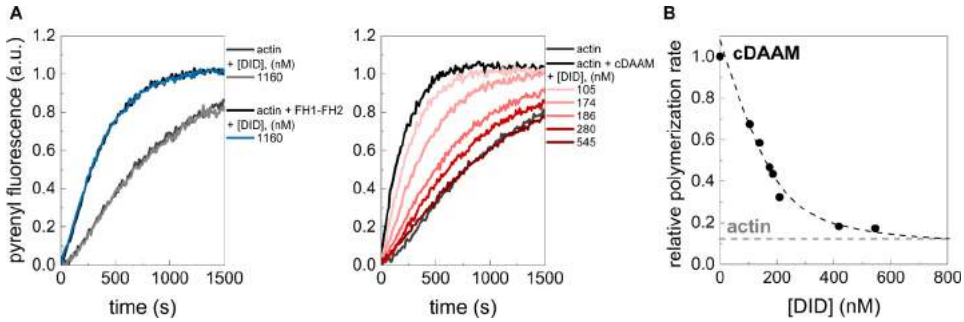

Figure 8. FH2/actin interaction is regulated through the DID/DAD-CT interaction. *A,* representative polymerization kinetics of actin in the absence and presence of DID, FH1–FH2, and cDAAM, as indicated. [actin] = 2 μM (containing 5% pyrenyl actin), [FH1–FH2] = 5 μM, [cDAAM] = 0.51 μM. *B,* relative polymerization rate of cDAAM catalyzed actin assembly as a function of DID concentration. *Dashed line* corresponds to the fit of the data using Equation 1. The fit gave half-inhibition of cDAAM by DID at 30.5 ± 14.31 nM. *a.u.*, arbitrary units. The relative rate of spontaneous actin assembly is indicated by *gray dashed line*.

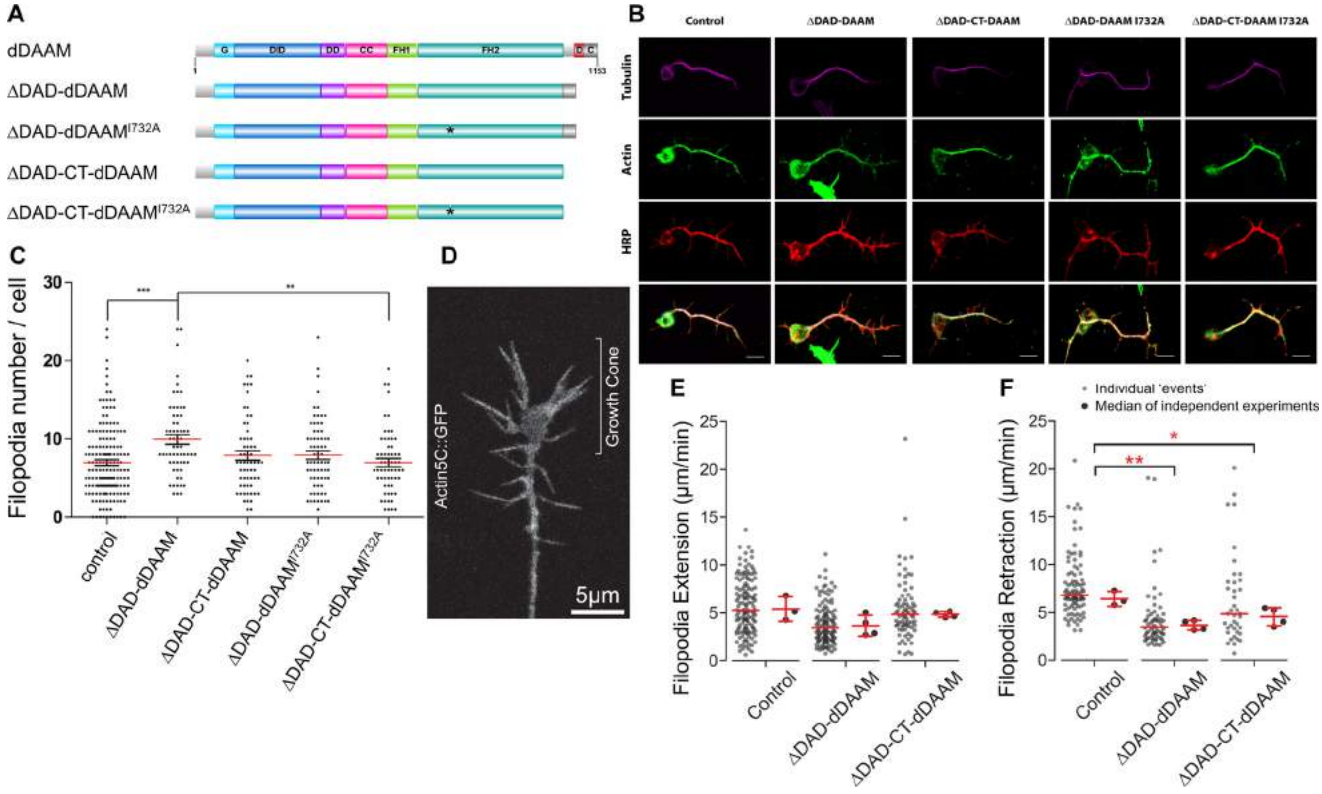

Figure 9. Constitutively active dDAAM induces filopodia formation in *Drosophila* primary neurons. *A,* domain organization of full-length *D. melanogaster* DAAM formin and of the constructs investigated in the *in vivo* experiments. Abbreviations are as in Fig. 1*A*. The position of the I732A mutation is highlighted by *asterisk*. The figure was made with Illustrator for Biological Sciences (57). *B,* representative images of primary neurons obtained from control or constitutively active dDAAM-overexpressing embryos, stained with tubulin (*magenta*), actin (*green*), and HRP (*red*). *Scale bar,* 5 μm. *C,* expression of ΔDAD-dDAAM (*c155>UAS-ΔDAD-dDAAM*, n = 62) construct induced a significant increase of filopodia number compared with control (*c155/+*, n = 162) and ΔDAD-CT-dDAAM I732A (*c155>UAS-ΔDAD-dDAAM I732A*, n = 60)-expressing cells. The other genotypes were not significantly different (*c155>ΔDADCT-dDAAM*, n = 61; *c155>ΔDADCT-dDAAM I732A*, n = 68). Data presented on the figure are given as mean ± S.E. Data were analyzed with Kruskal-Wallis for the whole-data set, followed by Dunn's post hoc test for multiple comparison. *D,* representative image from a time-lapse sequence of a neuronal growth cone expressing Actin5C::GFP. *Scale bar* = 5 μm (corresponding to supplemental Movie 1). *E,* comparison of filopodia extension rate showed no significant difference (one-way analysis of variance, p = 0.09; control, 5.4 ± 1.2, mean ± S.D., n = 3/134; ΔDAD-dDAAM, 3.6 ± 1.2, mean ± S.D., n = 4/118; ΔDAD-CT-dDAAM, 4.8 ± 0.3, mean ± S.D., n = 4/77). *F,* retraction rate is significantly lower in the case of ΔDAD and ΔDAD-CT overexpression, compared with the control filopodia (one-way analysis of variance, p = 0.0047; control, 6.4 ± 0.7, mean ± S.D., n = 3/91; ΔDAD-dDAAM, 3.6 ± 0.5, mean ± S.D., n = 4/63; ΔDAD-CT-dDAAM, 4.5 ± 0.9, mean ± S.D., n = 4/40).

To better understand the mechanisms of the actin-binding domains of DAAM in filopodia formation, filopodia dynamics was studied in primary neurons expressing ΔDAD-dDAAM or ΔDAD-CT-dDAAM. Filopodia dynamics was followed by co-expression of actin5C::GFP (Fig. 9*D*), and as expected, live imaging of 7–9 HIV neurons revealed an extensive movement of filopodia (supplemental Movie 1), including lateral displacement, collapse, stasis, and fusion. To characterize filopodia dynamics, we used extension and retraction as readouts (Fig. 9, *E* and *F*). We found that the overexpression of the truncated DAAM isoforms do not change significantly the extension rate as compared with control neurons, expressing actin5C::GFP alone (Fig. 9*E*). However, overexpression of the activated DAAM isoform (ΔDAD-dDAAM) leads to decreased filopodia retraction (Fig. 9*F*). This finding indicates that activated DAAM is probably involved in filopodia stabilization rather

Table 2
Properties of the C-terminal elements of different formins
Mm is *M. musculus* and *Dm* is *D. melanogaster*.

Formin	Main actin interacting module[a]	G-actin binding affinity	Nucleation activity in isolated form/contribution to FH2-mediated nucleation	Affecting G-actin interaction	Other effects in actin dynamics
Mm INF2 (12>)	**WH2-like/DAD sequence**	K_D ~0.06 μM 50 mM KCl	No/yes	Profilin interferes	Monomer sequestration, filament severing
Mm FMNL3 (14)	**WH2**-DAD-CT	K_D ~2–3 μM 50 mM KCl	Yes/yes	INF2 C terminus interferes mDia1 C terminus does not interfere	Inhibits elongation (~ nM)
Mm Dia1 (13)	**DAD**-CT	K_D ~100 μM 200 mM NaCl	Yes/yes	Profilin does not interfere	Accelerates elongation (~ μM)
Dm Capu (15)	**tail**	K_D ~20 μM 50 mM NaCl	No/yes	WH2, RPEL1 interfere Profilin does not significantly interfere	Inhibits elongation (>10 μM)
Dm DAAM (this study)	DAD-**CT**	K_D = 44.4 ± 2.85 μM 50 mM NaCl	No/yes	Profilin does not interfere WH2 interferes	Inhibits elongation (>40–50 μM)

[a] The main actin interacting elements of the C-terminal regions are highlighted in boldface.

than filopodia elongation, although it still remains possible that DAAM is also involved in the initial actin nucleation steps of filopodia formation. The retraction rate upon ΔDAD-CT–dDAAM overexpression is in between the wild-type control and that of ΔDAD-dDAAM (Fig. 9*F*), suggesting that the CT domain may have a minor role in filopodia stabilization.

Thus, the analysis of filopodia number and dynamics in primary neurons revealed that the CT domain of DAAM appears to contribute to filopodia formation *in vivo*, and it may also affect the dynamic behavior of filopodia.

Discussion

In this work we extended the characterization of the C-terminal elements of formins by analyzing the role of the DAD and CT regions of *Drosophila* DAAM in the regulation of actin dynamics both *in vitro* and *in vivo*. We showed that the DAD-CT tunes the nucleation activity and the proper filament end interactions of the FH1–FH2 domains of DAAM, as well as its ability to antagonize with CP.

Our data revealed that the DAD-CT region of DAAM can interact with actin *in vitro*; however, the binding of isolated DAD is very weak, and hence it is the CT region that is largely responsible for actin interaction (Fig. 3*A* and Table 1). The C-terminal regions of mDia1, INF2, and FMNL3 possess sequence elements characteristic of the N terminus of the actin-binding WH2 domains (12–14). Comparative sequence analysis of the DAD-CT regions of DAAM indicates some sequence similarity to WH2 domains, as well (Fig. 1*C*). The DAD region contains the conserved hydrophobic amino acid triplet of LL*XX*I, which mediates interactions between the N terminus of WH2 domains and the hydrophobic cleft of actin (34). However, the characteristic LKK(T/V) motif, which is essential for the actin binding of WH2 domains, is completely absent from the C terminus of DAAM (Fig. 1*C*). Similar sequence characters can be observed for the DAD of mDia1 and FMNL3, which also bind actin relatively weakly (Fig. 1*C* and Table 2) (13, 14). Conversely, INF2 possesses the LKK(T/V) motif that appears to strengthen its affinity to actin (Table 2) (12). The CT of DAAM is a relatively long (~40 aa) extension and predicted to be intrinsically disordered. Our mutational analysis indicates that the Arg/Lys residues in the CT region are central to efficient actin binding (Fig. 3*A*). Basic amino acids in the C terminus of mDia1, FMNL3, and Capuccino were shown to contribute to their actin affinity (13, 14, 47). These data suggest that the weak actin binding of the DAD region of formins might be attributed to the hydrophobic WH2-like amino acid triplet; however, other sequence elements that are present in the CT region appear to ensure a significantly stronger interaction.

The DAD-CT region of DAAM has similar affinity for free G-actin and profilin-bound G-actin (Fig. 3*A* and Table 1). We do not detect any indication for mutually exclusive binding between profilin and DAD-CT to monomeric actin, whereas DAD-CT is displaced by WH2 domains possessing a relatively long and disordered C-terminal extension (Fig. 3, *B* and *C*). Profilin interacts with the hydrophobic cleft of subdomains 1 and 3 of actin, which might interfere with the WH2-like binding mode of DAD. The long C-terminal half of WH2 extends along the negative surface patch of the actin molecule toward the pointed face, through interactions mainly controlled by electrostatic forces (32–34). The similar structural features and the competitive binding of DAAM CT and WH2 domains indicate that DAAM CT adapts a binding mode, which is similar to that of the C terminus of WH2. These considerations further support our conclusion that the main actin-binding element of DAD-CT is not the DAD but is the CT region (Fig. 10).

As opposed to mDia1 DAD, the isolated DAD-CT of DAAM cannot nucleate actin filaments on its own, even in its dimeric form maintained by GST (13). However, it markedly contributes to the nucleation efficiency of the FH2 domain, yet a properly functioning FH2 domain is absolutely essential for nucleation (Figs. 2, 4, and 5). The actin binding strengths of the FH1–FH2 and cDAAM constructs are apparently the same (Fig. 2*C* and Table 1). From this aspect the FH2 domain of DAAM differs from other formins, which requires the C-terminal regions for efficient G-actin binding (13, 22, 23). However, the more potent nucleation activity of cDAAM as compared with that of FH1–FH2 indicates that the presence of the DAD-CT region must change the structural and/or kinetic features of FH1–FH2 when in complex with actin. This is supported by our data, which indicate positive cooperativity between the association of FH2 and DAD-CT to actin, as well as structural considerations as discussed below.

Besides their role in stabilizing nucleation intermediaries, our results also indicate that the C-terminal regions can contribute to proper filament end interaction and to the processivity of DAAM. This is supported by the fact that cDAAM is more efficient in maintaining filament elongation in the pres-

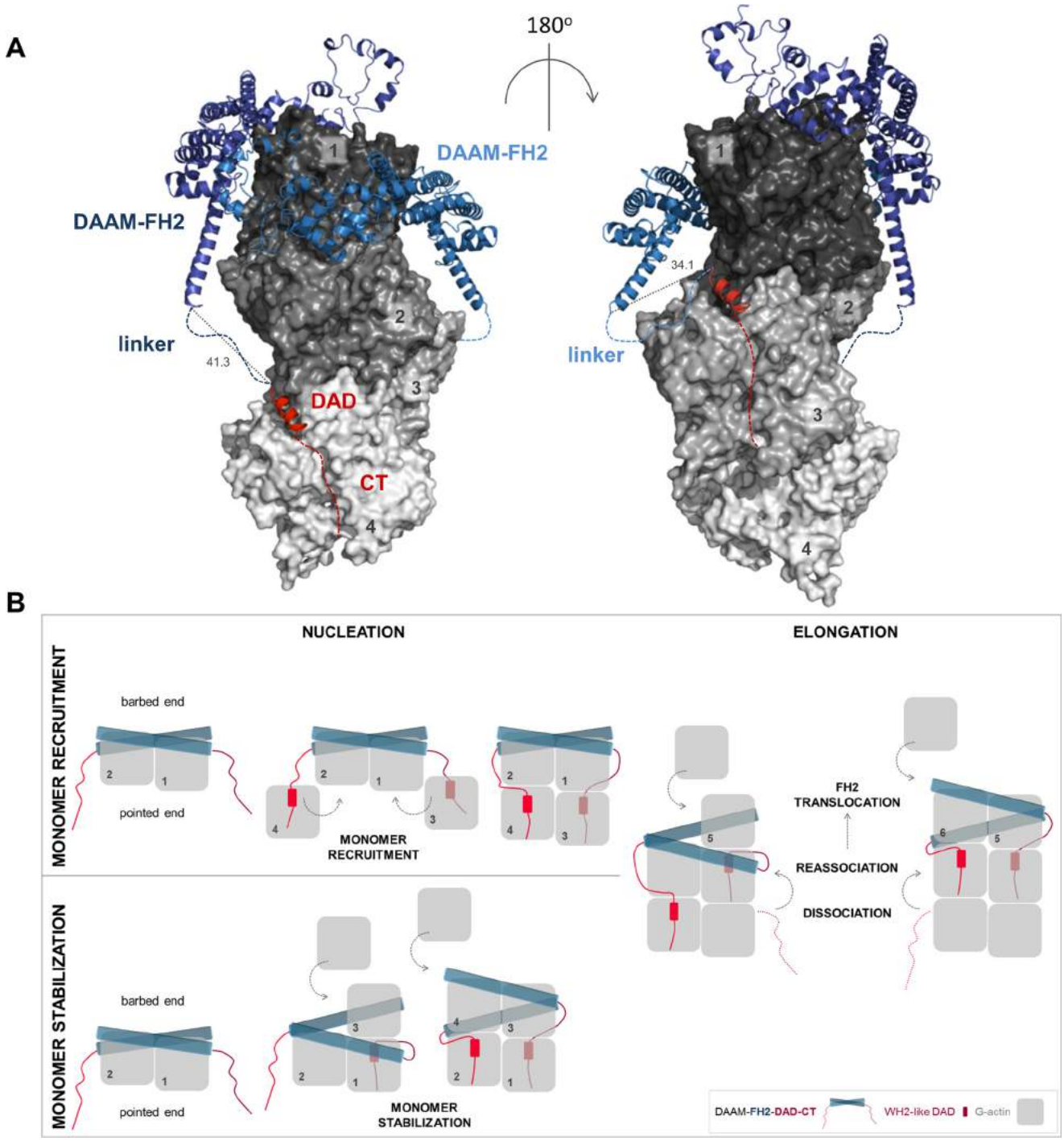

Figure 10. Structural model of the interactions of FH2, DAD, and CT with actin. *A,* model was generated using X-ray structures of complexes of FH2–actin and WH2–actin. Four actin subunits (*gray,* indicated by *numbers*) are shown according to their arrangement in the Oda's model (58). The FH2 dimer of DAAM (*blue*) and the DAD region of mDia1 (*red*) are represented as *ribbons*. *Red dashed lines* indicate the possible orientation of the disordered CTs of DAAM. *Blue dashed lines* indicate the ~20-aa linkers connecting the FH2 and DAD of DAAM. Distances are given in Å. The model was generated with PyMOL based on the alignment of following structures: Protein Data Bank codes: 4EAH ((48) FMNLFH2-TMR-actin); 2Z6E ((59) hDAAM-FH2); 2BAP ((60) mDia1-DAD); and 2A41 ((61) WIP-WH2). *B,* alternative model describing actin nucleation mediated by FH2-DAD-CT for low-affinity C-terminal formin regions. In this scenario, the binding of DAD-CT to actin requires increased affinity, which may be manifested through monomer capturing by FH2.

ence of capping protein than FH1–FH2 and that the DAD-CT region influences the effect of the I732A mutation on actin elongation (Figs. 5 and 6). Recent findings on the co-regulation of barbed-end dynamics by CPs and formins (*e.g.* mDia1, FMNL2, and human Daam1) propose the existence of a ternary or decision complex at the filament end (40, 43). Because of the overlapping binding sites of CPs and formins, the co-existence of these proteins at the filament end results in steric clashes, which can be resolved by the partial dissociation of both CPs and formin from the barbed end, as suggested by structural modeling (43). According to the proposed structural features, the main filament end interacting region of the formin in the

ternary complex is the αD helix in the knob region. Disrupting this region, by introducing the mutation in the conserved Ile residue, is expected to loosen the formin/barbed-end interaction and weaken its integrity in the ternary complex. This may result in a faster dissociation and/or slower association or complete removal of the formin, leaving the ends capped by CPs, consistently within our experiments (Fig. 6). Importantly, our results shed light on the importance of DAD-CT in the anti-capping activity of DAAM. The more efficient anti-capping activity of cDAAM as compared with FH1–FH2 (Fig. 6) indicates that the C-terminal regions of DAAM contribute to the stability of the ternary complex, which relies on both DAD and CT. Nevertheless, it seems that the loss-of-function defects in the FH2 domain regarding filament end interaction can be compensated by DAD-CT only in the absence of profilin and CPs. This indicates that in a complex biological context, *i.e.* filopodial elongation or sarcomeric thin filament lengthening, the FH2 domain of DAAM is essential for properly functioning barbed-end interactions.

What is the mechanistic view of the enhancement of FH2-mediated actin assembly by DAD-CT?

DAD-CT can stabilize the structure of the FH2 domain making it a more efficient nucleator, by which it would contribute indirectly, independent from its own actin binding ability, to the core activity of FH2. A similar mode of action was proposed for the FH1 domain of FMNL3 (48). Alternatively, the binding of isolated DAD-CT to actin suggests that DAD-CT can directly interact with actin in their complexes with FH1–FH2–DAD-CT to promote nucleation. In support of this, structural data predict that each of the DAD-CT regions in the FH1–FH2–DAD-CT dimer can establish contacts with an actin monomer (Fig. 10*A*). This would result in the stabilization of four actin subunits by DAAM, which would completely overcome the structural and kinetic barrier of actin assembly imposed by the nucleation phase. Accordingly, the current model proposes that the FH1–FH2-C terminus forms a tripartite machinery, in which the C terminus serves as a monomer recruitment motif (13, 48). This model implies that the actin monomers captured by DAD-CT would incorporate at pointed ends, which can be interfered with by profilin. In contrast, the model implicates that the affinity of the C-terminal of DAAM and some other formins, which is relatively weak in their isolated forms (Table 2), must be strengthened in their complexes with FH2. This might occur by FH2-mediated structural changes in the C-terminal regions. Alternatively, the FH2 domain by bringing actin subunits into the close proximity of DAD-CT could increase the apparent affinity of the C terminus. In this scenario, the low-affinity C-terminal regions of formins may be involved in the stabilization of the FH2–actin complex, whereas high-affinity C-terminal domains can mediate monomer recruitment (Fig. 10*B*). Besides nucleation, DAD-CT also supports the interaction of FH2 with the filament ends, as well as its anti-capping efficiency. This is manifested possibly through interactions of the DAD-CT with the sub-terminal actin subunits, consistently with the proposed structural model (Fig. 10) (48). In the presence of the C-terminal regions, the stair stepping of formins requires the dissociation and re-association of both FH2 and DAD-CT, which can influence the processive mode of filament end tracking, as suggested by our data and the work of others (15).

The contribution of the DAD-CT of DAAM in tuning the activities of the FH2 domain is supported by the analysis of its role in neuronal actin dynamics (Fig. 9). Our results point to the importance of the CT region in actin interactions, in good agreement with the biochemical data. Interestingly, the *in vivo* data suggest that the contributions of the FH2 and CT regions to filopodia formation are comparable. An explanation might be that the CT region of DAAM is not only important for actin interaction but it can also associate with other cytoskeletal regulators, which can contribute to the functioning of DAAM. As examples, Flightless I was shown to directly interact with the C terminus of DAAM and modulate its actin assembly activity; also other formins can bind microtubules that influence their interactions with actin (20, 47, 49).

In conclusion, the C terminus of DAAM shares similar properties to other formins with regard to actin binding and tuning the nucleation-promoting activity of the FH2 domain, as well as to its processive filament end tracking. We also demonstrate that DAD-CT makes the FH2 domain more efficient in antagonizing with capping protein. Our observations suggest that the effects of DAD-CT on the actin nucleation and elongation activities of DAAM are manifested by cooperative structural and/or kinetic stabilization of the interaction of FH2 with actin. Altogether, our work provides support for the idea that the DAD-CT region plays a significant role in modulation of the actin-assembling properties of the *Drosophila* member of the DAAM formin.

Experimental procedures

Protein purifications and modifications

For bacterial protein expression, cDNAs of DAAM subfragments (DID, 115–356 aa; cDAAM, 568–1153 aa; FH1–FH2, 568–1054 aa; cDAAMΔCT, 568–1116; DAD-CT, 1083–1153 aa; and DAD, 1083–1119 aa) and their mutated versions (FH1–$FH2^{I732A}$, $cDAAM^{I732A}$, $cDAAM^{Arg-Ala}$, and $DAD\text{-}CT^{Arg-Ala}$) (Fig. 1*A*) were inserted into pGEX-2T vector (Amersham Biosciences). Constructs were expressed as glutathione *S*-transferase (GST) fusion proteins in *Escherichia coli* BL21(DE3)pLysS strain (Novagen). Transformed bacteria were grown at 37 °C in Luria Broth powder microbial growth medium (Sigma). Protein expression was induced by addition of 1 mM isopropyl β-D-1-thiogalactopyranoside at A_{600} ~0.6–0.8. After overnight expression at 20 °C, the bacterial extracts were collected by centrifugation (10,000 × *g*, 15 min, 4 °C) and stored at −80 °C until use. For protein purification, the bacterial pellet was lysed by sonication in Lysis buffer (50 mM Tris-HCl, pH 7.6, 5 mM DTT, 50 mM NaCl, 5 mM EDTA, 1% sucrose, 10% glycerol supplemented with 1 mM PMSF, 5 mM $MgCl_2$, 0.1 mg/ml DNase, and Protease Inhibitor Mixture (Sigma P8465)). The cell lysate was ultracentrifuged (110,000 × *g*, 1 h, 4 °C). The supernatant was slowly loaded onto GSH resin (Amersham Biosciences) in a column. For FH domain-containing constructs, the column was sequentially washed with Lysis, Wash1 (50 mM Tris-HCl, pH 7.6, 5 mM DTT, 400 mM NaCl, 10% (v/v) glycerol, 1% (w/v) sucrose), ATP (50 mM Tris-HCl, pH 7.6, 5 mM DTT, 100 mM KCl, 10 mM $MgCl_2$, 0.25 mM ATP, 5% (v/v) glycerol, 1% (w/v) sucrose), and Wash2 (50 mM Tris-HCl, pH 7.6, 5 mM DTT, 50

mM NaCl, 5 mM $MgCl_2$, 10 mM KCl, 5% (v/v) glycerol, 1% (w/v) sucrose) buffers. For the C-terminal constructs, lacking the FH domains, the column was washed with Lysis and Wash2 buffers. The proteins were eluted by Wash2 buffer supplemented with 50 mM glutathione-reduced (Sigma G4251), concentrated (Vivaspin 30,000-Da cutoff), and loaded onto PD10 column (GE Healthcare 17-0851-01) for buffer exchange to Storing buffer (50 mM Hepes, pH 7.6, 5 mM DTT, 50 mM NaCl, 5% (v/v) glycerol, 1% (w/v) sucrose). Before flash-freezing in liquid nitrogen, the constructs were clarified by ultracentrifugation (300,000 × *g*, 30 min, 4 °C) and stored at −80 °C until use. Control experiments showed that a freeze/thaw cycle does not affect the functionality of the constructs (data not shown). Typically, 5–6 g of bacterial pellet yielded 1–1.2 mg/ml protein. The protein concentrations were measured spectrophotometrically using the extinction coefficients at 280 nm and molecular weights derived from the amino acid sequence (ExPASy ProtParam tool http://web.expasy.org/protparam/).[3] Actin was purified from rabbit skeletal muscle, gel-filtered on Superdex 200, and stored in G buffer (4 mM Tris-HCl, pH 7.8, 0.1 mM $CaCl_2$, 0.2 mM ATP, 0.005% NaN_3, 0.5 mM β-mercaptoethanol) according to standard protocols (50, 51). Actin was labeled at Lys^{328} by Alexa Fluor® 488 carboxylic acid succinimidyl ester (Alexa488NHS, Invitrogen) or at Cys^{374} by *N*-(1-pyrene)iodoacetamide (pyrene, Thermo Fisher Scientific) according to standard protocols (21, 28, 52). Mouse profilin 1 was purified as described previously and labeled with Alexa Fluor® C_5 568 maleimide (Alexa568C, Invitrogen) (28, 53). Heterodimeric mouse αβ CP and the WH2 domain-containing construct of SALS (SALS-WH2) were purified as described previously (28, 54).

General experimental considerations

Samples at each concentration were prepared individually for experiments. All measurements were performed at 20 °C. The sum of the volume of the proteins and the volume of their storing buffer were constant in the samples and represented a maximum 50% of the total volume of the sample. The concentrations given in the text are final concentrations. In all experiments Mg^{2+}-ATP-actin was used. The actin monomer-bound Ca^{2+} was replaced by Mg^{2+} by adding 200 μM EGTA and 50 μM $MgCl_2$ and incubating the samples for 5–10 min at room temperature.

Pyrenyl polymerization assays

The polymerization kinetics of Mg^{2+}-ATP–G-actin was measured using pyrene-actin. The actin concentration was 2 μM that containing 5 or 2% pyrenyl-labeled actin in the case of free G-actin and profilin–G-actin, respectively. In profilin-containing samples, the profilin concentration was 6 μM. The polymerization was initiated by the addition of 1 mM $MgCl_2$ and 50 mM KCl in the absence and presence of different proteins (for exact sample composition and concentrations, see the figure legends). The measurements were performed using a Safas Xenius FLX spectrofluorimeter (λ_{ex} = 365 nm, λ_{em} = 407 nm). To quantitatively analyze the effect of DAAM on actin assembly, the polymerization rates were determined from the slope of the pyrenyl traces at half-maximum polymerization. The relative polymerization rates were derived as the ratio of the polymerization rate measured in the presence of different amounts of DAAM and the polymerization rate of spontaneous actin assembly (Figs. 2*B* and 4*B*). For the quantitative analysis of the effect of DID on cDAAM-mediated actin assembly (Fig. 8*B*), the relative polymerization rate was derived as the ratio of the polymerization rate measured in the presence of cDAAM and different amounts of DID and the polymerization rate measured in the presence of cDAAM and in the absence of DID. The DID concentration dependence of the relative polymerization rate ($v_{relative}$) was fit by Equation 1,

$$v_{relative} = \left(1 - \frac{[cDAAM{:}DID]}{[cDAAM_0]}\right) \cdot v_0 + v_{min} \qquad \text{(Eq. 1)}$$

where v_0 and v_{min} are the relative polymerization rates in the absence and presence of saturating amounts of DID, respectively; [$cDAAM_0$] is the total cDAAM concentration, and [cDAAM: DID] is the concentration of the cDAAM–DID complex, which was derived from the quadratic binding equation.

The antagonistic effect of DAAM with CP was investigated as described (40). Briefly, profilin/G-actin assembly was initiated in the absence of CP and in the presence of different DAAM constructs (200 nM), and then CP at different concentrations was added after ~120 s to the protein mixtures. Polymerization rates (v) were derived over 40 s just before and 40 s after the addition of CP. The rates were plotted as the function of [CP], and data were fit by Equation 2.

$$v = v_0 - \left(\frac{v_0 - v_{min}}{1 + \frac{IC_{50}}{[CP_0]}}\right) \qquad \text{(Eq. 2)}$$

where v_0 and v_{min} are the polymerization rates in the absence and presence of saturating amounts of CP, respectively; [CP_0] is the total CP concentration, IC_{50} is the CP concentration required for 50% inhibition.

Steady-state fluorescence experiments

Steady-state anisotropy—To study the DAAM/G-actin interaction, the steady-state anisotropy of Alexa Fluor 488 succinimidyl ester-labeled Mg^{2+}-ATP-G-actin (Alexa488NHS–G-actin) was measured. Alexa488NHS–G-actin (0.2 μM) was incubated with latrunculin A (LatA, 4 μM) for 20 min. Then DAAM constructs were added at different concentrations, and the samples were further incubated for 1 h at 20 °C. In measurements when profilin was present, profilin (0.8 μM) was added to actin after the incubation with LatA, and the samples were further incubated for 30 min at 20 °C, prior to the addition of DAAM constructs. Note that due to the presence of LatA that prevents actin polymerization, the increase in steady-state anisotropy could not result from filament formation; it solely reflects the binding of DAAM constructs to actin. To study the salt dependence of the DAD-CT/G-actin interaction, the ionic strength was set by adding NaCl to the samples (for exact concentrations see Fig. 3*A*). Anisotropy measurements were performed using a Horiba Jobin Yvon spectrofluorometer (λ_{ex} = 488 nm, λ_{em} = 516 nm; slits, 5 nm). To study the interaction of

[3] Please note that the JBC is not responsible for the long-term archiving and maintenance of this site or any other third party hosted site.

DAD-CT with profilin/G-actin, steady-state anisotropy measurements were performed using Alexa Fluor 568C_5 maleimide-labeled profilin (Alexa568C–profilin). In these experiments Alexa568C–profilin (2 μM) was added to Mg^{2+}-ATP–G-actin (4 μM) bound to LatA (8 μM), and after a 30-min incubation at 20 °C, the samples were supplemented with DAD-CT at different concentrations and further incubated for 1 h at 20 °C. The measurements were performed using a Horiba Jobin Yvon spectrofluorometer (λ_{ex} = 578 nm, λ_{em} = 600 nm; slits, 5 nm). For quantitative analysis, the DAAM concentration dependence of the steady-state anisotropy (r) measured either in the absence or presence of profilin was fit by Equation 3,

$$\frac{r - r_A}{r_{AD} - r_A} = \frac{A_0 + D_0 + K_d - \sqrt{(A_0 + D_0 + K_d)^2 - 4A_0D_0}}{2D_0} \quad \text{(Eq. 3)}$$

where A_0 and D_0 are the total G-actin and DAAM concentration, respectively, r_A is the steady-state anisotropy of Alexa488NHS–G-actin/Alexa568C–profilin; r_{AD} is the steady-state anisotropy of Alexa488NHS–G-actin/Alexa568C–profilin at saturating amount of DAAM; and K_D is the dissociation equilibrium constant of the G-actin–AAM complex.

J(c) plot measurements—To investigate the effect of cDAAM^{I732A} on the amount of unassembled actin at steady-state critical concentration, measurements were performed as described (21, 28). The cDAAM^{I732A} concentration was 1 μM. For the analysis, $J(c)$ plots were generated ([actin] dependence of the fluorescence emission).

Total internal reflection fluorescence microscopy

The effects of DAAM constructs on the assembly of individual actin filaments were followed by TIRFM, as described previously (21, 28). Glass flow cells were incubated with 1 volume of *N*-ethylmaleimide myosin for 1 min and then washed with 2 volumes of myosin buffer (4 mM Tris-HCl, pH 7.8, 1 mM DTT, 0.2 mM ATP, 0.1 mM $CaCl_2$, 500 mM KCl, 1 mM $MgCl_2$, 0.2 mM EGTA) and 2 volumes of 0.1% (w/v) BSA. Finally, flow cells were equilibrated with 2 volumes of TIRFM buffer (0.5% (w/v) methylcellulose, 0.5% (w/v) BSA, 50 mM 1,4-diazabicyclo-[2,2,2]octane, 100 mM DTT in buffer F* (4 mM Tris-HCl, pH 7.8, 1 mM DTT, 0.2 mM ATP, 0.1 mM $CaCl_2$, 50 mM KCl, 1 mM $MgCl_2$, 0.2 mM EGTA)) before adding the protein mixture (for exact protein composition and concentration see the figure legends). To follow the assembly of free G-actin or profilin/G-actin in the absence and presence of DAAM, a mixture of G-actin (0.5 μM, containing 10% Alexa488NHS–G-actin) and different DAAM constructs in TIRFM buffer was injected into the flow cell. In profilin-containing samples, the profilin concentration was 2 μM. Images were captured every 10 s with an Olympus IX81 microscope equipped with a laser-based (491 nm) TIRFM module using an APON TIRF ×60 NA1.45 oil immersion objective and a CCD camera (Hamamatsu). Images were background corrected before analysis. For analysis of the number of filaments, images were captured 15 min after the initiation of actin polymerization. Filament number was derived from a 66 × 66-μm region of the images by using Fiji. Time-lapse images were analyzed by either the Multiple Kymograph plugin of Fiji or by manually tracking filament growth to derive the elongation rate of actin filaments. Filament length was converted to subunits using 370 subunits/μm filament (55). The elongation rate of actin filaments (v) was related to the critical concentration of actin assembly (cc ~0.1 μM (1, 2)) to the association rate constant of actin monomers to filament barbed ends (k_+) and to the total actin concentration ([G_0]) by Equation 4,

$$v = k_+([G_0] - cc) \quad \text{(Eq. 4)}$$

Actin filament binding and bundling assays

To investigate the interaction of DAD-CT with actin filaments, high-speed centrifugation experiments were performed and analyzed as described (21, 28). In control experiments, we found that the C-terminal constructs appear in the pellet in the absence of F-actin, however at significantly lower amounts than in the presence of actin filaments. Therefore, for quantitative analysis, the amount of self-pelleting DAAM protein was subtracted from the amount of DAAM sedimented in the presence of actin. The final F-actin concentration was 2.5 μM. To study the bundling activity of DAAM constructs, Mg^{2+}-ATP–G-actin (10 μM) was polymerized for 2 h at 20 °C by adding 1 mM $MgCl_2$ and 50 mM KCl. Actin filaments were diluted to 1 μM in F buffer (G buffer supplemented with 1 mM $MgCl_2$ and 50 mM KCl), in the absence and presence of different DAAM constructs and further incubated for 1 h at 20 °C. Samples were centrifuged (14,000 × *g*, 5 min, 20 °C), and then the supernatants were carefully removed and processed for SDS-PAGE analysis. The protein content of the supernatants was derived from Coomassie Blue-stained gels (Syngene Bioimaging System). Quantification of Coomassie Blue intensities was performed within the linear range of exposure identified by a calibration curve. The intensity values were corrected for the molecular weight of each protein. The relative amount of F-actin in the supernatant was derived as the ratio of the amount F-actin in the absence of any other protein to the amount F-actin in the presence of different proteins.

Genetics

The following fly stocks were used for *in vivo* overexpression: *ElavGAL4^{C155}* or *w;elavGAL4* were crossed to *w;UASΔDAD-DAAM, w;UASΔDAD-CT-DAAM, w;UASΔDAD-DAAM I732A, w;UASΔDAD-CT-DAAM I732A, w;UAS-ΔDAD-DAAM;UAS-Actin5C::GFP, w;UAS-ΔDAD-CT-DAAM;UAS-Actin5C::GFP.*

Primary cell cultures

Drosophila primary neuronal cells were obtained from stage 11 embryos following a protocol published by Sanchez-Soriano *et al.* (56) with some modifications. In brief, whole embryos were squashed in Schneider's *Drosophila* (Sigma) medium supplemented with 20% heat-inactivated fetal bovine serum (Sigma), 2 μg/ml insulin (Sigma), and penicillin/streptomycin solution (Lonza). Embryonic homogenates were spun at 380 × *g* for 4 min at room temperature. Pellets were resuspended in complete medium, and the cells were grown at 27 °C on glass

coverslips or in glass-bottom Petri dishes for live imaging (MaTek). For filopodia number analysis, primary neurons were fixed 6 h after plating in 4% formaldehyde for 30 min at room temperature. Cells were washed with PBST (PBS + 0.1% Triton X-100) and then blocked in 5% goat serum diluted in PBST for 10 min. Cells were incubated with primary antibodies overnight at 4 °C (mouse anti-tubulin 1:1000 (Sigma), rat anti-actin 1:200 (Babraham Bioscience), rabbit anti-HRP 1:200 (Jackson ImmunoResearch), diluted in blocking solution). After overnight incubation, cells were washed in PBST and then incubated with secondary antibodies for 1 h at room temperature (anti-mouse Alexa 405 1:600, anti-rat Alexa 488 1:600, and anti-rabbit Alexa 647 1:600 (Life Technologies, Inc.) diluted in blocking solution). Cells were washed in PBST, and then coverslips were mounted on microscope slides in 70% glycerol. Confocal images were collected with an Olympus FV1000 LSM microscope and edited with ImageJ software.

Live imaging and filopodia dynamics

Filopodia dynamics measurements were performed on 7–9 HIV neurons in culture using an LSM 880 confocal microscope (Zeiss) equipped with a ×40, 1.4 NA oil-immersion lens. To follow actin dynamics, we overexpressed Actin5C::GFP in the cell culture, using a pan-neuronal driver (Elav-Gal4). Imaging of the neurons was performed in glass bottom Petri dishes (MatTek Corp.) in growth media. Fluorescence was excited using the 488-nm line of the argon laser and recorded at a bandwidth of 500–550 nm at an acquisition rate of 1.27 Hz. Filopodia with recognizable extension and retraction phases were selected for further analysis. To measure the extension and retraction speed, kymographs were built using KymoReslice-Wide, a Fiji plugin dedicated to generate kymographs with improved contrast. Steepness was measured manually and converted to extension and retraction velocities in Excel (Microsoft).

Statistics

The data presented were derived from at least two independent experiments. Values are displayed as mean ± S.D. The number of independent experiments are given in the figure legends. The significance was calculated using two-sample *t* tests or *Z* tests considering the number of data and the variance (Excel, Microsoft). The data were analyzed by Kruskal Wallis or one-way analysis of variance considering the distribution of the data. By convention, $p \geq 0.05$ was considered as statistically not significant; *, $p < 0.05$; **, $p < 0.01$; ***, $p < 0.001$; and ****, $p < 0.0001$. The significance levels are given in the text and on the corresponding figure.

Author contributions—A. T. V. performed the experiments, analyzed the data, and prepared the digital images. I. F. performed the experiments, analyzed the data, and prepared the digital images. Sz. Sz., performed the experiments, analyzed the data, and prepared the digital images. E. M. performed the experiments. R. G. performed the experiments and analyzed the data. M. A. T., T. H., and R. P. performed the experiments and analyzed the data. G. C. S. T. read the article for intellectual content. J. M. conceived and designed the experiments, analyzed the data, and drafted the article. B. B. conceived and designed the experiments, performed the experiments, analyzed the data, drafted the article, prepared the digital images.

References

1. Bugyi, B., and Carlier, M. F. (2010) Control of actin filament treadmilling in cell motility. *Annu. Rev. Biophys.* **39,** 449–470
2. Pollard, T. D. (2007) Regulation of actin filament assembly by Arp2/3 complex and formins. *Annu. Rev. Biophys. Biomol. Struct.* **36,** 451–477
3. Pollard, T. D. (2016) Actin and actin-binding proteins. *Cold Spring Harb. Perspect. Biol.* 10.1101/cshperspect.a018226
4. Schönichen, A., and Geyer, M. (2010) Fifteen formins for an actin filament: a molecular view on the regulation of human formins. *Biochim. Biophys. Acta* **1803,** 152–163
5. Goode, B. L., and Eck, M. J. (2007) Mechanism and function of formins in the control of actin assembly. *Annu. Rev. Biochem.* **76,** 593–627
6. Breitsprecher, D., and Goode, B. L. (2013) Formins at a glance. *J. Cell Sci.* **126,** 1–7
7. Alberts, A. S. (2001) Identification of a carboxyl-terminal diaphanous-related formin homology protein autoregulatory domain. *J. Biol. Chem.* **276,** 2824–2830
8. Li, F., and Higgs, H. N. (2003) The mouse Formin mDia1 is a potent actin nucleation factor regulated by autoinhibition. *Curr. Biol.* **13,** 1335–1340
9. Otomo, T., Otomo, C., Tomchick, D. R., Machius, M., and Rosen, M. K. (2005) Structural basis of Rho GTPase-mediated activation of the formin mDia1. *Mol. Cell* **18,** 273–281
10. Otomo, T., Tomchick, D. R., Otomo, C., Machius, M., and Rosen, M. K. (2010) Crystal structure of the Formin mDia1 in autoinhibited conformation. *PLoS ONE* **5,** e12896
11. Rose, R., Weyand, M., Lammers, M., Ishizaki, T., Ahmadian, M. R., and Wittinghofer, A. (2005) Structural and mechanistic insights into the interaction between Rho and mammalian Dia. *Nature* **435,** 513–518
12. Chhabra, E. S., and Higgs, H. N. (2006) INF2 is a WASP homology 2 motif-containing formin that severs actin filaments and accelerates both polymerization and depolymerization. *J. Biol. Chem.* **281,** 26754–26767
13. Gould, C. J., Maiti, S., Michelot, A., Graziano, B. R., Blanchoin, L., and Goode, B. L. (2011) The formin DAD domain plays dual roles in autoinhibition and actin nucleation. *Curr. Biol.* **21,** 384–390
14. Heimsath, E. G., Jr., and Higgs, H. N. (2012) The C terminus of formin FMNL3 accelerates actin polymerization and contains a WH2 domain-like sequence that binds both monomers and filament barbed ends. *J. Biol. Chem.* **287,** 3087–3098
15. Vizcarra, C. L., Bor, B., and Quinlan, M. E. (2014) The role of formin tails in actin nucleation, processive elongation, and filament bundling. *J. Biol. Chem.* **289,** 30602–30613
16. Matusek, T., Djiane, A., Jankovics, F., Brunner, D., Mlodzik, M., and Mihály, J. (2006) The *Drosophila* formin DAAM regulates the tracheal cuticle pattern through organizing the actin cytoskeleton. *Development* **133,** 957–966
17. Matusek, T., Gombos, R., Szécsényi, A., Sánchez-Soriano, N., Czibula, A., Pataki, C., Gedai, A., Prokop, A., Raskó, I., and Mihály, J. (2008) Formin proteins of the DAAM subfamily play a role during axon growth. *J. Neurosci.* **28,** 13310–13319
18. Molnár, I., Migh, E., Szikora, S., Kalmár, T., Végh, A. G., Deák, F., Barkó, S., Bugyi, B., Orfanos, Z., Kovács, J., Juhász, G., Váró, G., Nyitrai, M., Sparrow, J., and Mihály, J. (2014) DAAM is required for thin filament formation and sarcomerogenesis during muscle development in *Drosophila*. *PLoS Genet.* **10,** e1004166
19. Bao, B., Zhang, L., Hu, H., Yin, S., and Liang, Z. (2012) Deletion of a single-copy DAAM1 gene in congenital heart defect: a case report. *BMC Med. Genet.* **13,** 63
20. Vogler, G., Liu, J., Iafe, T. W., Migh, E., Mihály, J., and Bodmer, R. (2014) Cdc42 and formin activity control non-muscle myosin dynamics during *Drosophila* heart morphogenesis. *J. Cell Biol.* **206,** 909–922
21. Barkó, S., Bugyi, B., Carlier, M. F., Gombos, R., Matusek, T., Mihály, J., and Nyitrai, M. (2010) Characterization of the biochemical properties and biological function of the formin homology domains of *Drosophila* DAAM. *J. Biol. Chem.* **285,** 13154–13169
22. Pring, M., Evangelista, M., Boone, C., Yang, C., and Zigmond, S. H. (2003) Mechanism of formin-induced nucleation of actin filaments. *Biochemistry* **42,** 486–496

23. Xu, Y., Moseley, J. B., Sagot, I., Poy, F., Pellman, D., Goode, B. L., and Eck, M. J. (2004) Crystal structures of a formin homology-2 domain reveal a tethered dimer architecture. *Cell* **116,** 711–723
24. Coué, M., Brenner, S. L., Spector, I., and Korn, E. D. (1987) Inhibition of actin polymerization by latrunculin A. *FEBS Lett.* **213,** 316–318
25. Bosch, M., Le, K. H., Bugyi, B., Correia, J. J., Renault, L., and Carlier, M. F. (2007) Analysis of the function of Spire in actin assembly and its synergy with formin and profilin. *Mol. Cell* **28,** 555–568
26. Pollard, T. D., and Cooper, J. A. (1984) Quantitative analysis of the effect of *Acanthamoeba* profilin on actin filament nucleation and elongation. *Biochemistry* **23,** 6631–6641
27. Renault, L., Bugyi, B., and Carlier, M. F. (2008) Spire and Cordon-bleu: multifunctional regulators of actin dynamics. *Trends Cell Biol.* **18,** 494–504
28. Tóth, M. Á., Majoros, A. K., Vig, A. T., Migh, E., Nyitrai, M., Mihály, J., and Bugyi, B. (2016) Biochemical activities of the Wiskott-Aldrich syndrome homology region 2 domains of sarcomere length short (SALS) protein. *J. Biol. Chem.* **291,** 667–680
29. Pollard, T. D. (1986) Rate constants for the reactions of ATP- and ADP-actin with the ends of actin filaments. *J. Cell Biol.* **103,** 2747–2754
30. Jaiswal, R., Breitsprecher, D., Collins, A., Corrêa, I. R., Jr., Xu, M. Q., and Goode, B. L. (2013) The formin Daam1 and fascin directly collaborate to promote filopodia formation. *Curr. Biol.* **23,** 1373–1379
31. Schutt, C. E., Myslik, J. C., Rozycki, M. D., Goonesekere, N. C., and Lindberg, U. (1993) The structure of crystalline profilin-β-actin. *Nature* **365,** 810–816
32. Didry, D., Cantrelle, F. X., Husson, C., Roblin, P., Moorthy, A. M., Perez, J., Le Clainche, C., Hertzog, M., Guittet, E., Carlier, M. F., van Heijenoort, C., and Renault, L. (2012) How a single residue in individual β-thymosin/WH2 domains controls their functions in actin assembly. *EMBO J.* **31,** 1000–1013
33. Dominguez, R. (2016) The WH2 domain and actin nucleation: necessary but insufficient. *Trends Biochem. Sci.* **41,** 478–490
34. Renault, L., Deville, C., and van Heijenoort, C. (2013) Structural features and interfacial properties of WH2, β-thymosin domains and other intrinsically disordered domains in the regulation of actin cytoskeleton dynamics. *Cytoskeleton* **70,** 686–705
35. Shimada, A., Nyitrai, M., Vetter, I. R., Kühlmann, D., Bugyi, B., Narumiya, S., Geeves, M. A., and Wittinghofer, A. (2004) The core FH2 domain of diaphanous-related formins is an elongated actin binding protein that inhibits polymerization. *Mol. Cell* **13,** 511–522
36. Lu, J., Meng, W., Poy, F., Maiti, S., Goode, B. L., and Eck, M. J. (2007) Structure of the FH2 domain of Daam1: implications for formin regulation of actin assembly. *J. Mol. Biol.* **369,** 1258–1269
37. Otomo, T., Tomchick, D. R., Otomo, C., Panchal, S. C., Machius, M., and Rosen, M. K. (2005) Structural basis of actin filament nucleation and processive capping by a formin homology 2 domain. *Nature* **433,** 488–494
38. Isenberg, G., Aebi, U., and Pollard, T. D. (1980) An actin-binding protein from *Acanthamoeba* regulates actin filament polymerization and interactions. *Nature* **288,** 455–459
39. Wear, M. A., Yamashita, A., Kim, K., Maéda, Y., and Cooper, J. A. (2003) How capping protein binds the barbed end of the actin filament. *Curr. Biol.* **13,** 1531–1537
40. Bombardier, J. P., Eskin, J. A., Jaiswal, R., Corrêa, I. R., Jr., Xu, M. Q., Goode, B. L., and Gelles, J. (2015) Single-molecule visualization of a formin-capping protein 'decision complex' at the actin filament barbed end. *Nat. Commun.* **6,** 8707
41. Ramabhadran, V., Gurel, P. S., and Higgs, H. N. (2012) Mutations to the formin homology 2 domain of INF2 protein have unexpected effects on actin polymerization and severing. *J. Biol. Chem.* **287,** 34234–34245
42. Romero, S., Le Clainche, C., Didry, D., Egile, C., Pantaloni, D., and Carlier, M. F. (2004) Formin is a processive motor that requires profilin to accelerate actin assembly and associated ATP hydrolysis. *Cell* **119,** 419–429
43. Shekhar, S., Kerleau, M., Kühn, S., Pernier, J., Romet-Lemonne, G., Jégou, A., and Carlier, M. F. (2015) Formin and capping protein together embrace the actin filament in a menage a trois. *Nat. Commun.* **6,** 8730
44. Harris, E. S., Li, F., and Higgs, H. N. (2004) The mouse formin, FRLα, slows actin filament barbed-end elongation, competes with capping protein, accelerates polymerization from monomers, and severs filaments. *J. Biol. Chem.* **279,** 20076–20087
45. Higashi, T., Ikeda, T., Shirakawa, R., Kondo, H., Kawato, M., Horiguchi, M., Okuda, T., Okawa, K., Fukai, S., Nureki, O., Kita, T., and Horiuchi, H. (2008) Biochemical characterization of the Rho GTPase-regulated actin assembly by diaphanous-related formins, mDia1 and Daam1, in platelets. *J. Biol. Chem.* **283,** 8746–8755
46. Liu, W., Sato, A., Khadka, D., Bharti, R., Diaz, H., Runnels, L. W., and Habas, R. (2008) Mechanism of activation of the formin protein Daam1. *Proc. Natl. Acad. Sci. U.S.A.* **105,** 210–215
47. Roth-Johnson, E. A., Vizcarra, C. L., Bois, J. S., and Quinlan, M. E. (2014) Interaction between microtubules and the *Drosophila* formin Cappuccino and its effect on actin assembly. *J. Biol. Chem.* **289,** 4395–4404
48. Thompson, M. E., Heimsath, E. G., Gauvin, T. J., Higgs, H. N., and Kull, F. J. (2013) FMNL3 FH2-actin structure gives insight into formin-mediated actin nucleation and elongation. *Nat. Struct. Mol. Biol.* **20,** 111–118
49. Higashi, T., Ikeda, T., Murakami, T., Shirakawa, R., Kawato, M., Okawa, K., Furuse, M., Kimura, T., Kita, T., and Horiuchi, H. (2010) Flightless-I (Fli-I) regulates the actin assembly activity of diaphanous-related formins (DRFs) Daam1 and mDia1 in cooperation with active Rho GTPase. *J. Biol. Chem.* **285,** 16231–16238
50. Spudich, J. A., and Watt, S. (1971) The regulation of rabbit skeletal muscle contraction. I. Biochemical studies of the interaction of the tropomyosin-troponin complex with actin and the proteolytic fragments of myosin. *J. Biol. Chem.* **246,** 4866–4871
51. Bugyi, B., Didry, D., and Carlier, M. F. (2010) How tropomyosin regulates lamellipodial actin-based motility: a combined biochemical and reconstituted motility approach. *EMBO J.* **29,** 14–26
52. Bugyi, B., Papp, G., Hild, G., Lõrinczy, D., Nevalainen, E. M., Lappalainen, P., Somogyi, B., and Nyitrai, M. (2006) Formins regulate actin filament flexibility through long range allosteric interactions. *J. Biol. Chem.* **281,** 10727–10736
53. Perelroizen, I., Marchand, J. B., Blanchoin, L., Didry, D., and Carlier, M. F. (1994) Interaction of profilin with G-actin and poly(L-proline). *Biochemistry* **33,** 8472–8478
54. Nag, S., Ma, Q., Wang, H., Chumnarnsilpa, S., Lee, W. L., Larsson, M., Kannan, B., Hernandez-Valladares, M., Burtnick, L. D., and Robinson, R. C. (2009) Ca^{2+} binding by domain 2 plays a critical role in the activation and stabilization of gelsolin. *Proc. Natl. Acad. Sci. U.S.A.* **106,** 13713–13718
55. Hanson, J., and Lowy, J. (1963) The structure of F-actin and of actin filaments isolated from muscle. *J. Mol. Biol.* **6,** 46–60
56. Sanchez-Soriano, N., Travis, M., Dajas-Bailador, F., Gonçalves-Pimentel, C., Whitmarsh, A. J., and Prokop, A. (2009) Mouse ACF7 and *Drosophila* short stop modulate filopodia formation and microtubule organisation during neuronal growth. *J. Cell Sci.* **122,** 2534–2542
57. Liu, W., Xie, Y., Ma, J., Luo, X., Nie, P., Zuo, Z., Lahrmann, U., Zhao, Q., Zheng, Y., Zhao, Y., Xue, Y., and Ren, J. (2015) IBS: an illustrator for the presentation and visualization of biological sequences. *Bioinformatics* **31,** 3359–3361
58. Oda, T., Iwasa, M., Aihara, T., Maéda, Y., and Narita, A. (2009) The nature of the globular- to fibrous-actin transition. *Nature* **457,** 441–445
59. Yamashita, M., Higashi, T., Suetsugu, S., Sato, Y., Ikeda, T., Shirakawa, R., Kita, T., Takenawa, T., Horiuchi, H., Fukai, S., and Nureki, O. (2007) Crystal structure of human DAAM1 formin homology 2 domain. *Genes Cells* **12,** 1255–1265
60. Lammers, M., Rose, R., Scrima, A., and Wittinghofer, A. (2005) The regulation of mDia1 by autoinhibition and its release by Rho*GTP. *EMBO J.* **24,** 4176–4187
61. Chereau, D., Kerff, F., Graceffa, P., Grabarek, Z., Langsetmo, K., and Dominguez, R. (2005) Actin-bound structures of Wiskott-Aldrich syndrome protein (WASP)-homology domain 2 and the implications for filament assembly. *Proc. Natl. Acad. Sci. U.S.A.* **102,** 16644–16649

SUPPLEMENTAL MATERIAL

THE ACTIVITIES OF THE C-TERMINAL REGIONS OF THE FORMIN PROTEIN DISHEVELED-ASSOCIATED ACTIVATOR OF MORPHOGENESIS (DAAM) IN ACTIN DYNAMICS

Andrea Teréz Vig[1], István Földi[2], Szilárd Szikora[2], Ede Migh[2], Rita Gombos[2], Mónika Ágnes Tóth[1], Tamás Huber[1], Réka Pintér[1], Gábor Csaba Talián[1], József Mihály[2], Beáta Bugyi[1,3,*]

* to whom the correspondence should be addressed: Beáta Bugyi, University of Pécs, Medical School, Department of Biophysics, Pécs, Szigeti str. 12, H-7624, Hungary, Phone: +36-72-536-265, E-mail: beata.bugyi@aok.pte.hu

Institutions:

[1] University of Pécs, Medical School, Department of Biophysics, Szigeti str. 12, Pécs, H-7624, Hungary

[2] Biological Research Centre, Hungarian Academy of Sciences, Institute of Genetics, MTA-SZBK NAP B Axon Growth and Regeneration Group, Temesvári krt. 62, Szeged, H-6726, Hungary

[3] Szentágothai Research Center, Ifjúság str. 34, Pécs, H-7624, Hungary

Supplemental movie 1. Filopodia dynamics in *Drosophila* primary neurons.
Time lapse sequence of filopodia dynamics of a neuronal growth cone expressing Actin5C::GFP. Scale bar = 5 μm, elapsed time is given in seconds.

The activities of the C-terminal regions of the formin protein disheveled-associated activator of morphogenesis (DAAM) in actin dynamics

Andrea Teréz Vig, István Földi, Szilárd Szikora, Ede Migh, Rita Gombos, Mónika Ágnes Tóth, Tamás Huber, Réka Pintér, Gábor Csaba Talián, József Mihály and Beáta Bugyi

J. Biol. Chem. 2017, 292:13566-13583.
doi: 10.1074/jbc.M117.799247 originally published online June 22, 2017